JPL- 701-174

JPL BASIC RESEARCH REVIEW

DRA

AS PRESENTED TO THE OAST RESEARCH COUNCIL OCTOBER 16 AND 17, 1972

(NASA-CR-136973) JPL BASIC RESEARCH EARTH REVIEW (Jet Propulsion Lab.) 178 p

N74-71716

Unclas
00/99 31047

JET PROPULSION LABORATORY
CALIFORNIA INSTITUTE OF TECHNOLOGY
PASADENA, CALIFORNIA

701-174

JPL BASIC RESEARCH REVIEW

AS PRESENTED TO THE OAST RESEARCH COUNCIL OCTOBER 16 AND 17, 1972

Compiled by:

John W. Lucas
Manager for Research and
Planetary Quarantine

Approved by:

Frank E. Goddard, Jr.
Assistant Laboratory Director for
Research and Advanced Development

JET PROPULSION LABORATORY
CALIFORNIA INSTITUTE OF TECHNOLOGY
PASADENA, CALIFORNIA

PREFACE

As was the case last year, the Jet Propulsion Laboratory is reporting to the OAST Research Council on those tasks that are considered to be basic research.

We wish to express our appreciation to Research Council members for informing themselves of and commenting on our basic research effort. The critique provided us last year was most useful, and we look forward to another mutually informative meeting.

CONTENTS

		Page
	PREFACE	iii
I.	AERODYNAMICS	
	VISCOUS TRANSONIC FLOW INVESTIGATIONS Donald Collins	1
	SUPPORT INTERFERENCE IN TRANSONIC WIND TUNNELS Wayne Marko	5
II.	FLUID MECHANICS	
	SHOCK WAVE-TURBULENT BOUNDARY LAYER INTERACTIONS – PSEUDO SHOCK REGION Robert Cuffel	11
	BOUNDARY LAYER EXPERIMENTAL STUDIES James Kendall	13
	BOUNDARY LAYER TRANSITION THEORY Leslie Mack	17
	NEW TECHNIQUES FOR SOLUTION OF NONLINEAR DIFFERENTIAL EQUATIONS Frank Estabrook	21
III.	FLIGHT MECHANICS	
	No basic research in this category	
IV.	ATMOSPHERIC AND SPACE PHYSICS	
	MONTE CARLO TRANSPORT CALCULATIONS George Thomas	23
	THEORETICAL STUDY OF THE RADIATING, VISCOUS HYPERSONIC BLUNT BODY PROBLEM Richard Passamaneck	27
	MEASUREMENTS OF THE STRUCTURE OF AN IONIZING SHOCK WAVE IN A HYDROGEN-HELIUM MIXTURE Lewis Leibowitz	29
V.	ENVIRONMENTAL SCIENCE	
	NOISE GENERATING MECHANISMS IN SUPERSONIC JETS S. Parthasarathy	33
	PHOTOCHEMISTRY OF AIR POLLUTION William DeMore	39
VI.	MATERIALS	
	CROSSLINK DENSITY AS REDUCTION PARAMETER FOR ELASTOMERS Jovan Moacanin	41
	VISCOELASTIC BEHAVIOR OF ELASTOMERS UNDERGOING CHEMICAL DEGRADATION Jovan Moacanin	47
VII.	STRUCTURES	
	No basic research in this category	
VIII.	PROPULSION	
	DYNAMICS OF JET IMPINGEMENT Jack Rupe	51
	MOLECULAR BEAM SAMPLING SYSTEM FOR COMBUSTION CHAMBERS John Houseman	55
	DETONATION PROPULSION Lloyd Back	59

Page

SOLID PROPELLANT COMBUSTION MODELING
R. N. Kumar 63

NETWORK POLYMER FORMATION
Harold Marsh 67

FINITE DEFORMATION THEORY
Jovan Moacanin 71

IX. POWER

SOLAR CELL RESEARCH
Richard Stirn 75

LASER BEAM PHOTOVOLTAIC CONVERSION
Richard Stirn 79

PULSE CHARGING OF BATTERIES
Werner von Hartmann 83

ANALYSIS OF LINEAR INDUCTION MACHINES
David Elliott 89

NaK-NITROGEN LIQUID METAL MHD CONVERTER
Donald Cerini 93

X. GUIDANCE AND NAVIGATION

No basic research in this category

XI. CONTROL

No basic research in this category

XII. COMMUNICATIONS AND INFORMATION SCIENCES

JPL ROBOT RESEARCH PROGRAM
William Whitney 97

Page

CODING THEORY AND LINEAR PROGRAMMING
Robert J. McEliece 103

XIII. LIFE SCIENCE

No basic research in this category

XIV. PHYSICS AND CHEMISTRY

LASER KINETICS
Gary Russell 107

METALLIC VAPOR DISCHARGE TUBE EXPERIMENT
Che Chen 111

SUPERSONIC ELECTRIC DISCHARGE COPPER VAPOR LASER
Noble Nerheim 115

NUCLEAR ZEEMAN MASER
Daniel Elleman 119

PHYSICS OF MOLECULAR INTERACTIONS
Wesley Huntress 121

ELECTRON IMPACT SPECTROSCOPY
Sandor Trajmar 125

THERMIONICS RESEARCH
Katsunori Shimada 129

LASER PLASMADYNAMIC GENERATOR
Katsunori Shimada 133

SUPERFLUID HELIUM ORBITAL EXPERIMENTS
Melvin Saffren 137

STUDY FOR A PHYSICS AND CHEMISTRY LABORATORY IN SPACE
Melvin Saffren 141

Page

INFRARED ACTIVE JOSEPHSON JUNCTIONS
Melvin Saffren 145

SUPERCONDUCTIVITY RESEARCH
Randall Kirschman 151

SUPERCONDUCTIVITY AT HIGH TEMPERATURE
Alan Rembaum 155

Page

ELECTRONIC PROPERTIES OF THIN INSULATING FILMS
Christer Svensson 161

MAGNETO-OPTIC INFORMATION STORAGE ON MnBi FILMS
George Lewicki 165

SPACE-CHARGE-LIMITED CURRENTS (SCLC) IN SOLIDS
Alex Shumka 169

AERODYNAMICS

D. J. Collins*

VISCOUS TRANSONIC FLOW INVESTIGATIONS

One of the most critical problems that has faced aircraft designers during the last decade, and will face them in the foreseeable future, is that of the influence of viscosity on the distribution of pressure on aerodynamic surfaces. Viscous interaction effects are particularly critical in the transonic speed regime, where gross changes in the flow over an aerodynamic surface can result from small perturbations in the boundary shape. Such changes are often introduced as a result of the separation of the viscous layer near the body and lead to gross modifications to the exterior inviscid flow.

As the focal point of the current program, we have initiated a coordinated experimental and theoretical study in order to fully understand the fundamental nature of viscous interactions in transonic flow, particularly flows exhibiting large degrees of turbulent separation. The initial experiments, conducted in the JPL 20-in. supersonic wind tunnel, have yielded substantial information on the nature of viscous interactions in both laminar and in turbulent flow. Of particular interest in regard to transonic scale effects are results from two circular-arc airfoil models, scaled so that the transonic tunnel parameter is held constant and studied under conditions for which the transonic similarity parameter is constant. These results demonstrate the concepts of inviscid similarity under conditions where viscosity is unimportant and show a marked deviation from inviscid similarity when viscous effects are dominant. From such tests, we hope to learn more about the similarity scaling for viscous-dominated flows.

The theoretical efforts initiated under this task have utilized the considerable expertise of Dr. Julian Cole and Dr. James Krupp of UCLA to formulate an inviscid theory from which computations can be made of the experimental flows. Thus, a direct comparison between theory and experiment has been made for both subcritical and supercritical airfoils in a bounded flow. The influence of the upstream and downstream boundary conditions and of the presence of solid walls has been included in these computations. The results indicate that for flows exhibiting vanishing degrees of separation, both the airfoil pressure distribution and the distribution of pressure along the wind tunnel boundary are correctly modeled by the inviscid theory. For flows exhibiting strong viscous effects, the pressure distribution on the airfoil surface is no longer adequately described by the inviscid theory.

The present experimental results have had an immediate application as a reference flow for the theoretical computations of Klineberg and Steger at the Ames Research Center. In these computations, Klineberger and Steger have succeeded in modeling a subcritical laminar viscous interaction using integral methods to represent the viscous layer and computing the outer inviscid flow by a finite-difference relaxation technique. Such computations are the first successful attempt at computing the entire viscid-inviscid interaction at transonic speeds.

The future course of the experimental program at the Jet Propulsion Laboratory will be directed toward the measurement of both the mean flow field and the details of the structure of those transonic flows which exhibit extensive turbulent separation. To facilitate these measurements, new instrumentation is being developed, including a laser doppler velocimeter and a laser interferometer. Simultaneously, the theoretical investigation is being extended to include viscous effects on the boundaries.

*Space Sciences Division, Physics Section

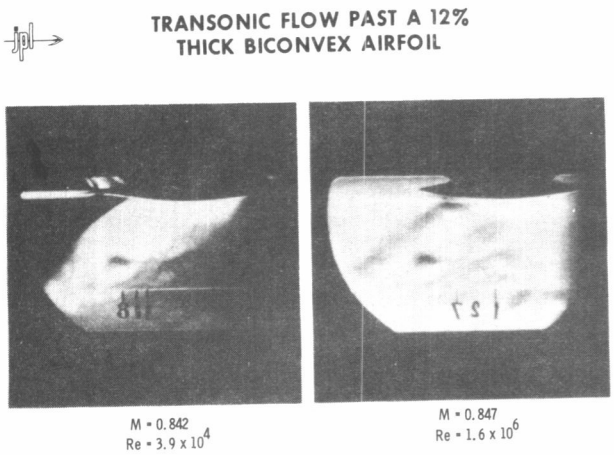

Figure 1.

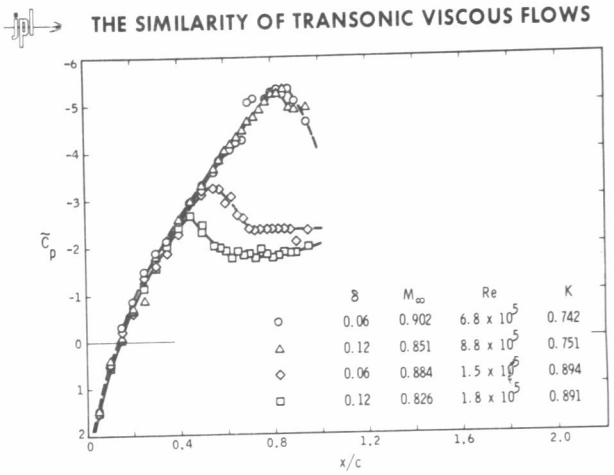

Figure 2.

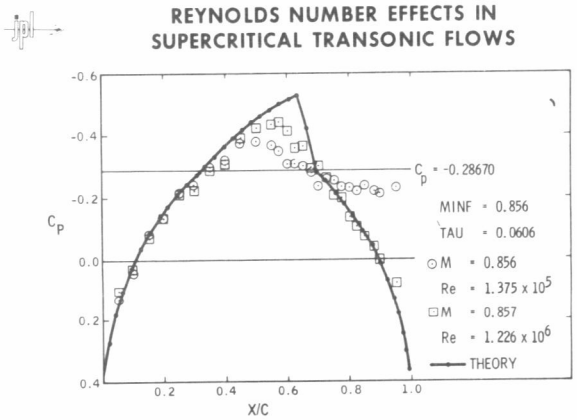

Figure 3.

REYNOLDS NUMBER EFFECTS IN SUPERCRITICAL TRANSONIC FLOWS

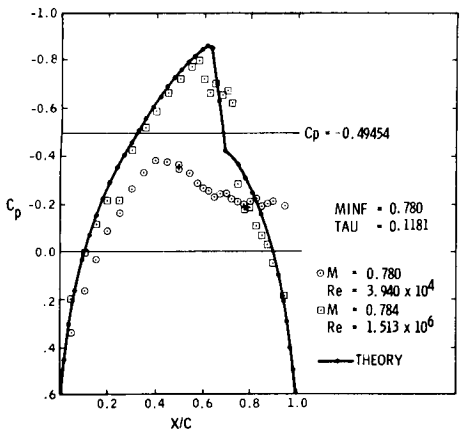

Figure 4.

COMPARISON WITH THE THEORY OF KLINEBERG AND STEGER

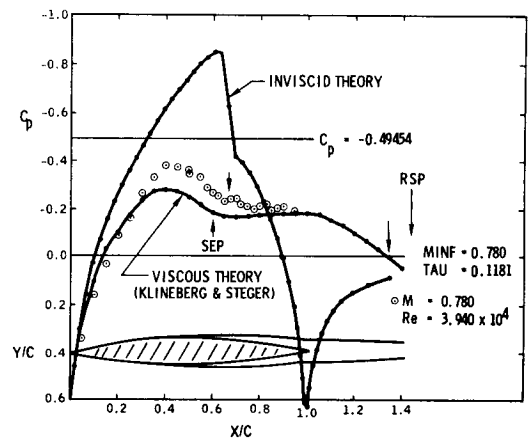

Figure 5.

Wayne Marko*

SUPPORT INTERFERENCE IN TRANSONIC WIND TUNNELS

The performance and economic justification of aircraft are in many cases dependent on the critical transonic drag and drag rise onset. However, our ability to adequately predict transonic performance has not always been satisfactory. Although considerable wind tunnel data related to this problem has been obtained over the years, no general procedure for assessing support interference and its influence on aircraft performance has been established.

The test program described herein avoided the confusion which results from studying too many parameters. Support interference was studied simply by comparing the drag obtained with models on supports in the wind tunnel and in free-flight under identical conditions. The free-flight drag data have been obtained in the same wind tunnel, with the same size models and under the same flow conditions.

Three phases of programs were outlined in the last JPL Basic Research Review (Document 701-135):

(1) free-flight technique adaption and technique transference

(2) problem definition and acquisition of basic data

(3) fundamental studies which included the telemetry of sting interference free base pressure measurements.

All three phases have been successfully completed, and data are being analyzed and prepared for reporting. By necessity, this basic research review presents only a few program highlights.

The principal configuration in this program is the HIRAD-10 with fins, a configuration which has undergone extensive testing at Langley Research Center in connection with their transonic transport development program.

In addition, three basic configurations, a 10-deg cone, a 60-deg blunt cone, and a sphere have been tested. All configurations had boundary layer transition trips.

The test program was conducted in the NASA Ames Research Center 6 by 6-foot supersonic wind tunnel during two test periods. The first was in January 1972 and the second in May of the same year. The sum of the test periods equaled about eight weeks of single shift operation. The test program received considerable support from the Ames Experimental Investigations Branch Staff.

The sting support drag data from the two tests, five months apart, compare very well with each other. These data impart confidence as to the repeatability of the sting supported results which are, in turn, related to the accuracy of the force balance measurements and similarity of the boundary layer. The free-flight drag measurements also present an excellent self-consistent picture of the transonic drag rise for the configurations tested. What is important then, is the comparison of free-flight results with those of the sting support method. Comparative free-flight and sting support results on three of the basic configurations tested, the two cones and the sphere, indicate small sting effects when reasonably small stings were used. In the case of the sphere and blunt body, the normal shocks occurred near the maximum diameter and trailing edge, respectively, initiating separated flow which blanketed the entire base area and reduced the influence of the sting. In the case of the cone, sting effects were minimized when a 0.6-in. diameter sting was used ($d_s/D = 0.4$). With larger, 1.0-in.-diam stings, the wake shock moved perceptibly closer to the base and the total drag increased appreciably.

While the configurations just described were subject to minimal sting effects for small stings, comparative sting support and free-flight tests indicate that the sting has an appreciable effect on the drag in the transonic regime for the

*Applied Mechanics Division, Aerophysics Section

fuselage-like configurations tested. The free-flight data show both an earlier drag-rise by 0.02 and a level difference of about 15%. The surprising feature is that the drag-level difference persists well below the drag-rise region, throughout the Mach range tested; that is, at least down to M = 0.85. If it is assumed that a difference in the base pressure is the reason for the 15% difference, then the sting-supported base pressure coefficients should be about 0.3 more positive than that of the free-flight values. Results from the base-pressure studies indicate the opposite to be true in spite of the larger-than-anticipated scatter in the base-pressure data telemetered from the free-flight models. Therefore, as the difference in the drag levels of the sting-supported and free-flight models cannot be explained by the difference in base pressure, it must be assumed that significant interference caused by the sting support extends well forward of the base and results in an increase in the pressure level on the aft portion of the body. Additional testing should be done to confirm and quantify this conclusion.

Comparative tests using the wind tunnel free-flight technique have applications in other areas. Future investigations should include: comparative tests in wind tunnels of different configuration, additional base pressure telemetry measurements with refined telemetry equipment, blockage tests to probe the phenomena observed at the NASA Langley Research Center for the fuselage-like configurations in the same facility, and, finally, comparative free-flight and support studies on airplane-like configurations.

FIRST YEAR PROGRAM

- FREE-FLIGHT TECHNIQUE DEVELOPMENT AND TECHNIQUE TRANSFERENCE
- PROBLEM DEFINITION AND ACQUISITION OF BASIC DATA
- FUNDAMENTAL STUDIES

Figure 1.

ACCOMPLISHMENTS

- PERFORMED COMPARITIVE DRAG EXPERIMENTS USING FREE-FLIGHT AND STING SUPPORT TECHNIQUES IN THE SAME WIND TUNNEL
- INVESTIGATED DIFFERENT SUPPORT SYSTEMS
- INVESTIGATED EFFECTS OF STING DIAMETER
- MEASURED BASE PRESSURE USING FREE FLIGHT TELEMETRY AND STING SUPPORT TECHNIQUES

Figure 2.

TEST CONFIGURATIONS

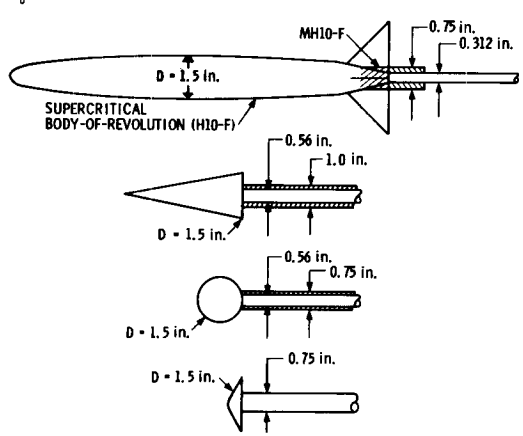

Figure 3.

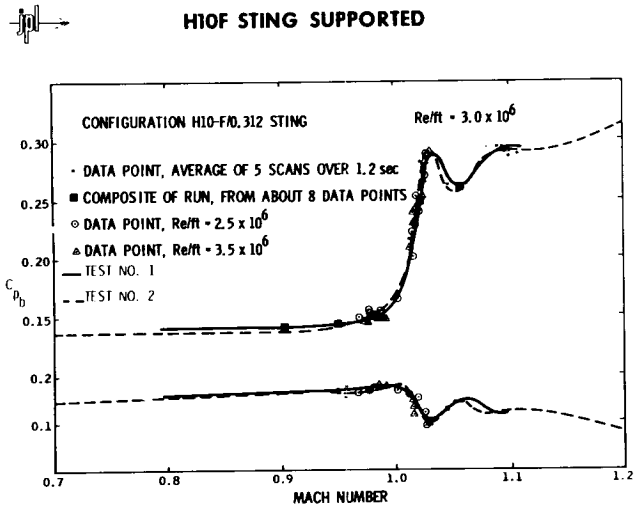

Figure 4.

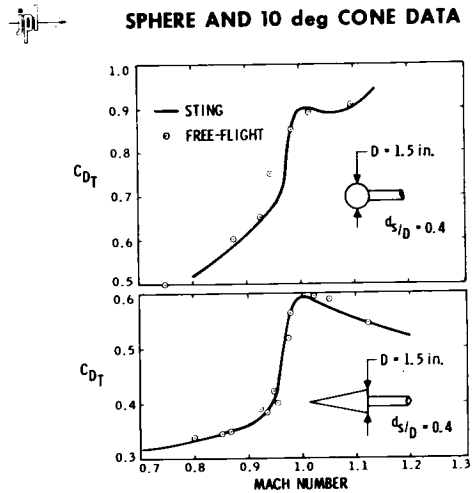

Figure 5.

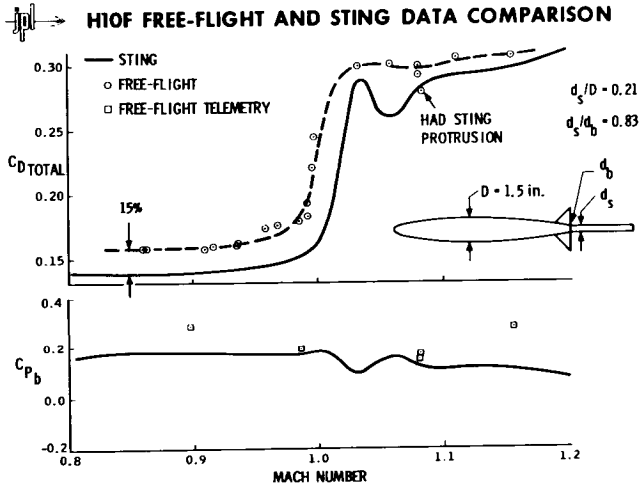

Figure 6.

SUMMARY

- FREE FLIGHT AND STING SUPPORT TESTS
- SAME FACILITY - AMES 6 x 6 ft TRANSONIC TUNNEL
- MACH 0.8 TO 1.2
- DRAG OF A SPHERE AND 10° CONE ARE RELATIVELY INDEPENDENT OF MEASUREMENT TECHNIQUE
- STING SUPPORT TESTS OPTIMISTICALLY PREDICT DRAG FOR A FUSELAGE SHAPE AND DELAYED DRAG RISE WHEN COMPARED WITH FREE-FLIGHT DATA
- IT IS SUGGESTED THAT AIRCRAFT PERFORMANCE PREDICTIONS MAY BE SERIOUSLY DEGRADED BY THE EFFECTS SHOWN

Figure 7.

POSSIBLE FUTURE WORK

- COMPARISON OF DATA OBTAINED USING FREE-FLIGHT TECHNIQUE IN SEVERAL FACILITIES
- OBTAIN ADDITIONAL BASE PRESSURE TELEMETRY DATA
- INVESTIGATE BLOCKAGE PHENOMENA WITH FREE-FLIGHT MODELS
- PERFORM COMPARITIVE STUDIES ON AIRPLANE-LIKE CONFIGURATIONS

Figure 8.

FLUID MECHANICS

R. F. Cuffel*

SHOCK WAVE-TURBULENT BOUNDARY LAYER INTERACTIONS--PSEUDO SHOCK REGION

This study of the strong compression process found in channel flows, which is referred to as a pseudo-shock region or multiple-shock region, was initiated because of the substantially increased wall heat transfer and the scarcity of information on the flow process. This investigation, which was terminated in FY'72, was the last of a series of studies of various flow phenomena found in an axisymmetric diffuser.

A schematic of the flow field and the wall and centerline static pressures, normalized by the wall value at the inlet of the pseudo shock region, are shown in Fig. 1. The dashed line, δ , indicates the edge of the velocity boundary layer. Pitot, static, and thermocouple probes were traversed across the flow at the five locations indicated.

The pseudo-shock region began downstream of Position 1. The static pressure increased along the wall, extending from the wall into the flow. This resulted in the compression, deceleration, and thickening of the boundary layer. The boundary layer was unable to withstand this adverse pressure gradient and separated. The beginning of the separated flow region was established by bleeding ammonia through the pressure taps and observing the traces in the ammonia sensitive paint on the walls. The thickness of the reverse flow region was 4% of the wall radius at Position 3. The thick subsonic flow region formed in this separation process continued to grow downstream as the flow decelerated.

The compressive turning of the flow inward beyond the separated flow region generated a Mach-disk-like shock near the centerline. The subsonic flow region downstream of this normal shock disappeared as the flow accelerated. The outer edge of the viscous slipstream grew into the boundary layer forming a totally viscous flow.

Analysis of the measurements between Positions 3 and 5 revealed that radial variations decreased while the static pressure increased along the streamlines. The total pressure, however, increased along the convergent streamlines in the core flow region near the centerline and throughout most of the subsonic flow region near the wall. In the large annular region between the total pressure decreased along the divergent streamlines.

The walls were externally cooled, the wall-to-total-gas temperature ratio being 0.44. The thermal boundary layer was slightly thicker than the velocity boundary layer throughout this region. The heat transfer measurements shown in Fig. 2 are similar in shape to the wall static pressure measurements. In the oblique shock reflection regions upstream, the heat-transfer coefficient ratio varied like the 0.8 power of the wall static pressure ratio, as was typical of other investigations. In the pseudo-shock region, the dependence is much less, being like the 0.6 power for this test.

Internal flow measurements throughout a pseudo-shock region revealed only one Mach-disk-like shock emanating from the embedded separated flow region. This strong compression is predominantly a viscous process.

*Propulsion Division, Research and Advanced Concepts Section

PSEUDO SHOCK REGION

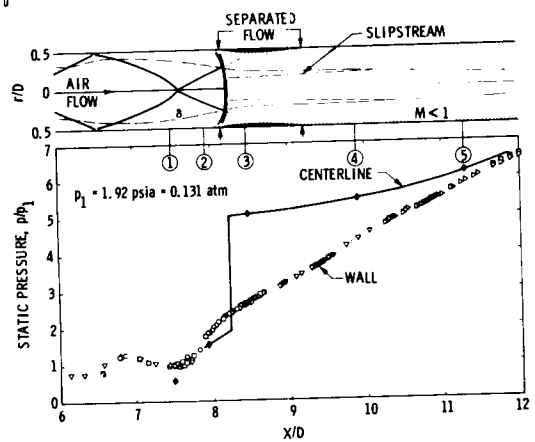

Figure 1.

HEAT TRANSFER

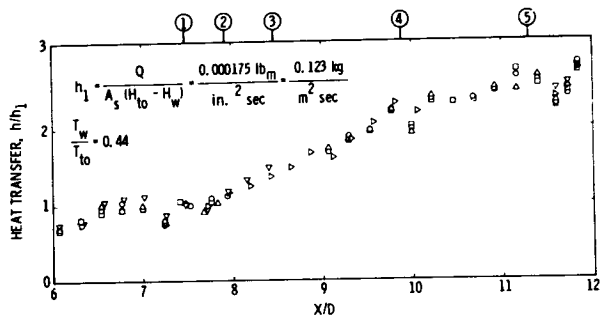

Figure 2.

CONCLUSIONS

PSEUDO SHOCK REGION

- ONE MACH DISK
- VISCOUS COMPRESSION PROCESS

Figure 3.

BOUNDARY LAYER EXPERIMENTAL STUDIES

Supersonic boundary layer transition is often regarded as a process for which there is no explanation. In contrast, the present experiments are carried out with the belief that a boundary layer is a fluid-dynamic amplifier with definite response characteristics which can be understood. The work seeks to evaluate these characteristics in terms of the available theory and to guide theory where improvement should be made.

Much of the work during the past year concerned measuring transition on a 10-deg, half-angle cone at Mach 2 and 4.5 in support of a cooperative program recommended by the NASA Transition Study Group. The objectives are indicated in Fig. 1. By use of the hot-wire anemometer, the transition location has been recorded for small increments of azimuth angle, angle of attack, and wall temperature. Of interest in the assessment of firing range data, it has been found that transition is insensitive to the cone tip temperature and is correlated rather well with the wall temperature in the vicinity of transition.

A portion of the above work has been aimed at further establishing the relevance of stability theory to wind tunnel transition results. The amplification rate of the natural fluctuations on the cone in the presence of wind tunnel sound was determined. Figure 2 shows that for adiabatic conditions, the observed amplification rate resembles that predicted for a 30-deg wave angle. The wave angle is not known in actuality, but 30 deg is probably a reasonable average. When the wall is cooled, the amplification is suppressed, a result consistent with the observed rearward movement of transition.

As is indicated in the foregoing, the comparison between theory and experiment requires knowledge of the wave obliqueness angle, a quantity not readily measured. In recent tests, the wave obliqueness has been controlled to a considerable extent in the manner shown in Fig. 3. The tunnel is operated with laminar wall layers. By means of air jets on the two sidewalls and on the ceiling of the tunnel, strips of turbulent flow can be created or inhibited at will. Each strip emits waves of a rather definite directionality. Figure 3 shows the response of a laminar layer on a test plate to waves emanating from the ceiling which impinge upon the plate in a nearly two-dimensional pattern, and to waves from the sidewalls, which impinge obliquely. The considerable difference in fluctuation growth is consistent with expectation from theory. A detailed comparison will be available soon.

In addition, this technique has enabled the detection of non-linearity in the fluctuation growth, a matter of considerable importance in comparing experimental results with linear theory. As shown in Fig. 4, the response of the boundary layer on the test plate to the oblique waves from both walls can be much greater than twice the response to waves from either wall alone. The streamwise development of non-linearity is given.

Because the realization of a so-called quiet tunnel, being considered elsewhere, is likely to require some time, attempts have been and will be made to reduce the sound in the usual type of tunnel. A number of exploratory investigations were made. Tunnel wall cooling showed a benficial trend, but further work will be needed to indicate whether an important gain can be made.

*Space Sciences Division, Physics Section

EXPERIMENTAL ACTIVITIES

- CONE TRANSITION
  - COOLED; HEATED TIP
  - TIP BLUNTNESS
  - ANGLE OF ATTACK
  - VIBRATION
- FORCING AND INSTABILITY IN NOISY TUNNEL
  - EFFECT OF COOLING
  - TWO-DIMENSIONAL vs OBLIQUE SOUND WAVES
  - NON-LINEARITY
- REDUCTION OF TUNNEL SOUND

Figure 1.

FLUCTION GROWTH ON A 10° CONE

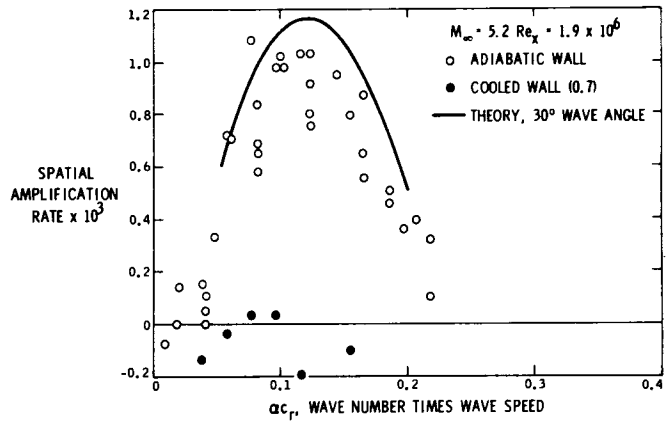

Figure 2.

WAVE OBLIQUENESS EXPERIMENTS

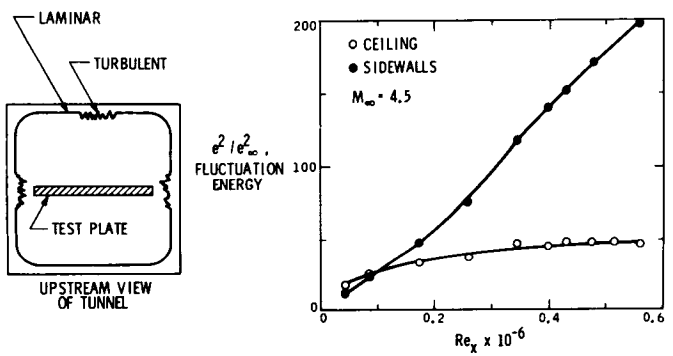

Figure 3.

NON-LINEARITY IN A BOUNDARY LAYER

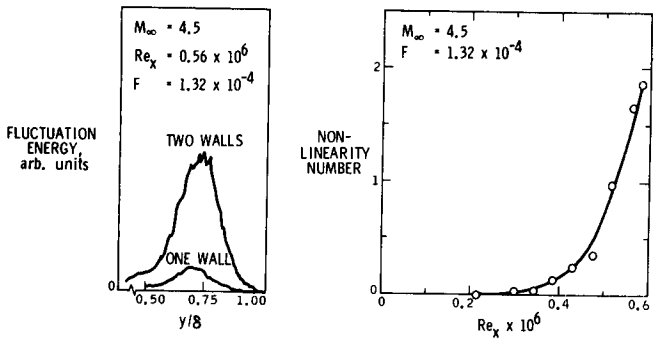

Figure 4.

FUTURE WORK

- COORDINATION WITH THEORY
  - COOLED WALL
  - PRESSURE GRADIENT
  - HYPERSONIC FLOW
- EXPLORATORY STUDIES
  - ROUGHNESS ELEMENTS
  - THREE-DIMENSIONALITY
  - NON-LINEARITY
- REDUCTION OF TUNNEL SOI'

Figure 5.

L. Mack*

BOUNDARY LAYER TRANSITION THEORY

Linear stability theory usually deals with only a single mode out of what is believed to be an infinite number. An exception is the dynamically unstable supersonic boundary layer, where multiple unstable modes exist and have been studied theoretically and identified experimentally. The incompressible Blasius boundary layer is the simplest example of a dynamically stable boundary layer, i.e., as the Reynolds number, R_x, approaches infinity no unstable modes can exist. For a complete understanding of instability phenomena and their connection with transition, it is essential to know all the possible disturbances that can exist in such a boundary layer. Numerous investigations have been carried out of the complete eigenvalue spectrum at finite Reynolds numbers for Couette and plane Poiseuille flow, but only a single incomplete investigation has been made of a boundary-layer flow. All of the higher modes found in these studies are stable. Only the fundamental or Tollmien-Schlichting wave can be unstable. On the contrary, Raetz has claimed that additional unstable disturbances do exist in a Blasius boundary layer. These disturbances are a special type of oblique spatial disturbances, and their existence would be of great importance to the transition problem.

A careful study has been carried out of both Raetz-type disturbances and the complete eigenvalue spectrum of two-dimensional temporal disturbances for flat-plate boundary layers. Even with Raetz's own method of locating eigenvalues, no evidence of his amplified disturbances could be found. However, his method, which consists of plotting in the complex c (wave velocity) plane the two curves formed by the zeroes of the real and imaginary parts of the secular determinant and looking for intersections, proved to be ideal for finding unknown higher modes. Because of severe numerical problems associated with the 6-place tabulated values of the Blasius velocity profile that were being used, the Blasius boundary layer was replaced by the asymptotic suction boundary layer for the study of the complete spectrum.

The main result was the discovery of a new class of distrubances with c_r, the phase velocity, near unity. In the free stream, these distrubances are primarily viscous, or vorticity, waves. There is an orderly sequence of values of c_i starting near $c_i = 0$. The first 20 modes have been calculated, and the sequence appears to extend indefinitely in the negative c_i direction. All modes are damped, but those with c_i near zero can persist for many cycles if once excited. In addition to this family, there are other modes apparently scattered at random over the complex c plane which include the fundamental or Tollmien-Schlichting wave. These higher modes are similar to the fundamental in that the inviscid solution dominates in the free stream.

It has been established that the "viscous" family also exists for spatial distrubances, and for the Blasius boundary layer. The number of modes in the "inviscid" family appears to depend upon the velocity profile. The eigenvalues of all of the modes except one go to zero as $R_x \longrightarrow \infty$. The remaining mode approaches the single eigenvalue of the inviscid stability equation.

*Space Sciences Division, Physics Section.

EIGENVALUE PROBLEM

- ORR-SOMMERFELD EQUATION: $(U - c)(\phi'' - \alpha^2\phi) - U''\phi = -\frac{i}{\alpha R}(\phi^{IV} - 2\alpha^2\phi'' + \alpha^2\phi)$
- MEAN FLOW: BOUNDARY LAYER $U(y)$, AS $y \to \infty$, $U = U_1$

$$\begin{pmatrix} u'(y) \\ v'(y) \end{pmatrix} = \begin{pmatrix} f(y) \\ \alpha\phi(y) \end{pmatrix} \exp\left[i(\alpha x - \omega t)\right]$$

TEMPORAL: REAL α COMPLEX $c = \omega/\alpha = c_r + ic_i$

SPATIAL: REAL ω COMPLEX $\alpha = \alpha_r + i\alpha_i$

- BOUNDARY CONDITIONS: $y = 0$, $u' = 0$, $v' = 0$; $y \to \infty$ $\begin{pmatrix} u' \\ v' \end{pmatrix} \to$ SOLUTION OF O - S EQUATION WITH $U = U_1$
- PROBLEM: GIVEN R AND α, FIND ALL POSSIBLE ω (OR c) FOR WHICH BOUNDARY CONDITIONS ARE SATISFIED.

Figure 1.

METHOD OF FINDING EIGENVALUES

- SECULAR DETERMINANT $D = \begin{vmatrix} f^{(1)}(0) & f^{(2)}(0) \\ \phi^{(1)}(0) & \phi^{(2)}(0) \end{vmatrix} = D_r + iD_i$

FOR GIVEN α, R TEMPORAL D_r AND D_i ARE FUNCTIONS OF c_r AND c_i

- IF c IS EIGENVALUE, $D_r(c_r, c_i) = 0$ $D_i(c_r, c_i) = 0$

SOLVE FOR c_r, $c_r = F_r(c_i)$ $c_r = F_i(c_i)$

- PLOT F_r AND F_i IN COMPLEX c PLANE. INTERSECTION POINTS ARE EIGENVALUES.
- ALL INTERSECTION POINTS ARE VERIFIED TO BE EIGENVALUES BY AUTOMATIC SEARCH PROCEDURE WHICH WORKS IN IMMEDIATE VICINITY OF EIGENVALUE.

Figure 2.

CALCULATION CONDITIONS

- WITH 6-PLACE BLASIUS BOUNDARY LAYER TABLES USED AS INPUT, THERE ARE SEVERE NUMERICAL DIFFICULTIES WHEN $c_r \to 1$
- WITH ASYMPTOTIC SUCTION VELOCITY PROFILE

$$U(y) = 1 - \exp\left(\frac{v_w y}{\nu}\right)$$

U, U' CAN BE COMPUTED IN DOUBLE PRECISION AT EACH INTEGRATION STEP AND THERE ARE NO NUMERICAL PROBLEMS

- CALCULATIONS DONE WITH ASYMPTOTIC SUCTION PROFILE AND TEMPORAL DISTURBANCES AT

$R_{\delta^*} = 500$

$\alpha_{\delta^*} = 0.1543$

$v_w = -0.002\ U_1$

Figure 3.

EIGENVALUE SPECTRUM OF ASYMPTOTIC SUCTION PROFILE

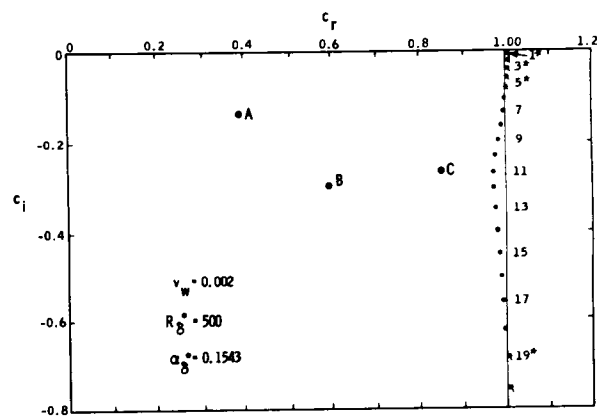

Figure 4.

RESULTS

TWO TYPES OF DISTURBANCES

- MODES A, B, C
  - SIMILAR TO TOLLMIEN-SCHLICHTING WAVES
  - IN FREE STREAM, MOSTLY INVISCID SOLUTION
- MODES 1 - 20 etc.
  - IN FREE STREAM, MOSTLY VISCOUS SOLUTION, WHICH IS

$$u' = \exp\left\{\pm\left[\alpha^2 + i\alpha R(1-c)\right]^{1/2} y\right\} \exp\left[i(\alpha x - \omega t)\right]$$

+ SIGN FOR $c_r > 1$

- SIGN FOR $c_r < 1$

  - c_r ALWAYS NEAR 1.0

THIS FAMILY ALSO EXISTS FOR

- BLASIUS BOUNDARY LAYER
- SPATIAL DISTURBANCES

Figure 5.

EIGENFUNCTIONS OF MODES A, B AND C OF ASYMPTOTIC SUCTION PROFILE

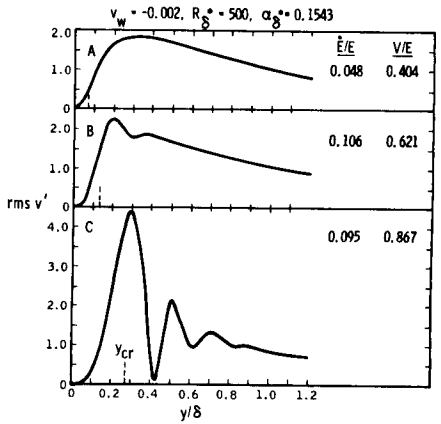

Figure 6.

EIGENFUNCTIONS OF MODES 4*, 5* AND 6 OF ASYMPTOTIC SUCTION PROFILE

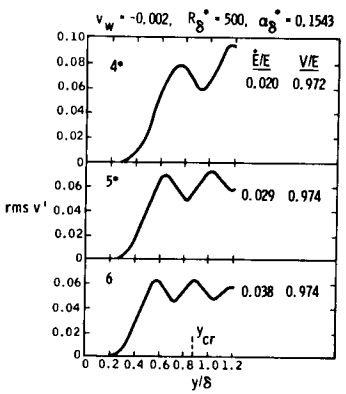

Figure 7.

EIGENFUNCTIONS OF MODES 8, 11 AND 18 OF ASYMPTOTIC SUCTION PROFILE

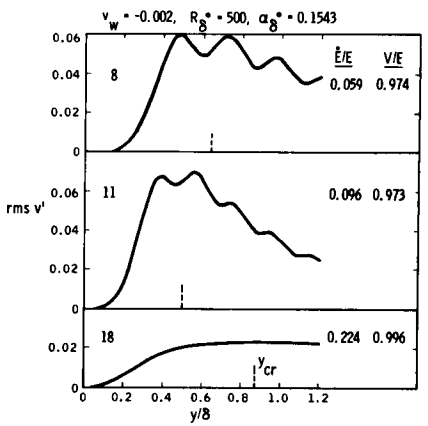

Figure 8.

RTOP 501-06-01
Computations/Aerodynamics
Frank B. Estabrook*

NEW TECHNIQUES FOR SOLUTION OF NONLINEAR DIFFERENTIAL EQUATIONS

Under this task we have formulated general theories of the analytic properties – and, in particular, the symmetry and conservation properties – of sets of partial differential equations and ordinary differential equations. The mathematics used in these theories is modern differential geometry, especially the calculus of exterior differential forms. Originated by É. Cartan in the first half of this century, it is only now appearing in a few advanced engineering and applied mathematics texts and courses. The use of differential forms has been shown to be the most powerful and elegant way to treat traditional disciplines of applied mathematics: ordinary differential equations and partial differential equations. It also provides a uniform symbolic notation which can be programmed for manipulation by high-speed computers.

We hope that one result of our work will be to make this new mathematical technique more accessible to applied mathematicians and engineers. Especially, our new results should be immediately useful to numerical analysts searching for optimum techniques for calculating quantitative solutions.

This theory brings all the *ad hoc* techniques previously known into a single, systematic mathematical language. We have so far treated, in more or less detail, the various following topics:

(1) invariance transformations
(2) general similarity solutions
(3) generalized characteristics
(4) integral conservation theorems
(5) change of variable and functional substitutions
(6) variational principles
(7) Hamiltonian methods.

This last year we first performed a series of analyses of simple, well-known, nonlinear partial differential equations (e.g., Burger's Equation, the Korteweg-de Vries Equation, one-dimensional isentropic flow), both to test our own understanding, and to exercise the completed computer capability we have developed for analytical manipulation of differential forms. We found the invariance groups of these equations, similarity solutions, conservation laws, potentials, etc. In the case of Burger's Equations we found, by systematic introduction of potentials, the surprising, but already known, linearization by functional substitution. For the Korteweg-de Vries Equation we had hoped to find a similar breakthrough, but our systematic procedure told us that, in fact, none exists.

Also, we have this year formulated and precisely defined the concept of *generalized characteristic*. A paper on this is almost completed and will be submitted soon. It is well known that integrations along Riemann characteristics is an extremely useful numerical and analytic technique, provided they exist! That is, roughly speaking, in regimes, where a flow, for example, is supersonic. But we have now shown that more general preferred paths sometimes exist which have the same property of reducing the effective number of independent variables – and these *generalized* characteristics can be used perhaps to smoothly join elliptic and hyperbolic regimes. It is too soon to foresee the results of this research, but we are presently trying out these ideas on the simplest equation of transonic flow.

Finally, an extensive paper is presently being completed applying the calculus of exterior forms to sets of first-order ordinary differential equations or, equivalently, to higher order differential equations. The first result, which to our surprise is apparently new, is clear proof that *all* sets of ordinary differential equations can, in principle, be thrown into Hamiltonian form. This means that the whole classical apparatus can be used: Poisson brackets, Poincare's integral invariants, Hamilton's variational principle, Lagrange's equations. At the suggestion of Julian Cole (UCLA) we are including a careful analysis of the invariance group of a set of ordinary differential equations, which S. Lie, Cole and others have shown to be a key to finding integration methods that are simple quadratures.

*Space Sciences Division, Physics Section.

ANALYTICAL TECHNIQUES FOR TREATMENT OF NONLINEAR DIFFERENTIAL EQUATIONS

- INVARIANCE TRANSFORMATIONS
- GENERAL SIMILARITY SOLUTIONS
- GENERALIZED CHARACTERISTICS
- INTEGRAL CONSERVATION THEOREMS
- CHANGE OF VARIABLE AND FUNCTIONAL SUBSTITUTION
- VARIATIONAL PRINCIPLES
- HAMILTONIAN METHODS

Figure 1.

CURRENT RESEARCH

- DIFFERENTIAL FORMS ON THE COMPUTER
  (BURGER'S EQUATION, KORTEWEG-DE VRIES EQUATION)
- GENERALIZED CHARACTERISTICS
  (CALCULATION OF TRANSSONIC FLOWS)
- ORDINARY DIFFERENTIAL EQUATIONS
  (NEW EXISTENCE PROOF FOR HAMILTONIANS)

Figure 2.

ATMOSPHERIC AND SPACE PHYSICS

George Thomas*

MONTE CARLO TRANSPORT CALCULATIONS

Transport of photons in nonisothermal shock layers has been studied using the Monte Carlo (random sampling) technique. No restrictions are placed on the radiation source term, which may consist of either volume emission sources (lines, continua, or molecular bands) and/or surface sources (reflecting walls or external light sources).

In the transport of radiation there exists a single parameter, temperature, which characterizes the essential nonlinearity of the problem in a nonisothermal medium. This simplifies the problem and suggests the following scheme for its solution: From an initial (arbitrary) temperature distribution a source distribution is constructed and a population of independent photons is generated. An estimate is made of the probability of the following two events:

(1) the photons escape through a boundary of the system
(2) the photons are absorbed within the system.

A tally is kept of the number of photons crossing all internal and external boundaries. These results are used in conjunction with the macroscopic transport equations to suggest a new temperature distribution. This iterative process is continued until the results of the current cycle agree with the preceding cycle; i.e., the system has converged.

*Applied Mechanics Division, Aerophysics Section.

BLUNT BODY PROBLEM WITH A BLOWN LAYER DUE TO MASSIVE ABLATION

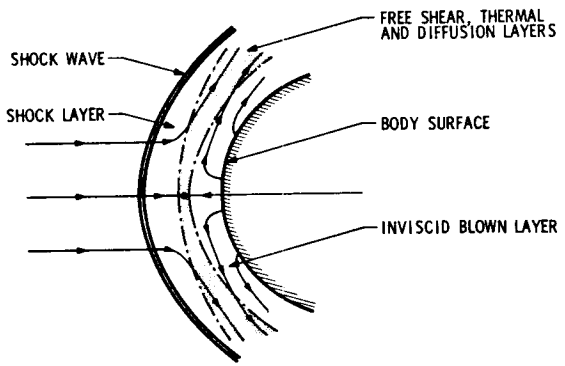

Figure 1.

ONE DIMENSIONAL SLAB

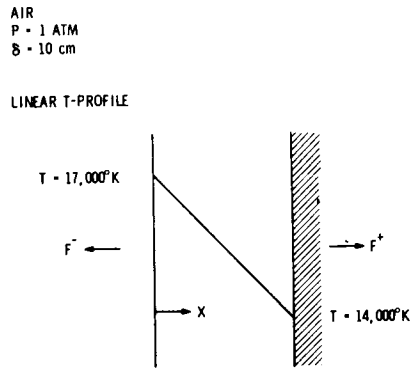

Figure 2.

3 STEP MODEL

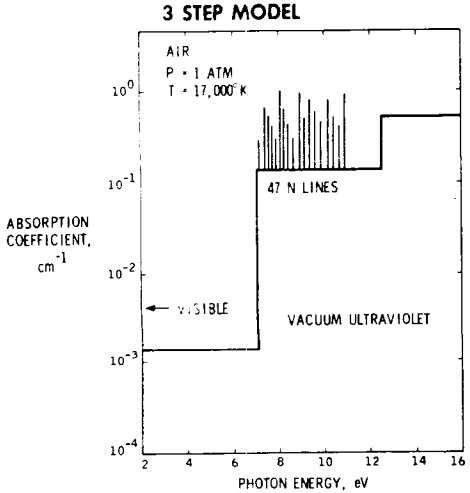

Figure 3.

MONTE CARLO TRANSPORT CALCULATIONS

- RANDOM SAMPLING TECHNIQUE FOR SOLVING PHYSICAL PROBLEMS
- TEMPERATURE INTRODUCES THE ESSENTIAL NON-LINEARITY
- STATE OF PHOTON SPECIFIED BY SET:

$$S = S(X, \mu, \nu, W)$$

- SET (X, μ, ν) MAY BE REGARDED AS RANDOM VARIABLES SPECIFIED BY PROBABILITY DIST FUNCTIONS
- RANDOM SAMPLING TECHNIQUES USED TO GENERATE SEQUENCE OF PHOTON HISTORIES:

$$S_0, S_1, S_2, \cdots, S_N$$

Figure 4.

FLOW DIAGRAM

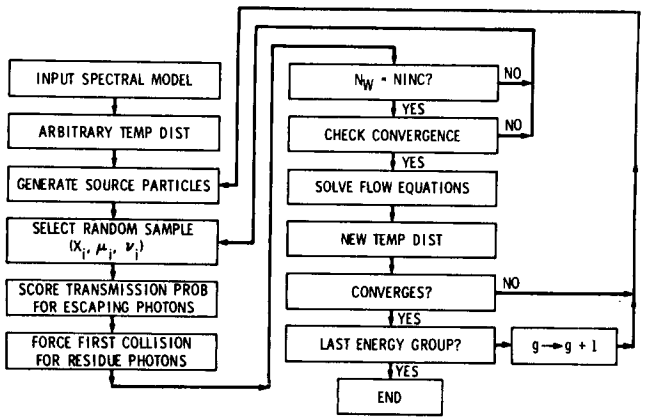

Figure 5.

TRICKS FOR EFFICIENT MONTE CARLO

ACCURACY ~ $\sqrt{N}$

- IMPORTANCE SAMPLING
- BIASED DISTRIBUTIONS
- CONVERGENCE CRITERIA
- SYMMETRY CONSIDERATIONS

Figure 6.

NON-ISOTHERMAL FLUX

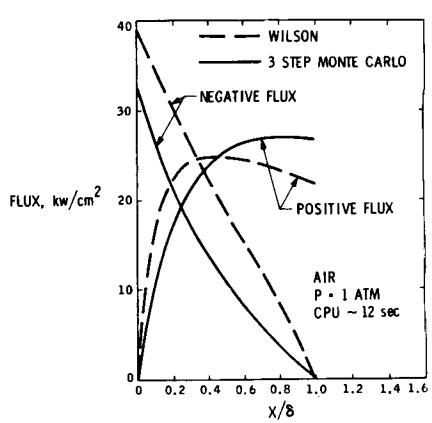

Figure 7.

ADVANTAGES OF MONTE CARLO CODE

- VERY FAST ~ 3 sec PER ENERGY GROUP
- MAY ALSO USE "FROZEN" PROBABILITIES TO SPEED UP ITERATIVE CYCLES
- ACCURACY ~ VERY FINE GRIDS
- HANDLES PROBLEMS OF GREATER COMPLEXITY THAN POSSIBLE WITH EXISTING TECHNIQUES

Figure 8.

Richard Passamaneck*

THEORETICAL STUDY OF THE RADIATING, VISCOUS HYPERSONIC BLUNT BODY PROBLEM

The viscous, radiating hypersonic flow past an axially symmetric blunt body is analyzed based on the Navier-Stokes equations plus a radiative equation of transfer derived from the Milne-Eddington differential approximation. The fluid is assumed to be a perfect gas with constant specific heats, a constant Prandtl number, P, or order one, a viscosity coefficient varying as a power, ω, of the temperature, and an absorption coefficient varying as the first power of the density. The gray gas assumption is invoked thereby making the absorption coefficient independent of the spectral frequency. The limiting form of the solutions is studied as the freestream Mach number, M, freestream Reynolds number, R, the inverse of the Bouguer number $(Bu)^{-1}$, (all based on the nose radius), and the temperature ratio across the shock wave, $\Gamma = \epsilon M^2$, go to infinity and the density ratio across the shock wave, $\epsilon = (\gamma - 1)/(\gamma + 1)$, goes to zero.

The method of matched asymptotic expansion is used in the analysis and it is shown that there is a precursor radiation region ahead of the fluid mechanical shock wave in which the convected energy is balanced by the divergence of the heat flux. A small transition region between the precursor region and the shock structure exists in which convection, heat conduction and divergence of heat flux are present in the energy equation. The three-region fluid mechanical shock structure follows the transition region with the exception that an emission-dominated region exists between the outer region and the middle region of the shock structure. Also at the end of the shock structure there is a radiation relaxation region in which the radiative intensity increases to the equilibrium value with a corresponding decrease in temperature (radiative cooling). Next follows the conventional shock layer of two or three regions depending on the ratios of the viscous to inviscid terms.

The gray gas assumption does not identically satisfy the radiative transfer equation and thus yields the Bouguer number as a similarity as well as the Boltzmann number. The thick and thin approximations commonly used do not yield both similarity parameters independently and therefore "full similarity" cannot be attained as it can with the gray gas assumption mentioned above. This analysis also showed a 16% reduction of the temperature, for a monotonic gas, in the radiation relaxation region between the shock wave structure and the shock layer. This reduction in temperature results in a 50% reduction in radiative heating.

*Applied Mechanics Division, Aerophysics Section.

ASSUMPTIONS

- NAVIER STOKES EQUATIONS ARE VALID
- PERFECT GAS
- CONSTANT SPECIFIC HEATS
- $\mu \sim T^{\omega}$
- HEAT CONDUCTION IS GIVEN BY FOURIER'S LAW
- GRAY GAS - $\alpha \neq g(\nu)$
- MILNE - EDDINGTON DIFFERENTIAL APPROXIMATION
- $\alpha \sim \rho T^{n}$

Figure 1.

RADIATING, VISCOUS HYPERSONIC BLUNT BODY FLOW

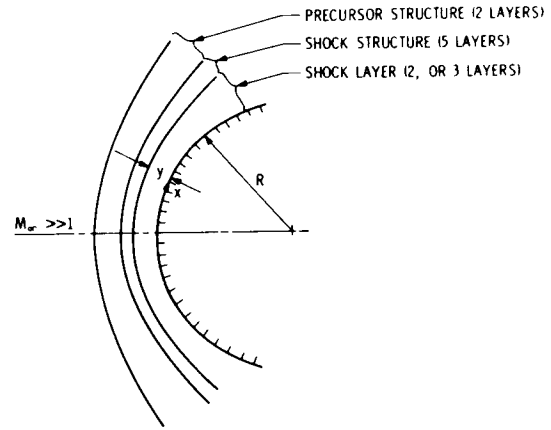

Figure 2.

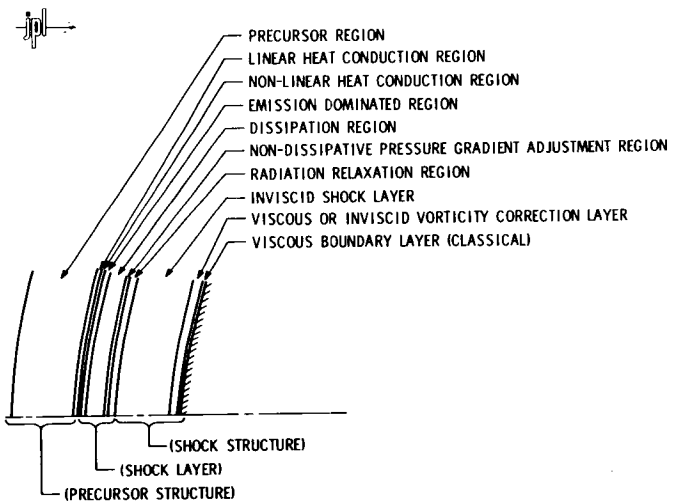

Figure 3.

SUMMARY

- FULL SIMILARITY IS ATTAINED
- A RADIATION RELAXATION REGION IS FOUND
- THE TEMPERATURE IN THE RELAXATION REGION DECREASES BY 16% WHICH RESULTS IN A 50% REDUCTION OF RADIATION HEATING TO THE BODY
- THE ABOVE DECREASES IN TEMPERATURE AND RADIATIVE HEATING ARE CONSISTANT WITH SHOCK TUBE EXPERIMENTS USING A MONATONIC GAS

Figure 4.

Lewis P. Leibowitz*

MEASUREMENTS OF THE STRUCTURE OF AN IONIZING SHOCK WAVE IN A HYDROGEN-HELIUM MIXTURE

While shock structure during ionization relaxation has been a subject of recent research for air, the noble gases, and alkali-metal vapors, the knowledge of hydrogen ionization relaxation is limited. An understanding of shock structure in hydrogen-helium mixtures is needed to determine the importance of non-equilibrium flow during atmospheric entry of probes of the outer planets. The presence of a thick nonequilibrium layer in the entry body flow-field could result in a significant reduction in the estimated radiative heating that the probe must be designed to withstand. In the present study, shock tube measurements and numerical analysis have been performed in order to understand the ionization and thermal processes which govern the shock structure in hydrogen-helium mixtures.

The ionization process of a hydrogen-helium mixture has been studied in an electric arc shock tube (Figs. 1, 2) using hydrogen line and continuum emission measurements. A reaction scheme is proposed which includes hydrogen dissociation and a two-step excitation-ionization mechanism for hydrogen ionization by atom-atom and atom-electron collisions (Figs. 3, 4). Agreement has been achieved between numerical calculations and measurements of emission intensity as a function of time for shock velocities from 13 to 20 km/sec in a 0.208 H_2 - 0.792 He mixture (Figs. 5-7). The electron temperature was found to be significantly different from the heavy particle temperature during much of the ionization process. Similar time-histories for $H\beta$ and continuum emission indicate upper level populations of hydrogen in equilibrium with the electron concentration during the relaxation process. The expression for the rate constant for excitation of hydrogen by atom-atom collisions that best fit the data was

$$k_{AA} = 4.0 \times 10^{-17}\left(\frac{8kT}{\pi\mu}\right)^{1/2} \exp(-10/kT)\ \mathrm{cm}^3\ \mathrm{sec}^{-1}$$

where it has been assumed that the excitation cross section is the same for hydrogen and helium collision partners. The electron-atom excitation rate constant,

$$k_3 = 7.5 \times 10^{-16}\left(\frac{8kT_e}{\pi\mu_e}\right)^{1/2} \exp(-10/kT_e)\ \mathrm{cm}^3\ \mathrm{sec}^{-1}$$

determined from this investigation, was in agreement with recent electron beam cross section measurements.

*Applied Mechanics Division, Aerophysics Section.

EXPERIMENTAL APPARATUS

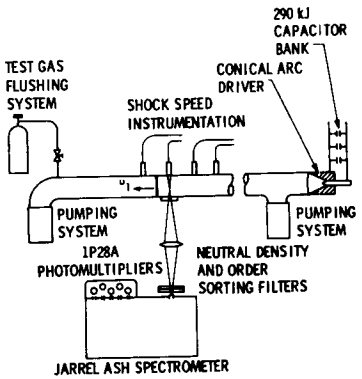

SPECTRAL INTERVALS

SPECIES	λ, nm	Δλ nm
Cr	425.4	0.5
He	447.1	0.5
H_2	462.8	1.0
H	486.1	0.5
$H^+ + e$	514.5	1.0

Figure 1.

EMISSION INTENSITY MEASUREMENT

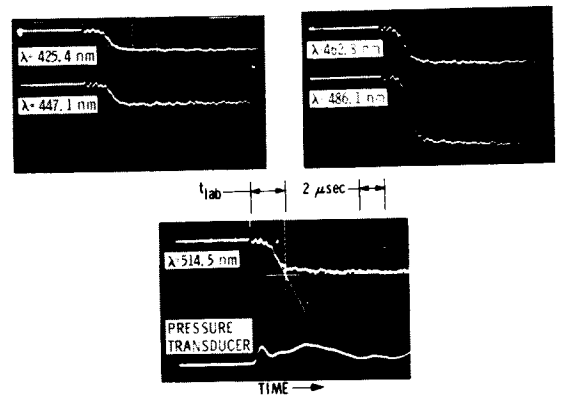

Figure 2.

REACTION MECHANISM

1. $H + e \rightleftharpoons H^+ + e + e$
2. $He + e \rightleftharpoons He^+ + e + e$
3. $H + e \rightleftharpoons H^* + e$
4. $He + e \rightleftharpoons He^* + e$
5. $H + H \rightleftharpoons H^* + H$
6. $H + He \rightleftharpoons H^* + He$
7. $H_2 + He \rightleftharpoons H + H + He$
8. $H_2 + H_2 \rightleftharpoons H + H + H_2$
9. $H_2 + H \rightleftharpoons H + H + H$
10. $H_2 + H^+ \rightleftharpoons H + H + H^+$
11. $H_2 + e \rightleftharpoons H + H + e$

Figure 3.

CALCULATED CONCENTRATIONS AND TEMPERATURES

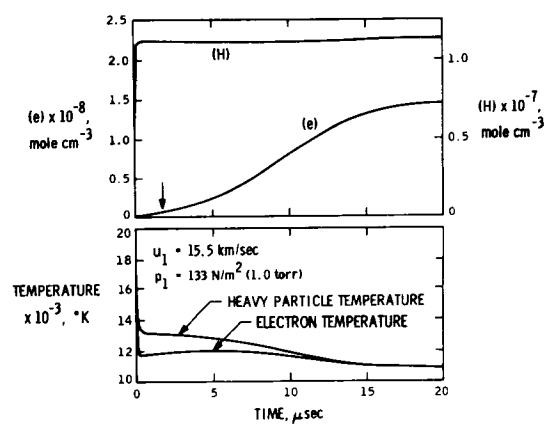

Figure 4.

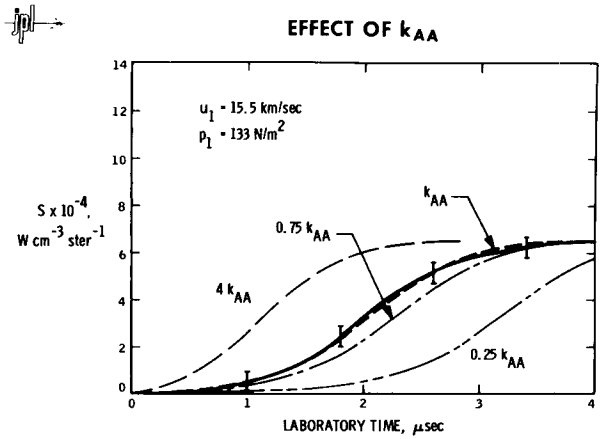

Figure 5.

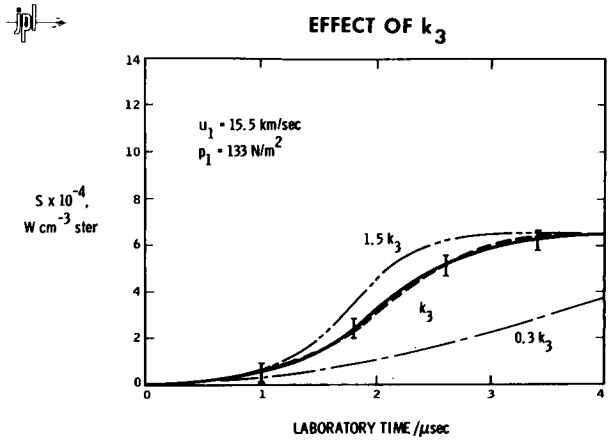

Figure 6.

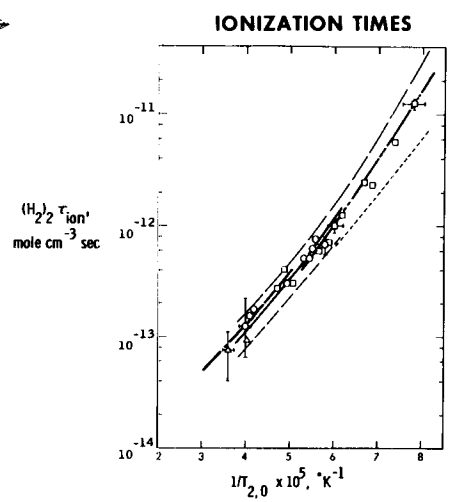

Figure 7.

ENVIRONMENTAL SCIENCE

S. Parthasarathy*

NOISE GENERATING MECHANISMS IN SUPERSONIC JETS

Noise reduction from high-speed flows has become an important environmental problem. An investigation of noise sources in jets will provide a better understanding of noise-generating mechanisms, and it is believed that this will lead to methods of noise control.

Turbulence, which consists of fluctuations of fluid properties such as density, pressure, temperature and velocity, generates sound in a compressible medium. These sound waves propagate outwards with the speed of sound. In turbulence, the fluctuating quantities are related to the complex equations of motion, whereas in sound, they are related to the simple equations of acoustics.

For a given flow, a basic description of the noise field is obtained by measurement of the sound pressure levels in various frequency bands. Equivalently, evaluation of the autocorrelations at various positions will also describe the noise field. Then from plots of the contours of equal sound pressure level in a particular frequency band, the apparent stationary source for that band may be located by following the locus of similar points on the different contours (such as in the direction of maximum noise propagation). From such plots, a given flow will be described in terms of a number of stationary sources located on the jet axis, one for each frequency band. Information about the motion of the sources, their growth and decay, however, are not available from such a description, but can be obtained from cross correlations.

The theory of a correlation method as applied to the evaluation of the autocorrelation function (or intensity and spectrum) of stationary and moving noise sources is presented. The use of this method is illustrated by numerical examples. Also, the application of this method to jet noise is discussed. Stationary sources are considered first, and then the theory is extended to moving sources such as those that occur in jet flows. Both subsonic and supersonic jets are considered.

*Propulsion Division, Research and Advanced Concepts Section

OBJECTIVES

- OBTAIN A CORRELATION BETWEEN THE DENSITY FLUCTUATIONS AND THE INTENSITY AND FREQUENCY SPECTRUM OF THE NOISE RADIATED FROM SUPERSONIC JETS

Figure 1.

NOISE GENERATION

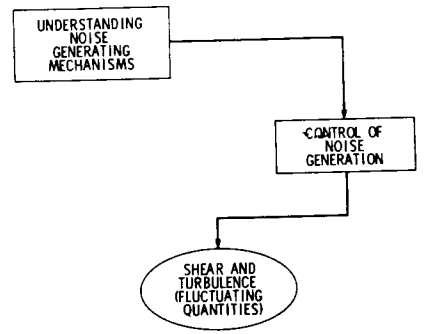

Figure 2.

APPROACH

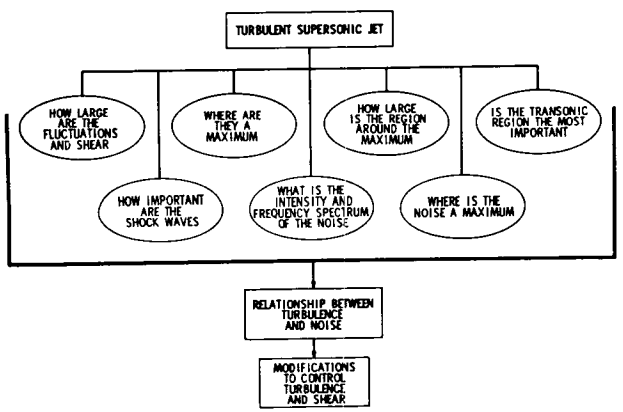

Figure 3.

APPROACH

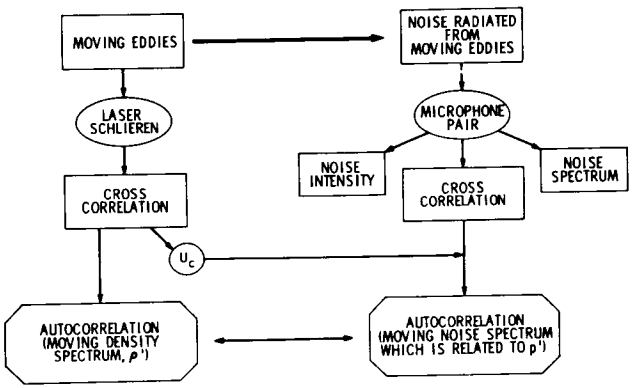

Figure 4.

STATIONARY NOISE SOURCES

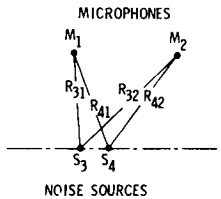

$p(t)$ = FLUCTUATING SOUND PRESSURE PRODUCED BY NOISE SOURCES

$$p_1(t) = \frac{S_3\left(t - \frac{R_{31}}{c}\right)}{R_{31}} + \frac{S_4\left(t - \frac{R_{41}}{c}\right)}{R_{41}}$$

$$p_2(t) = \frac{S_3\left(t - \frac{R_{32}}{c}\right)}{R_{32}} + \frac{S_4\left(t - \frac{R_{42}}{c}\right)}{R_{42}}$$

Figure 5.

CORRELATIONS

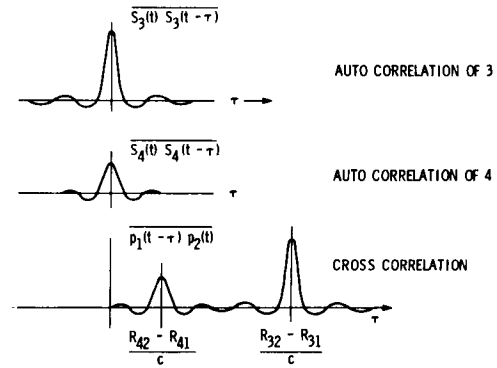

Figure 6.

NOISE SOURCES IN SUBSONIC MOTION

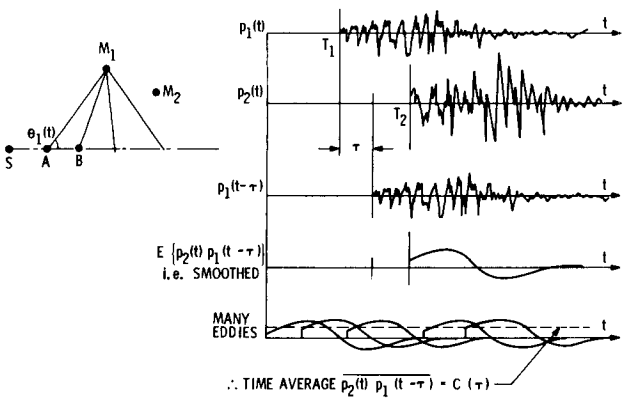

Figure 7.

MOVING SOURCES

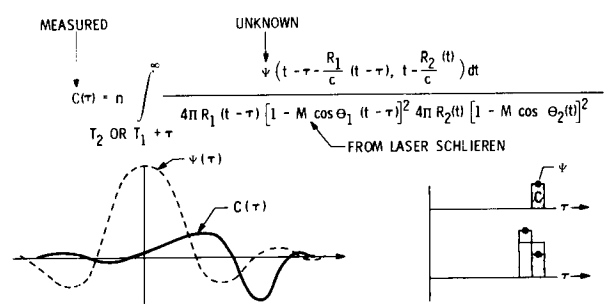

Figure 8.

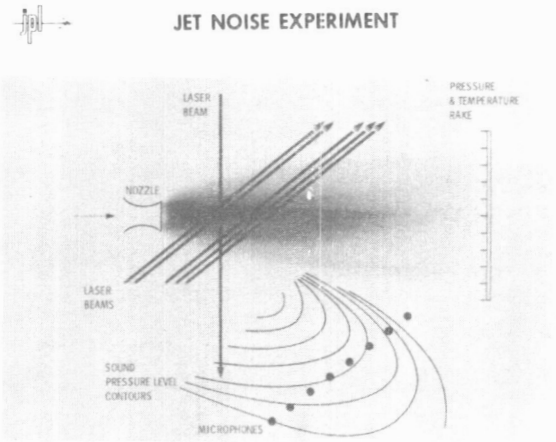

Figure 9.

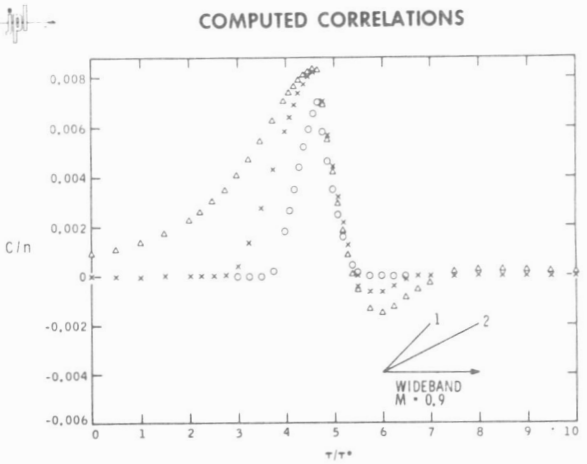

Figure 10.

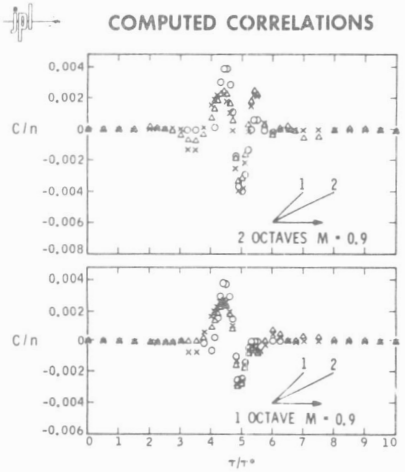

Figure 11.

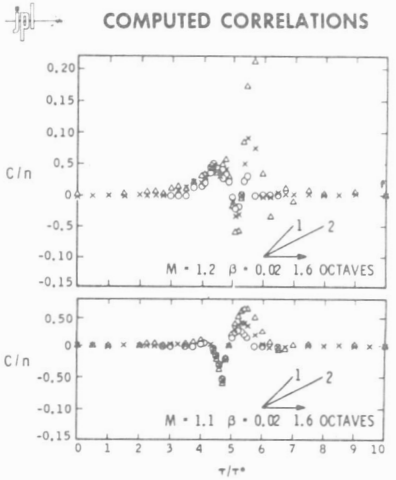

Figure 12.

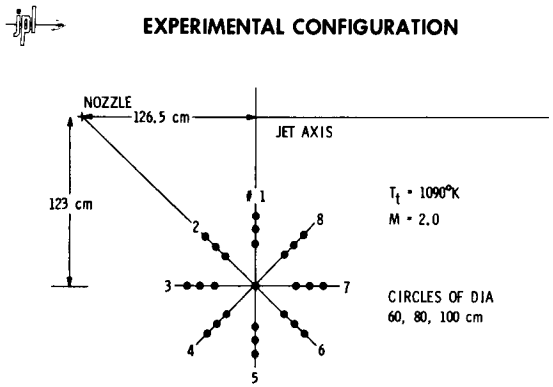

Figure 13.

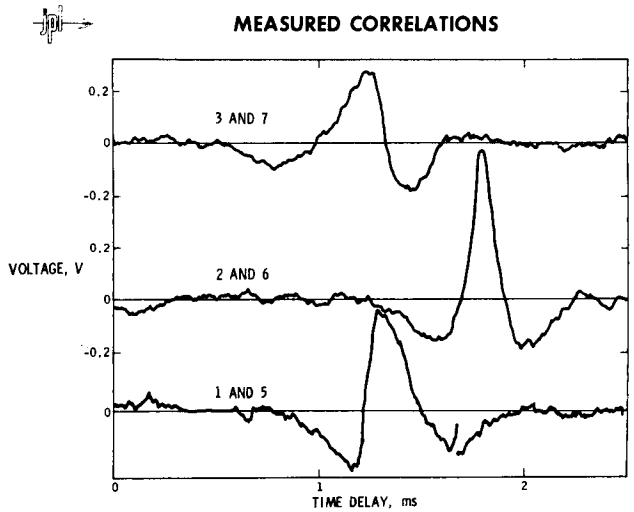

Figure 14.

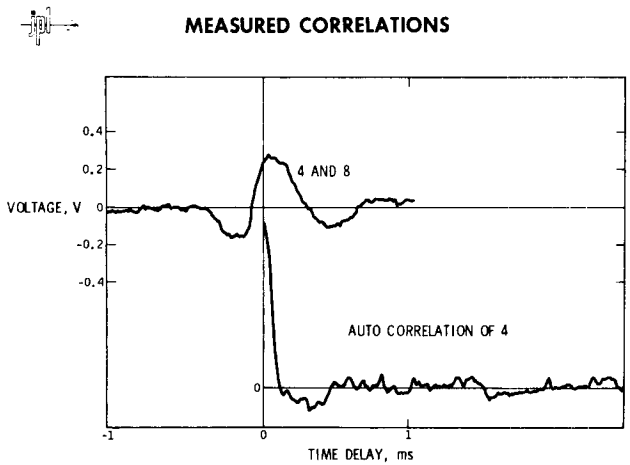

Figure 15.

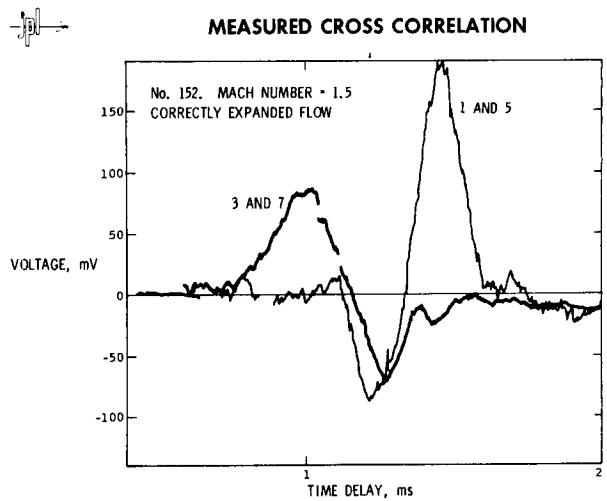

Figure 16.

SUMMARY

- NOISE SOURCES IN SUPERSONIC JETS
- $M \leq 2$
- $T_t \leq 1650°K$ (2500°F)
- SPECTRAL AND GEOMETRIC NOISE INTENSITY DISTRIBUTIONS
- FLUCTUATING DENSITY DISTRIBUTIONS
- CORRELATION BETWEEN DENSITY FLUCTUATIONS AND NOISE INTENSITY
- CONTROL OF NOISE SOURCES

Figure 17.

SENSORS

- FLOW CONDITIONS
  - COLD JET AT ROOM TEMPERATURE
    - SUBSONIC FLOW
    - SUPERSONIC FLOW

Figure 18.

FLOW CONDITIONS

- MACH NUMBER BETWEEN 1 AND 2
- STAGNATION TEMPERATURE UP TO 1650°K (2500°F)
- UNDER, OVER AND CORRECTLY EXPANDED JETS

Figure 19.

SENSORS

- FLUCTUATING QUANTITIES MEASURED

• MICROPHONE PROBE	STATIC PRESSURE	BB&N
• HOT WIRE PROBE	VELOCITY	ULTRASYSTEMS
• PIEZOELECTRIC CRYSTAL PROBE	STAGNATION PRESSURE	GE
• CROSSED LASER BEAMS	DENSITY	JPL

Figure 20.

W. DeMore*

PHOTOCHEMISTRY OF AIR POLLUTION

Mechanisms of $O(^1D)$ Reactions. Studies of the reaction of $O(^1D)$ with methane have been completed and extended to the $O(^1D)$ + ethane reaction. In each case the major primary reaction paths have been identified and detailed mechanisms leading to final product distribution have been formulated.

A technique has been developed for measuring the primary yield ratio of $O(^1D)$ to $O(^3P)$ in a photochemical process. The method is based on the reaction of atomic oxygen with isobutane and involves the measurement of relative peak areas of isomeric alcohols by gas chromatography. This approach is being applied to a problem of ozone photolysis which is pertinent to stratospheric chemistry.

Photolysis of Ozone. Ozone photolysis at wavelengths near 3000 Å is an important source of $O(^1D)$ in the stratosphere. However, there is some uncertainty concerning the relative yields of $O(^1D)$ and $O(^3P)$ in this region because the mechanism of ozone photolysis shows a strong wavelength dependence. We are currently measuring the wavelength dependence of the $O(^1D)/O(^3P)$ ratio using the method described in the preceding paragraph.

Mechanisms of Ozone Chain Decomposition. Photolysis of aqueous solutions of ozone has demonstrated that chain destruction of ozone occurs by the sequence of reactions

$$OH + O_3 \longrightarrow HO_2 + O_2$$

$$HO_2 + O_3 \longrightarrow OH + 2O_2$$

This appears to be the only direct evidence for this mechanism, which has often been proposed in connection with the effect of water on ozone destruction. Our previous work has suggested that such a mechanism cannot be operative in the gas phase. We are presently initiating experiments on the photolysis of gaseous water in the presence of ozone. This work will have application concerning the effect of high-flying aircraft on stratospheric ozone and also the influence of water on the presence of ozone in the Mars atmosphere.

Construction of New Apparatus. A large, all-quartz, temperature-controlled photochemical cell has been constructed and is being used for several of the experiments described in the foregoing paragraphs. This apparatus incorporates a unique optical filtering system developed in this laboratory which permits steady-state experiments using the 1849 Å line from a mercury lamp with no interference from the 2537 Å line.

*Space Sciences Division, Physics Section

MECHANISMS OF $O(^1D)$ REACTIONS

$O(^1D) + CH_4$	$\rightarrow CH_3 + OH$	90%
	$\rightarrow CH_2O + H_2$	10%
$O(^1D) + C_2H_6$	$\rightarrow C_2H_5 + OH$	59%
	$\rightarrow CH_3 + CH_2OH$	27%
	$\rightarrow CH_3CHO + H_2$	3%
	$\rightarrow C_2H_4 + H_2O$	~3%
	$\rightarrow$ OTHER PRODUCTS	8%

Figure 1.

MEASUREMENT OF $O(^1D)/O(^3P)$ RATIO

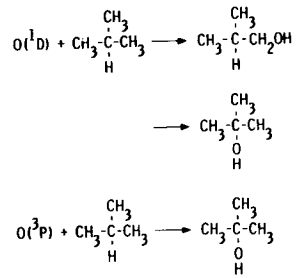

Figure 2.

PHOTOLYSIS OF OZONE

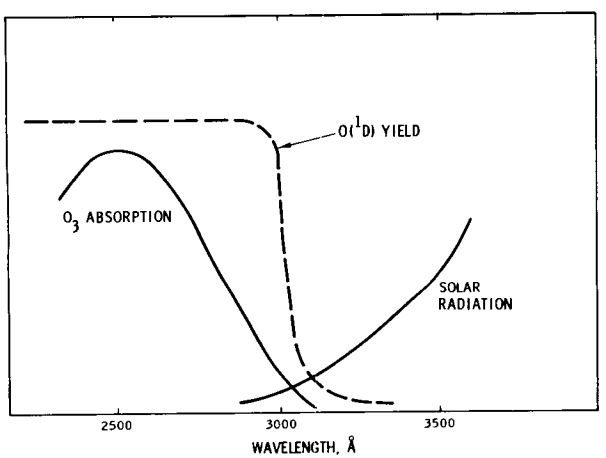

Figure 3.

EFFECT OF WATER ON OZONE

AQUEOUS SOLUTIONS:

$H_2O \xrightarrow{1849A} H + OH$

$H + O_3 \rightarrow OH + O_2$

$OH + O_3 \rightarrow HO_2 + O_2$

$HO_2 + O_3 \rightarrow OH + 2O_2$

GAS PHASE:

$OH^\circ + O_3 \rightarrow H + 2O_2$

$H + O_3 \rightarrow OH^\circ + O_2$

Figure 4.

MATERIALS

Jovan Moacanin*

CROSSLINK DENSITY AS REDUCTION PARAMETER FOR ELASTOMERS

For several years a systematic study of the mechanical properties of both gum and filled elastomers has been carried out at JPL, the goal being to develop a comprehensive theory for their mechanical properties up to and including rupture. From such a theory, test methods and analyses could evolve which on one hand would help engineering design by being able to predict behavior over a wide range of use conditions and on the other would provide guidance to the chemist in selecting the most effective compounds for a particular need.

Previous work showed that for elastomers in uniaxial deformation, a reduced failure surface is generated in stress-strain-time coordinates. Here, cross-link density, ν_e, is used to normalize stress and a factor a_x, which is inversely proportional to a power of ν_e, to reduce the time scale. Experimental studies carried out during the past year showed that the same reduction properties apply to both uniaxial and biaxial deformation. This is an extremely important result. In addition to the obvious practical utility of being able to use uniaxial test data to carry out multiaxial analyses, these results suggest great simplifications in the development of a multiaxial non-linear viscoelastic theory.

Further studies in uniaxial deformation included the effect of the filler on the elastomer behavior. It was observed that the shape of the failure surface plotted in logarithmic coordinates remained unchanged. This proves that the filler contribution is factorable. Because of difficulties in unambiguously determining ν_e in a filled fluorosilicone (the elastomer which was studied), the filler contribution could not be assessed quantitatively.

From an analysis of literature data, however, the functional form of the filler contribution was determined.

Future work will center on a study of SBR elastomer filled with HAF carbon black, because, for this system, test specimens with known ν_e values can be obtained and, hence, from the test data along with the known functional form for the filler contribution, the effect of the filler will be quantified.

*Propulsion Division, Polymer Research Section

RTOP 501-01-10
Viscoelastic Properties of Polymers
RTOP 502-04-45
Solid Propellant Research
Jovan Moacanin

CONCLUSIONS

- UNIAXIAL TEST DATA GENERATE A THREE DIMENSIONAL FAILURE SURFACE IN STRESS-STRAIN-TIME COORDINATES:

$$\sigma_b, \epsilon_b, t_b$$

- A REDUCED SURFACE IS OBTAINED BY INVOKING TIME-TEMPERATURE AND TIME-CROSSLINK DENSITY EQUIVALENCE:

$$\frac{\sigma_b T_0}{\nu_e T}, \epsilon_b, \frac{t_b}{a_T a_X}$$

- THE SURFACE IS INDEPENDENT OF TEST MODE

Figure 1.

BIAXIAL STRESS-STRAIN DATA

- STRIP BIAXIAL DEFORMATION AND THE $W(\lambda_1, \lambda_2, \lambda_3)$ SEPARABILITY POSTULATE GIVE:

$$W_e'(\lambda_1) = \frac{t_1 - t_2}{\lambda_1}$$

- EXTENSION OF UNIAXIAL RESULTS SUGGEST THAT ν_e SHOULD BE NORMALIZING FACTOR FOR BIAXIAL DEFORMATION:

$$\frac{{}^1W_e'(\lambda_1)}{{}^1\nu_e} = \frac{{}^2W_e'(\lambda_1)}{{}^2\nu_e}$$

Figure 2.

NORMALIZATION OF BIAXIAL DATA BY ν_e

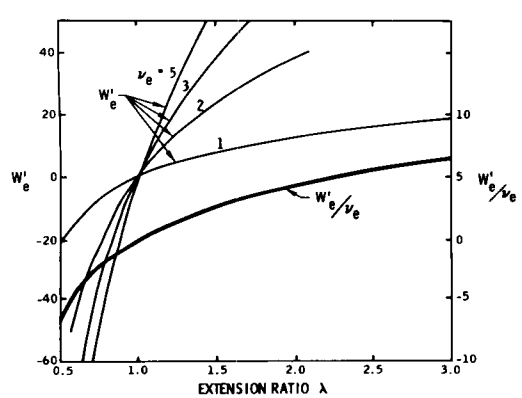

Figure 3.

TIME DEPENDENCE

IF THE STORED ENERGY FUNCTION IS SEPARABLE, THEN EXPECT SAME TIME DEPENDENCE AND SAME TIME REDUCTION PROPERTY FOR ν_e FOR BOTH UNIAXIAL AND BIAXIAL DEFORMATION:

$$t'/a_x' = t''/a_x''$$

WHERE

$$a_x \propto \nu_e^{-m}$$

Figure 4.

UNIAXIAL AND BIAXIAL STRESS RELAXATION

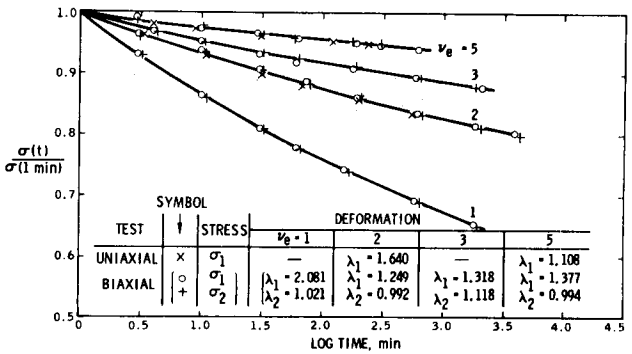

Figure 5.

TIME-CROSSLINKING SHIFT FACTOR FOR SBR AT 26°C

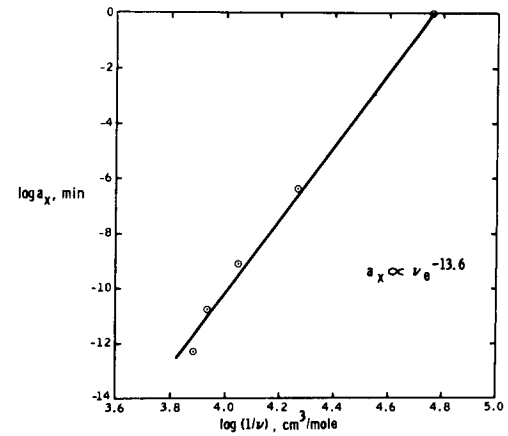

Figure 6.

EFFECT OF FILLER

- FOR UNFILLED ELASTOMER NORMALIZED COORDINATES ARE:

$$\frac{\sigma_b}{\nu_e}\frac{T_o}{T},\ \epsilon_b,\ \text{AND}\ \frac{t_b}{a_T a_x}$$

- FOR FILLED ELASTOMER NORMALIZED COORDINATES MUST BE MODIFIED

$$\nu_e \longrightarrow \nu_e\, h(\phi)$$

$$a_x \longrightarrow a_x a_\phi$$

Figure 7.

FLUOROSILICONE RUBBER FOR VARYING ν_e, ϕ

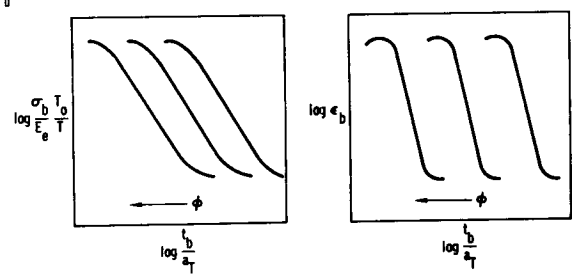

Figure 8.

FUNCTION FOR FILLER CONTRIBUTION TO MODULUS

- FLUOROSILICONE RESULTS DEMONSTRATE FACTORIZABILITY OF FILLER CONTRIBUTION, BUT NEED INDEPENDENT ESTIMATE FOR ν_e TO DETERMINE NUMERICAL VALUES
- A FUNCTION OF THE FOLLOWING FORM FITS ALL THE KNOWN DATA FOR SBR AND CARBON BLACK FILLER

$$h(\phi) = \left(1 + \frac{1.25 \frac{\phi}{\phi_m}}{1 - \frac{\phi}{\phi_m}}\right)^2$$

Figure 9.

MODULUS vs FILLER CONTENT AT CONST. ν_e FOR SBR

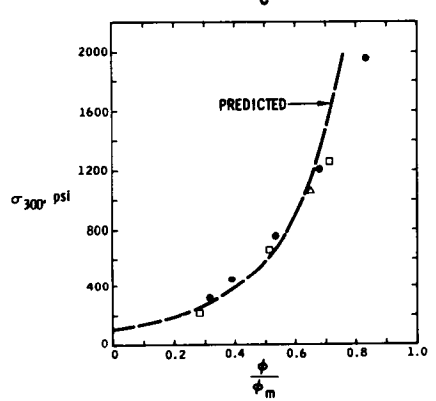

Figure 10.

RELATIVE MODULUS FROM SWELLING FOR NATURAL RUBBER

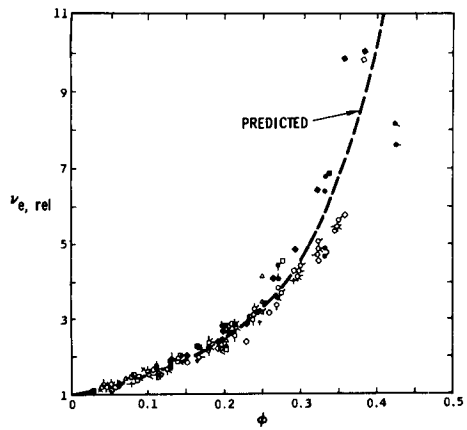

Figure 11.

CONCLUSIONS

- FILLER CONTRIBUTION CAN BE FACTORED OUT
- FORM OF CONTRIBUTION OF FILLER TO MODULUS KNOWN
- TIME SHIFT FACTOR a_ϕ TO BE DETERMINED

Figure 12.

FUTURE WORK

EXPERIMENTS IN PROGRESS ON SBR-HAF CARBON BLACK FORMULATIONS OF KNOWN ν_e AND ϕ LEVELS WILL BE USED TO DETERMINE EFFECT OF FILLER ON TIME SCALE.

Figure 13.

Jovan Moacanin*

VISCOELASTIC BEHAVIOR OF ELASTOMERS UNDERGOING CHEMICAL DEGRADATION

Numerous recent applications require elastomeric materials which can perform for very long times under stringent conditions. For anticipated space missions to outer planets, lifetimes of over ten years are needed. For high-speed aircraft, economics dictate minimum lifetimes of three years under conditions of extreme temperature cycling. Components for artificial hearts will have to withstand 10^9 cycles of stretching or bending over a ten-year period.

A theoretical framework to interpret behavior when both mechanical relaxation and chemical degradation are occurring simultaneously was discussed last year. In this theory, the response of such relaxing-reacting materials is described in terms of parameters which all can be measured from independent experiments. The fundamental postulate underlying this theory is that the viscoelastic behavior at a given time is entirely determined by the crosslink density of the elastomer at the same time. This postulate permits separation of viscoelastic from chemical degradation kinetics parameters.

It became apparent, however, that a very sensitive experimental method was necessary in order to test and further develop the theory. Using temperature as a parameter, for example, is unsatisfactory, because changes in temperature affect both chemical degradation and mechanical relaxation.

The experimental approach which has been developed during the last year is based on the photolysis of the disulfide bond at 2700 Å

$$-S-S- \xrightarrow{UV} -S\cdot + \cdot S-$$

A disulfide containing constituent was used to introduce this linkage into castable polyurethane elastomer formulations. This elastomer can be subjected to any test mode, such as stress relaxation, creep, or constant strain-rate. Chain scission is then induced at will by using pulsed or continuous UV.

Preliminary experiments showed that typically a two minute burst of light may induce a 10% decrease in crosslink density. Such a change can be considered to be "instantaneous" relative to relaxation measurements of a few hours duration. This type of condition will enable a number of experiments to be carried out on quantitative investigations of coupling between scission reactions and mechanical relaxation.

*Propulsion Division, Polymer Research Section

APPROACH

DEVELOP THEORY FROM: KNOWLEDGE OF VISCOELASTIC BEHAVIOR OF STABLE ELASTOMERS AND BEHAVIOR WITH DEGRADATION AT QUASI-EQUILIBRIUM (CHEMORHEOLOGY), AND

POSTULATE THAT FOR GIVEN CROSSLINK DENSITY THERE IS A UNIQUE CREEP CURVE INDEPENDENT OF HISTORY.

Figure 1.

CREEP RESPONSE FOR SINGLE CHANGE IN CROSSLINK DENSITY

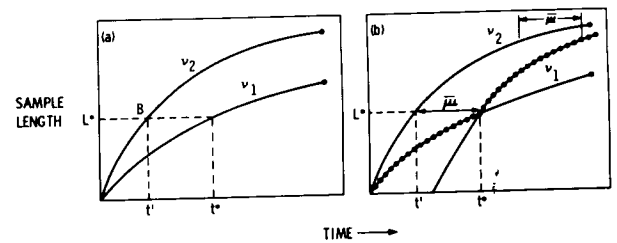

Figure 2.

NEW EXPERIMENTAL APPROACH

- NORMALLY MECHANICAL RELAXATION AND CHEMICAL DEGRADATION OCCUR SIMULTANEOUSLY
- DIFFICULT TO SEPARATE EFFECTS EXPERIMENTALLY
- INTRODUCE PHOTO-LABILE LINKS INTO ELASTOMER NETWORK
- USE PHOTOLYSIS TO INDUCE "AGING" AT WILL WITHOUT AFFECTING OTHER TEST CONDITIONS

Figure 3.

TEST PRINCIPLE

$$-S-S- \xrightarrow{UV} -S\cdot \quad \cdot S-$$

- INCORPORATE DISULFIDE LINKAGE IN CONVENTIONAL POLYURETHANE BINDER FORMULATION
- DURING MECHANICAL RELAXATION EXPERIMENTS, INDUCE CHAIN SCISSION INCREMENTS WITH BURSTS OF UV

Figure 4.

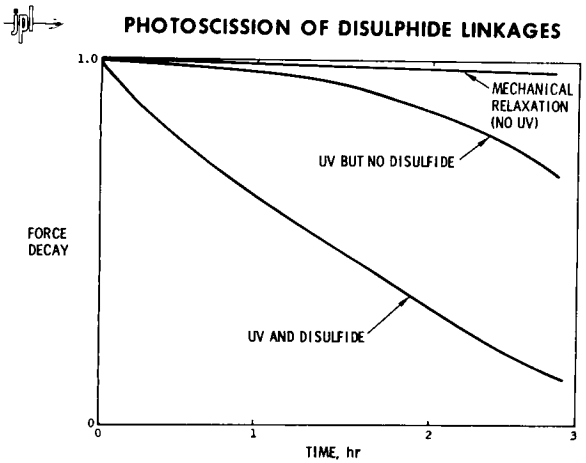

Figure 5.

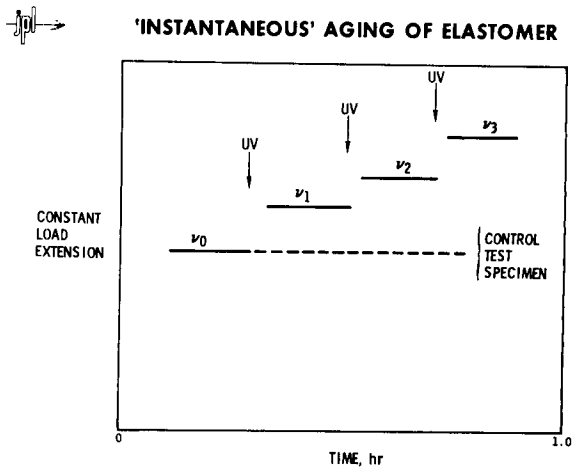

Figure 6.

CONCLUSIONS

SYSTEM DEVELOPED FOR EXPERIMENTAL STUDY OF COUPLING OF AGING REACTIONS WITH MECHANICAL RELAXATION

Figure 7.

FUTURE WORK

- TEST THEORY ON ELASTOMERS WHERE "INSTANTANEOUS" CROSSLINK DENSITY CHANGE CAN BE INDUCED
- GENERALIZE RESULTS TO CONTINUOUS CHANGES
- EXTEND STUDY TO TIME-TO-BREAK

Figure 8.

PROPULSION

J. H. Rupe*

DYNAMICS OF JET IMPINGEMENT

Introduction. The studies of the dynamics of jet impingement, as carried out at JPL, emphasize aspects relevant to liquid rocket injector design. Hence, the problem is couched in terms of the impingement of liquid jets, covering both like-on-like impingement and unlike impingement.

Review. At the Basic Research Review of December, 1971 (JPL Document 701-135) I described a significant extension to the solution for the jet-impingement flow field which was based on the concept of a singly stagnated jet. The essential observation was that the classical identical-jet problem, wherein both jets stagnate, is actually a unique case of the more general situation noted above. The topology of the several possible flow fields are illustrated in Fig. 2.

Some of the consequences of adopting this model can be predicted from a two-dimensional analysis, and these results were presented previously. We also showed a movie of the metastable flow field produced by impingement of identical three-dimensional jets *having uniform velocity profiles.* Hence, there was some preliminary evidence that the concept would be pertinent to three-dimensional systems.

Inferences of Theory. In some of the recent investigations, we have attempted to extend these concepts to three-dimensional sprays in order to clarify some of the anomalies that have plagued our previous work as well as prove the relevance of the two-dimensional results. It seemed particularly important to determine:

(1) the impact of backflow on the consistently low values previously observed for effluent *mass* flow

(2) the degree to which bifurcation modified the expected effluent *mixture* ratio

(3) the existence of the predicted discontinuity for equal stagnation pressure jets

(4) the extent to which a modified weighting factor (based on effluent mass flow in lieu of injected mass flow) used in the determination of the uniformity criterion would improve consistency of observations.

Overall Objective. The objectives are to verify these two-dimensional "predictions" but with a three-dimensional system.

The Global Experiment. The experimental apparatus that was to be replaced with a global experiment is shown schematically in Fig. 3. Although this apparatus has been used successfully for many years and yields a great deal of detailed information about the spray, our interest here was in the gross features of the three-dimensional spray that might be inferred from the theory. Thus the so-called global apparatus shown in Fig. 4 was devised in order to simulate the gross features of the original collector. It can be seen that the injected spray is separated into three regions. The first intercepts the portion normally accounted for by the rotating cross collector ($\alpha = 100^{\circ}$), the second intercepts that portion which would not either be collected or considered as backflow ($100^{\circ} < \alpha < 180^{\circ}$), leaving a third region into which the backflow is injected. A quantitative value for backflow is obtained from the difference between the injected mass flows and the two collected mass flows.

Experimental Results. The results of a series of collections obtained with this appartus are summarized in Fig. 5. It is noted that the ordinate represents the fraction of the injected flow collected in the several regions, while the abscissa represents a spectrum of dynamic pressure ratio obtained with a given total injected flow rate.

It is seen that (1) the effluent flow is indeed dominated by the high stagnation pressure jet, (2) the transition takes place at a stagnation pressure ratio of unity, (3) the region between 100° and 180° exhibits similar characteristics, and (4) the backflow is mainly comprised of fluid from the stagnation jet. Thus the essential features of the two-dimensional prediction are retained in three-dimensional sprays.

This conclusion is also borne out in Fig. 6, where these same data are superimposed on the two-dimensional prediction and clearly show the discontinuity in effluent mass fraction for stagnation pressure unity which occurs when the inflow mass fraction is about 0.55 (for these nonidentical jets).

Summary of Results. It has been shown experimentally that the implications of the two-dimensional theory have been verified.

*Propulsion Division, Liquid Propulsion Section

Although not proven here, it is now intuitively obvious that the jet velocity profiles will affect the backflow, as the low velocity portion of the jet will stagnate prior to penetrating the stagnation region.

Considerations for Injector Design. These results suggest several new constraints on the designer of injectors for liquid propellant rockets. In particular, the following is noted:

(1) From stability considerations, impinging jets, whether unlike or like-on-like, should be designed to operate with unequal stagnation pressures.

(2) From the standpoint of mixture ratio control, the designer should attempt to optimize relative to the *effluent* mixture ratio rather than the injected mixture ratio. This implies that an improved uniformity criterion is now possible.

(3) From the standpoint of heat transfer and compatibility with the injector face, the backspray should, whenever possible, be fuel-rich and, in any event, be controlled to minimize reactions in the vicinity of the face.

DYNAMICS OF JET IMPINGEMENT

- INTRODUCTION
- REVIEW
  - FLOW FIELD TOPOLOGY
- INFERENCES OF 2-DIMENSIONAL THEORY
  - EFFLUENT MASS FLOW ALWAYS LESS THAN TOTAL IN FLOW
    - CONSISTENT WITH PREVIOUS EXPERIENCE
  - EFFLUENT MASS FLOW HIGHEST FOR NON-BIFURCATED JET
    - NOT PREVIOUSLY CHECKED
    - BACKFLOW DOMINATED BY BIFURCATED JET
  - TRANSITION OCCURS AT EQUAL STAGNATION PRESSURES
  - UNIFORMITY CRITERION WEIGHTING FACTORS SHOULD BE MODIFIED
- OBJECTIVE
  - VERIFY 2-DIMENSIONAL CONCEPTS IN 3 DIMENSIONS
- APPROACH
  - A GLOBAL EXPERIMENT IN 3 DIMENSIONS

Figure 1.

2-DIMENSIONAL JET IMPINGEMENT
THE GENERAL CONFIGURATION – NONIDENTICAL JETS

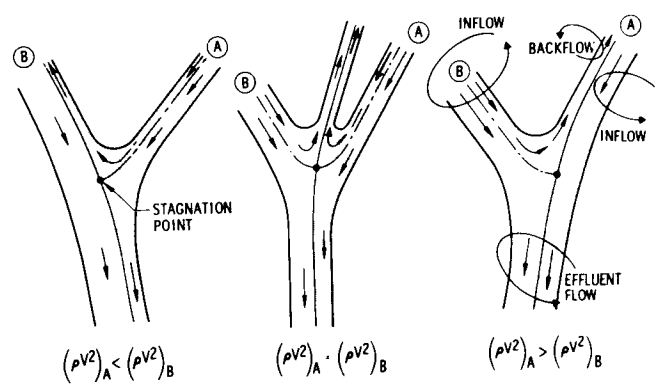

Figure 2.

ROTATING CROSS COLLECTOR

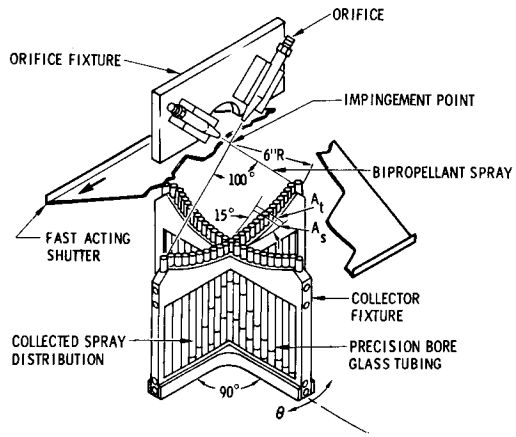

Figure 3.

GLOBAL COLLECTOR

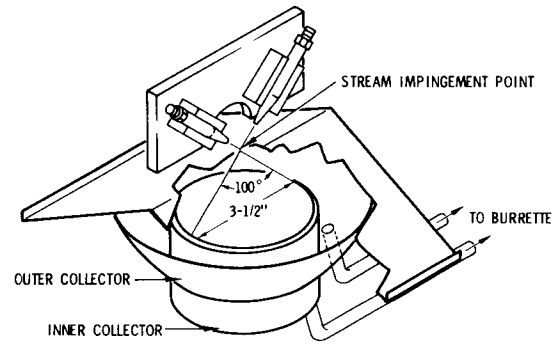

Figure 4.

PERCENT COLLECTED USING THE GLOBAL COLLECTOR

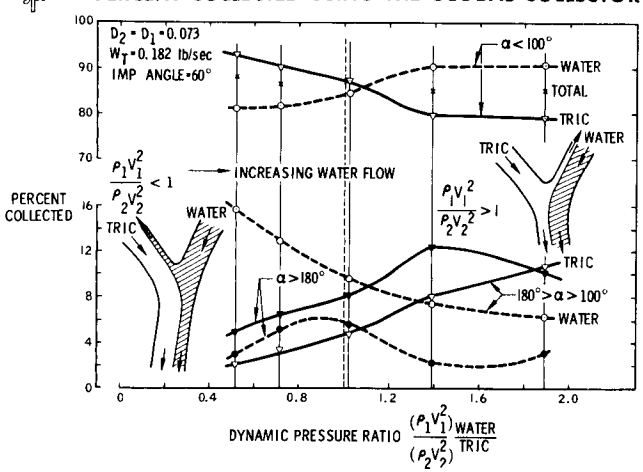

Figure 5.

3-DIMENSIONAL COMPARISON WITH 2-DIMENSIONAL THEORY

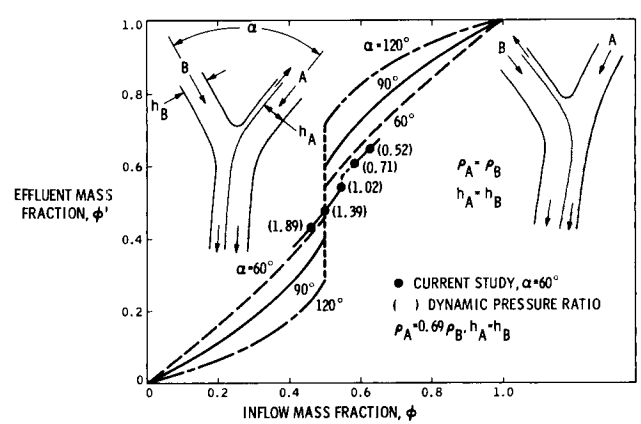

Figure 6.

DYNAMICS OF JET IMPINGEMENT SUMMARY OF RESULTS

- THE IMPLICATIONS OF THE 2-DIMENSIONAL THEORY HAVE BEEN VERIFIED EXPERIMENTALLY
  - ANOMALOUS EFFLUENT FLOWS EXPLAINED
  - LOW EFFLUENT FLOW FOR THE BIFURCATED JET CONFIRMED
  - TOPOLOGICAL TRANSITION OCCURS AT EQUAL STAGNATION PRESSURES
  - ADJUSTMENT OF UNIFORMITY CRITERION WEIGHTING FACTORS WILL IMPROVE CORRELATIONS
- NON-UNIFORM PROFILES PROBABLY IMPACT BIFURCATION. THE INFLUENCE OF THIS JET PROPERTY SHOULD BE ELUCIDATED.

Figure 7.

IMPACT ON INJECTOR DESIGN CONSTRAINTS

- FOR STABILITY

  JETS SHOULD BE NON-IDENTICAL -- i.e. NON-EQUAL STAGNATION PRESSURES
- FOR MIXTURE RATIO CONTROL

  JETS SHOULD SATISFY AN IMPROVED UNIFORMITY CRITERION

  IMPACT OF JET BIFURCATION ON THE MIXING FACTOR CAN BE MINIMIZED
- FOR COMPATIBILITY AND $\dot{q}$ CONTROL

  BACKSPRAY SHOULD BE MINIMIZED AND MIXTURE RATIO BE CONTROLLED

Figure 8.

John Houseman*

MOLECULAR BEAM SAMPLING SYSTEM FOR COMBUSTION CHAMBERS

The prediction of rocket engine performance has been developed to the point where a computer program is now available that takes the properties of the propellant spray into account. The molecular beam sampling system in this project has been developed to measure the mass and mixture ratio distribution of injector elements with highly reactive propellant systems. In addition, the nature and the concentration of the reactive species is detected. These additional measurements will yield the required reaction time for completion of the combustion process.

During the past year, the molecular beam sampling system shown in Fig. 1 was constructed. The system contains an experimental rocket combustion chamber with an unlike doublet injector element. The conventional nozzle has been replaced with a multiple nozzle end plate, containing 29 holes of 0.147-in. dia. Each of the sonic nozzles will be sampled, and, from the gas analysis, the local temperature and flow rate can be calculated. The mass and mixture ratio distribution of a particular injector element can thus be measured, and the Rupe mixing efficiency E_m can be calculated.

The gas sample from a particular nozzle is converted into a molecular beam by expansion through three orifices into three stages of vacuum. The molecular beam reaches velocities above Mach 10 within several sampling orifice diameters, resulting in temperatures below 200°R. The chemical composition thus becomes frozen, as only several hundred collisions take place over the cooling path, whereas chemical reactions require tens of thousands of collisions. A 300 ft^3/min Stokes mechanical pump provides a five torr vacuum in the first stage.

The inner core of the beam passes through a small skimmer orifice (0.020-in. dia.) into the second level of vacuum. The skimmer is designed to prevent shock formation in front of the skimmer orifice. The inner core of the beam finally reaches the ionizer of a quadrupole mass spectrometer in the third stage of vacuum.

Figure 2 shows an expanded view of the equipment before assembly. The rocket engine with the unlike doublet injector is on the left-hand side, while the quadrupole is on the right-hand side of the illustration.

Figure 3 shows the water-cooled heat shield which contains many small holes so that a water spray is formed in front of the shield. The hot exhaust gases from the many small nozzles are thus cooled, except for the nozzle being sampled. A small gap is left between the nozzle and the heat shield tip to provide a controlled leak from the nozzle towards the atmosphere. The nozzle flow rate was measured as a function of gap distance as shown in Fig. 4. The illustration shows the sample nozzle on the left with the heat shield tip on the right. An area ratio of $4\ \delta/D = 1$ is used in operation to insure that the nozzle is subsonic and that the sonic plane is formed on the outer gap annulus, where it does not interfere with the central path of the sample beam.

The results of a hot firing with N_2H_4/N_2O_4 propellants is shown in Fig. 5. The mass spectrometer output signal is plotted on a logarithmic scale versus the mass number. The significant result is that the mass spectrum of the sample shows that nitrogen tetroxide, hydrazine, and ammonia exist simultaneously at the engine centerline sampling spot, as shown by the signals at mass numbers 46, 31, and 17, respectively. Thus, the feasibility of measuring reactive species with the molecular beam system has been demonstrated.

Future work will concentrate on measuring the mass and mixture ratio distribution of unlike doublets, first for the N_2O_4/N_2H_4 system, and then for F_2/N_2H_4 and FLOX/MMH.

*Propulsion Division, Liquid Propulsion Section

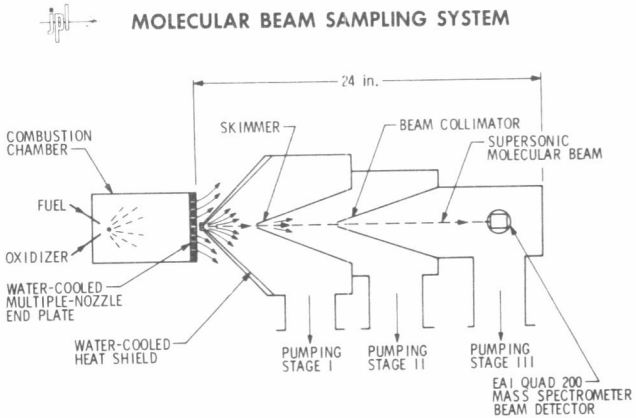

Figure 1.

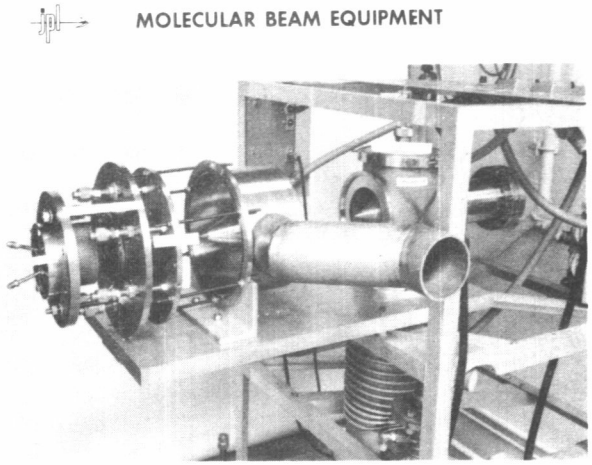

Figure 2.

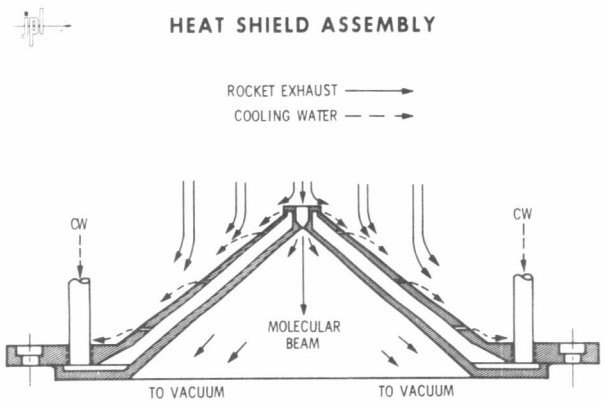

Figure 3.

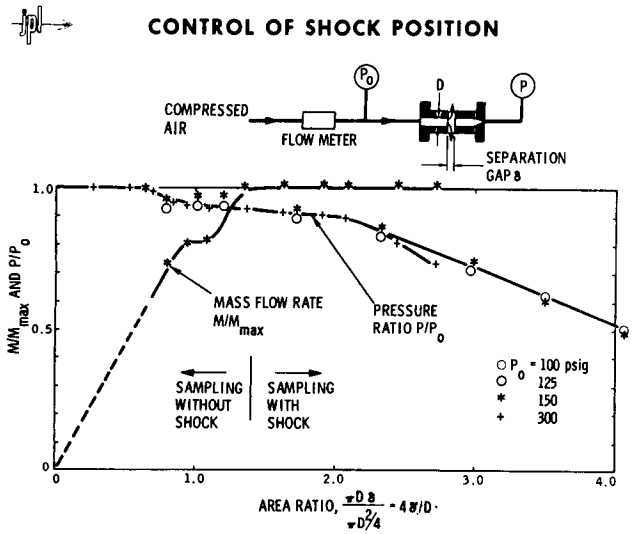

Figure 4.

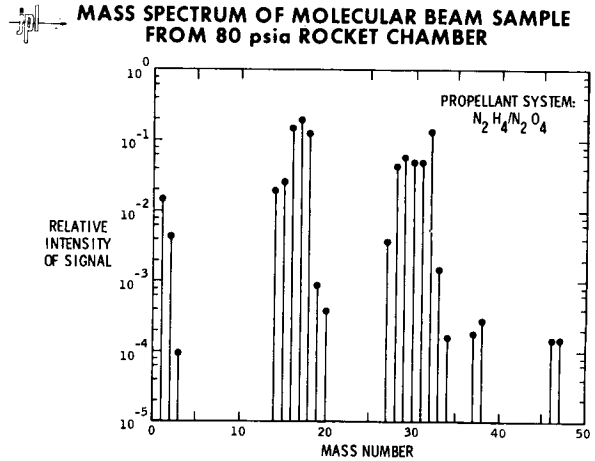

Figure 5.

Lloyd H. Back*

DETONATION PROPULSION

This investigation was motivated by interest in providing propulsion over a wide range of planetary ambient conditions or densities from a near-vacuum to a high density. Of particular interest are the high-density planetary atmospheres (Jupiter, Saturn, and Venus) where conventional propulsion performance would become relatively poor because of the high ambient pressures. For example, a chamber pressure as high as 2000 atm would be required to choke a nozzle operating at an ambient pressure of 1000 atm and, therefore, structural problems would be severe. The detonation propulsion concept utilizes the momentum of the ambient gas set into motion in the nozzle by the products of detonation. It has application to various propulsion devices such as attitude control engines, maneuver engines, and main high thrust engines. The concept involves intermittent detonation of high explosives at the apex of a nozzle and is being developed at JPL through a combined experimental and theoretical investigation. This investigation, which began in FY'72 and will be in progress during FY'73, had not been reported at the last Basic Research Review.

The concept, as currently envisioned, might employ a solid explosive mounted on a rotating wheel with the explosive being fired by an electric detonator or by a laser beam. To avoid problems associated with the intermittent mechanical feeding of a solid explosive, a liquid explosive concept is also being considered. In this concept, advantage is being taken of storing the liquid explosive and sensitizer separately for increased reliability and safety. The two components are then mixed in appropriate proportions and discharged at the apex of a nozzle, where they are detonated by shock waves. The strength of these shock waves must be on the order of about 10,000 atm (a laser beam is guided by fibre optics to a window covered with a metallic film which is exploded by the absorption of the laser pulse). Alternately, a paste or slurry explosive might be used which would offer the ease of position and chemical stability of a solid charge with the ease of management and flexibility of use of a liquid.

Experiments were carried out with nozzles of various shape. "Datasheet" was used as the explosive material. The nozzles were attached to a sled and were fired once, in a vertical position. Measurements were made in the atmosphere or in a tank over a range of ambient pressures from 0.06 to 1000 psia with either nitrogen and/or air as the ambient gas. A movie of the engine firing revealed the plume of the hot, luminous gases exhausted.

The general trend exhibited by the data for the nozzles with relatively small divergence indicates that the mean specific impulse I is relatively constant (being approximately 230 s) at the lower ambient pressures or densities and then it increases at the higher ambient pressures (being about 280 s at 1000 psia). The results indicate that even at relatively low ambient pressures, the performance exceeds that of monopropellant propulsion, e.g., for anhydrous hydrazine (80% ammonia dissociated) the mean specific impulse is 160 s for a sonic nozzle. In the experiments, the performance was less for the nozzles with relatively large divergence. By filling the 10-deg, 6-in.-long nozzle with water, a mean effective specific impulse of about 2100 s was achieved in a firing.

Application of the global conservation principles indicated the importance of the ratio of the mass of ambient gas in the nozzle to the mass of gas generated in the explosion, denoted by σ. In the low ambient density regime, i.e., $\sigma << 1$, the mean specific impulse is independent of the ambient pressure or density, and this is in accordance with the measurements. Also, the influence of the divergence factor λ is in the same direction as indicated by the data. The measured value of I is about 3/4 of the maximum value of 320 s predicted, presumably because not all of the thermal energy is converted into kinetic energy. To place the measurements in perspective with the global considerations, note that for the 10-deg-6 in. nozzle, for example, $\sigma = 1$ at a pressure of 4 atm (59 psia).

The more important situation is in the higher ambient density regime, i.e., $\sigma >> 1$, where the basic dependence $I \propto \sqrt{\rho_a}$ indicates the enhanced performance anticipated at higher ambient pressures or densities. Although the mean specific impulse does begin to increase with ambient pressure, the square root dependence predicts a larger increase than that observed experimentally up to ambient pressures of 1000 psia at which tests have been made so far. For the 10-deg-6 in. nozzle the estimated value of I is 1300 s at 1000 psia. It is felt that the reduced strength of the shock wave that propagates along the nozzle setting the ambient gas into motion with relatively lower speeds at the higher pressure explains the larger overestimate of the actual momentum of the ambient gas in the regime $\sigma >> 1$. Clearly, in order to obtain more definitive information, modeling of the actual flow and wave phenomena is required.

Activities planned for FY'73 include the construction of a demonstration unit for pulsed mode operation and the extension of the analysis of flow and wave phenomena.

*Propulsion Division, Research and Advanced Concepts Section

SCOPE OF INVESTIGATION

- MOTIVATED BY INTEREST IN PROPULSION OVER A WIDE RANGE OF PLANETARY AMBIENT CONDITIONS OR DENSITIES
- PARTICULAR INTEREST IN HIGH DENSITY PLANETARY ATMOSPHERES WHERE CONVENTIONAL PROPULSION BECOMES POOR BECAUSE OF HIGH BACK PRESSURES
- UTILIZES MOMENTUM OF AMBIENT GAS SET INTO MOTION IN NOZZLE BY PRODUCTS OF DETONATION
- APPLICATION TO VARIOUS PROPULSION DEVICES (ATTITUDE CONTROL ENGINES, MANEUVER ENGINES AND MAIN, HIGH THRUST ENGINES)
- CONCEPT BEING DEVELOPED AT JPL - PULSED MODE OPERATION
- COMBINED EXPERIMENTAL AND THEORETICAL INVESTIGATION

Figure 1.

DETONATION PROPULSION CONCEPT

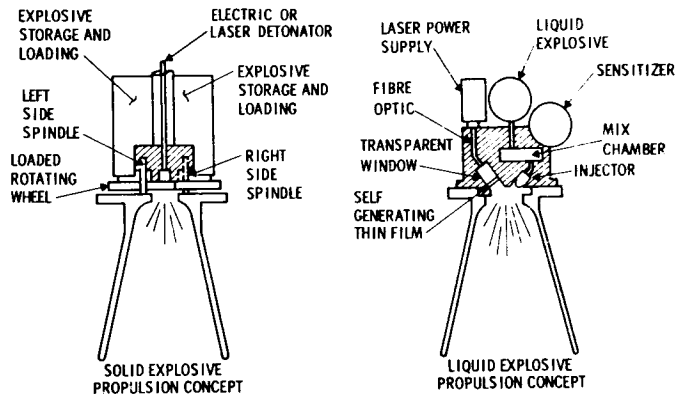

Figure 2.

EXPERIMENTS

- NOZZLES WITH VARIOUS SHAPES:

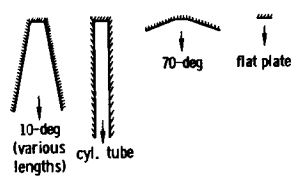

- EXPLOSIVE MATERIAL - DETASHEET - HIGH EXPLOSIVE $\frac{E_\alpha}{m_e} = 1180 \frac{cal}{gm} (2120 \frac{Btu}{lbm})$
- VARIABLE AMBIENT DENSITY OR PRESSURE: P_a: 3 mm Hg (0.058 psia) TO 1000 psia
- AMBIENT GAS - NITROGEN AND/OR AIR, CO_2, ALSO WATER
- MEAN SPECIFIC IMPULSE: $I = \frac{\int F dt}{m_e g_c}$
- SLED-NOZZLE: VERTICAL FIRING

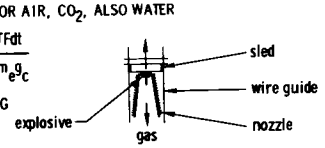

Figure 3.

MOVIE - ENGINE FIRING

- 10 deg NOZZLE - 6 in. LONG
- 1.5 gm "DETASHEET"
- P_a ATMOSPHERIC
- AMBIENT GAS - AIR

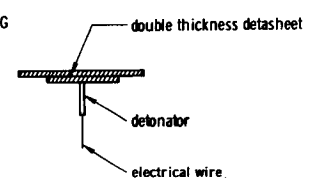

Figure 4.

EXPERIMENTAL RESULTS

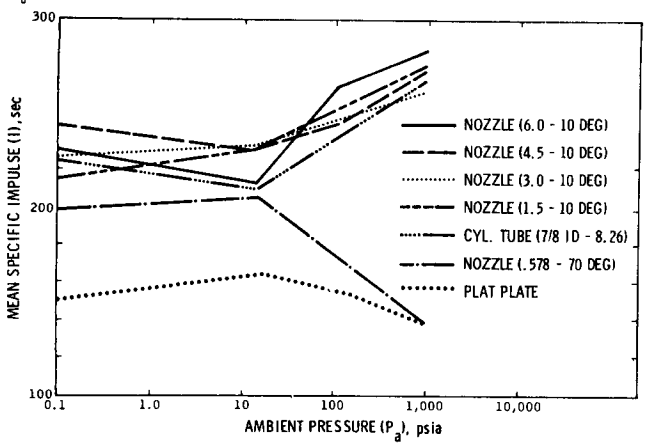

Figure 5.

GLOBAL CONSERVATION PRINCIPLES

- MOMENTUM BALANCE: $\int F dt = \lambda m \bar{u}$

  where $\lambda = \frac{1}{2}(1 + \cos\theta)$ divergence factor

  m = mass of gas in nozzle

  $\bar{u}$ = average velocity

  $\int F dt$ = total impulse

- ENERGY BALANCE: $E_\alpha = m H_t$

  where E_α = explosive energy

  H_t = total enthalpy

- FOR COMPLETE CONVERSION OF TOTAL ENTHALPY INTO KINETIC ENERGY:

$$\bar{u} = \sqrt{2 g_c H_t}$$

Figure 6.

MEAN SPECIFIC IMPULSE AND OPERATIONAL REGIMES

EFFECTIVE MEAN MAXIMUM SPECIFIC IMPULSE:

$$I = \lambda \sqrt{\frac{2}{g_c}} \sqrt{\frac{E_\alpha}{m_e}} \sqrt{\underbrace{\frac{m}{m_e}}_{1+\sigma}}$$

IMPORTANT PARAMETER: $\sigma = \frac{m_a}{m_e}$ (mass of ambient gas in nozzle) / (mass of gas generated in explosion)

REGIMES:

LOW AMBIENT DENSITY: $\sigma \ll 1$, $m \cong m_e$

$$I = \lambda \sqrt{\frac{2}{g_c}} \sqrt{\frac{E_\alpha}{m_e}}$$ independent of ambient density or pressure

$I = \lambda$ (320) sec for detasheet

HIGH AMBIENT DENSITY: $\sigma \gg 1$, $m \cong m_a$

$$I = \lambda \sqrt{\frac{2}{g_c}} \sqrt{\frac{E_\alpha}{m_e}} \sqrt{\underbrace{\frac{m_a}{m_e}}_{\sigma}}$$

BASIC DEPENDENCE FOR A NOZZLE OF GIVEN SHAPE, i.e., $m_a = \rho_a V$

$$I \propto \sqrt{\rho_a}$$

Figure 7.

PLANNED ACTIVITIES

- CONSTRUCTION OF DEMONSTRATION UNIT EMPLOYING LASER INITIATION AND THIXOTROPIC EXPLOSIVE
- CONTINUE ANALYTICAL INVESTIGATION OF FLOW AND WAVE PHENOMENA INCLUDING INTERACTION WITH THE STRUCTURE

Figure 8.

R. N. Kumar*

SOLID PROPELLANT COMBUSTION MODELING

This program is aimed at obtaining a better understanding of the time-independent and oscillatory combustion of AP**/composite propellants; analytical and experimental investigations are undertaken.

The aim of the analytical work is a coherent interpretation of diverse experimental data with a few unifying concepts. It is hypothesized that the overall rate-controlling reactions are more likely to be in the low-temperature condensed phase than in the high-temperature vapor phase. As a variety of propellants use the same oxidizer (AP), and as the fuels used (polymers) are similar, the basic condensed phase degradation reactions are common to all such propellants. The vapor-phase chemical reaction rates are hypothesized to be controlled by the molecular mixing rates of fuel and oxidizer vapors. In comparison with experimental data, the analyses realistically predict AP/propellant static and dynamic burning characteristics, including a few that have remained inconsistent with previous theories.

Two separate experimental programs are undertaken. One of them is concerned with measuring the rates of growth and decay of acoustic waves in a device widely known as the T-burner. The current experiments have indicated the strong influence of convection on oscillatory burning. The limiting amplitude of pressure fluctuations can vary by more than a factor of three, depending on whether the velocity fluctuations are either parallel to or normal to the burning surface. Also, rich harmonics have been observed in the pressure - time traces when the burning area of the propellant far exceeds the burner cross-sectional area. The harmonic content and the limiting amplitude are found to be affected by the initial wall temperature, revealing the important role of heat transfer to the inert walls.

The other experimental program is concerned with the effects of propellant compositional variables on oscillatory combustion behavior. Four propellants are formulated with different particle sizes of the oxidizer, keeping all other variables identical. The propellants are fired in a simple device called the L-star burner, where the bulk mode instability is readily excited. Stability maps are obtained with a very economical firing program. For each of the propellants, a certain mean pressure has been found (in numerical agreement with theoretical considerations) above which no bulk-mode oscillations are observed. Color movies have shown the non-simple physical processes in the chamber during some of the instability modes. In a subprogram with two propellants of widely different mechanical properties, with practically identical chemical compositions, the oscillatory combustion characteristics are found to be essentially identical.

The following are the principal results of the work to date:

(1) a coherent theory for the time-independent and oscillatory combustion of AP/composite propellants

(2) data from laboratory scale burner experiments for the interpretation of actual rocket motor instability; importance of convective flux and heat loss to the inert walls in T-burners

(3) accurate stability maps for propellants with systematically designed heterogeneity

(4) graphic display, through moving pictures, of the non-simple processes during bulk mode instability.

The research work is continuing in all of these areas.

*Research Fellow in Jet Propulsion, California Institute of Technology.
**Ammonium perchlorate.

SCOPE OF RESEARCH

- MODELING OF AP/COMPOSITE PROPELLANT COMBUSTION
  - AIM: INTERPRET APPARENTLY DIVERSE EXPERIMENTAL DATA
- T-BURNER EXPERIMENTS WITH JPL T-17 PROPELLANT
  - AIM: INTERPRET BROWNLEE'S RESEARCH IN LIGHT OF NON-ISENTROPIC PRESSURE COUPLING
- L-STAR BURNER EXPERIMENTS
  - AIM: STUDY PROPELLANT COMPOSITIONAL VARIABLES AS THEY INFLUENCE OSCILLATORY BEHAVIOR AT LOW CHAMBER PRESSURES

Figure 1.

COMBUSTION MODELING

- AIM: A SIMPLE MODEL SHOULD EXPLAIN:
  - AP PYROLYSIS DATA
  - AP DEFLAGRATION DATA
  - PROPELLANT STEADY COMBUSTION CHARACTERISTICS
  - PROPELLANT OSCILLATORY COMBUSTION CHARACTERISTICS

Figure 2.

FUNDAMENTAL HYPOTHESES

- OVERALL RATE CONTROL BY CONDENSED PHASE REACTIONS
- VAPOR PHASE MIXING RATE LESS THAN VAPOR PHASE KINETIC RATES

Figure 3.

ANALYTICAL RESULTS

- REQUIRE:
  - THERMOPHYSICAL CONSTANTS, k, c, MP, . . . | GENERALLY AVAILABLE
  - KINETIC DEGRADATION RATES, $B \cdot \exp(-E/RT)$ | GENERALLY AVAILABLE
  - GAS-PHASE DIFFUSIVE-MIXING RATES | THEORIES INADEQUATE; EXPERIMENTS MAY BE NEEDED

AND PREDICT TYPICALLY:

Figure 4.

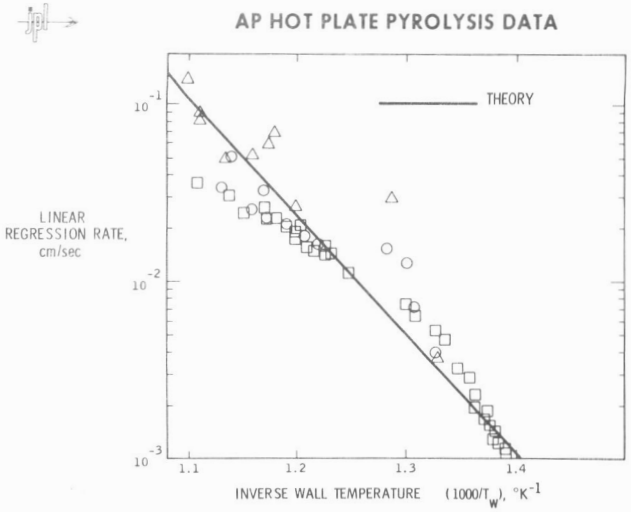

Figure 5.

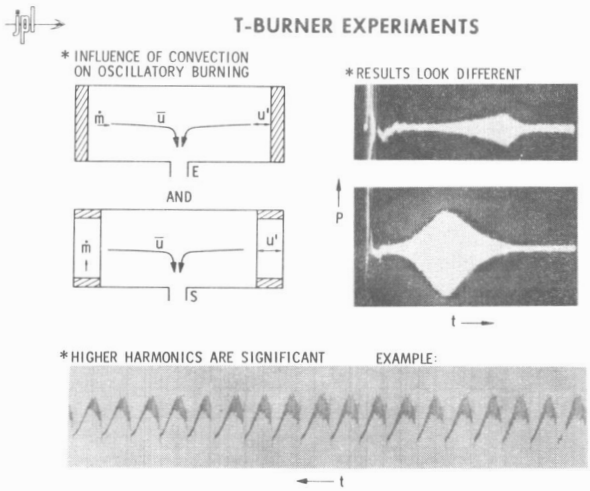

Figure 6.

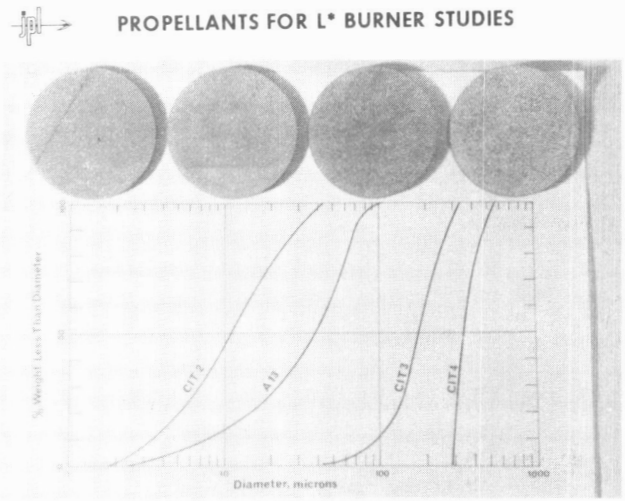

Figure 7.

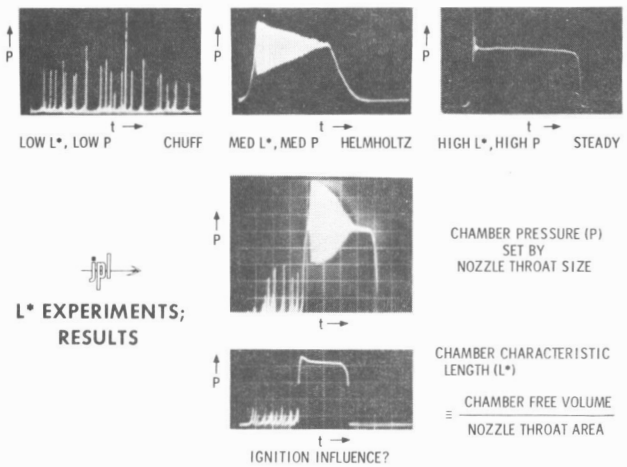

Figure 8.

THE L* BURNER

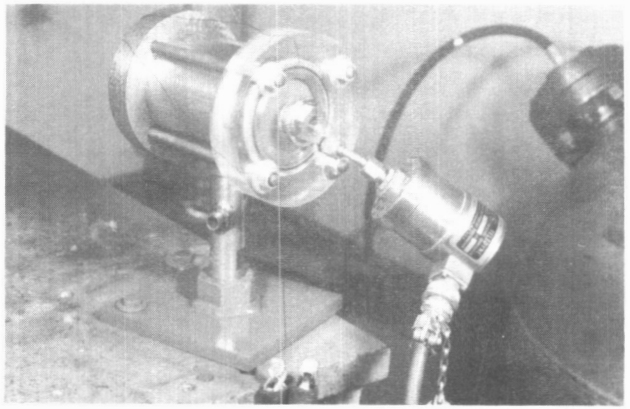

Figure 9.

TYPICAL STABILITY MAP

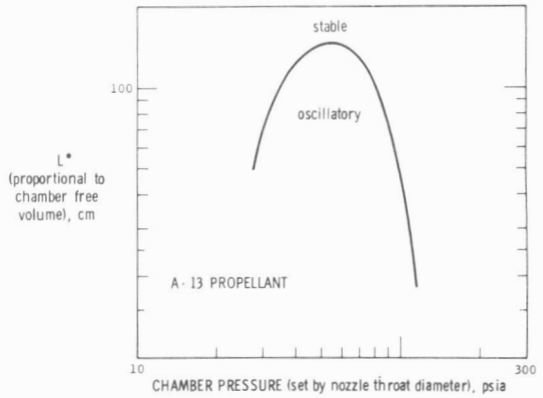

Figure 10.

SIGNIFICANCE OF RESEARCH

- UNIFIED THEORY
- T-BURNER EXPERIMENTS
  - DATA FOR INTERPRETATION OF ROCKET FIRINGS
  - IMPORTANCE OF CONVECTION
  - IMPORTANCE OF HEAT LOSS
- L-STAR BURNER EXPERIMENTS
  - CONDENSED PHASE DETAILS
  - STABILITY MAPS
  - GRAPHIC VISUALIZATION

Figure 11.

NETWORK POLYMER FORMATION

H. E. Marsh, Jr.*

General Models. This work deals with network polymers that are generated by the reactions between polyfunctional molecules (see Fig. 2). Whereas, as described in the previous review, expressions for gelation derived from two different theories were equivalent for simple (3/2) trifunctional systems, this was not the case for complex (3/3) systems. The latter class is illustrated in Fig. 3 as having branch units of both chemical polarities. Agreement between the two models was achieved by adoption in one of them of a more specific rule for one of the probability steps in the derivation. (See Figs. 5 and 6.) Further theoretical studies are being made to interpret the lack of correlation in (3/3) systems between experiment and theory.

Applications. The critical degree of branching, α_c, which is based on composition (see Fig. 4), and the corresponding physical state of incipient gelation are valuable in theoretical studies. However, because polymers in this state are almost liquids, α_c is of little use in formulating more highly cured elastomers. The number of effective chains, ν_e, referred to by Moacanin in his paper in this document entitled "Crosslink Density as a Reduction Parameter for Elastomers," would be useful if it could be calculated from composition. A method was developed, based on the gelation relationships being discussed here, for predicting the number of effective chains from composition and extent of cure. This method starts with counting the relative number of four different kinds of branching units after reactions have occurred, as shown in Fig. 9. Evidence for the correctness of this approach is found in the equivalence of the expression for sol-gel ratio, an intermediate parameter, with that given by Flory (J. Amer. Chem. Soc. *63*, 3083 [1941]).

Another problem encountered in the formulating of liquid elastomers arises as special kinds of non-ideality specific to each chemical curing system. For example, urethane systems have, in addition to the main (A+B) reaction, a side reaction not permitted in ideal models. As can be seen in Fig. 10, this side reaction results in the formation of branch units additional to those introduced as trifunctional molecules. Furthermore, the number of extra branch units depends on the number of urethane links previously formed. A new expression describing a model which accounts for the side reaction and the consequent branch units has been derived.

Combination of the new urethane model with the method for predicting the number of effective chains appears to have promise for formulating liquid urethane elastomers. A preliminary test of the combined model with the data of four distinct solid propellant formulations shows good correlation between estimated effective chains and tensile strength. (See Fig. 11.) Of particular interest is prediction of high tensile strength produced by side-reaction-generated branch units in the case in which a low molecular weight prepolymer was used without the usual addition of a trifunctional ingredient.

Work will continue in both areas discussed in this review. With regard to the lack of agreement between model and experiment for complex (3/3) systems, efforts will be concentrated on finding reasonable perturbations of the model that can account for the deviation. The combined urethane/effective chain model will be tested against available data of a large variety of solid propellant formulations. Pending success of such testing, the model will be used to design experiments the purpose of which will be the comparison of the relative qualities of new prepolymers on a basis of equivalent network structure.

*Propulsion Division, Solid Propellant Engineering Section.

MODEL FOR FLORY-TYPE DERIVATION

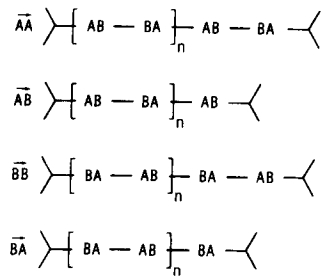

$$\alpha = \alpha_{AA} + \alpha_{AB} + \alpha_{BB} + \alpha_{BA}$$

Figure 5.

A GENERAL RELATIONSHIP FOR (3,2,1/3,2,1) SYSTEMS

WHERE $1/(1+Q)$ & $Q/(1+Q)$ REPRESENT RELATIVE CONCENTRATIONS OF A & B BRANCH UNITS

$$\alpha = \frac{\frac{1}{1+Q}\left(P_A P_B \sigma_B \rho_A + P_A \rho_B\right) + \frac{Q}{1+Q}\left(P_A P_B \sigma_A \rho_B + P_B \rho_A\right)}{1 - P_A P_B \sigma_A \sigma_B}$$

Q (BASED ON TOTAL COMPOSITION) $= r\rho_B/\rho_A$

Q(BASED ON NETWORK COMPOSITION)

$$= \frac{1}{2}\left\{\sigma_A \rho_B/\rho_A - \sigma_B + \left[(\sigma_B - \sigma_A \rho_B/\rho_A)^2 + 4r\rho_B/\rho_A\right]^{1/2}\right.$$

THE LATTER IS CORRECT

Figure 6.

A POSSIBLE CAUSE OF NON-AGREEMENT BETWEEN THEORY AND EXPERIMENT IN (3/3) SYSTEMS

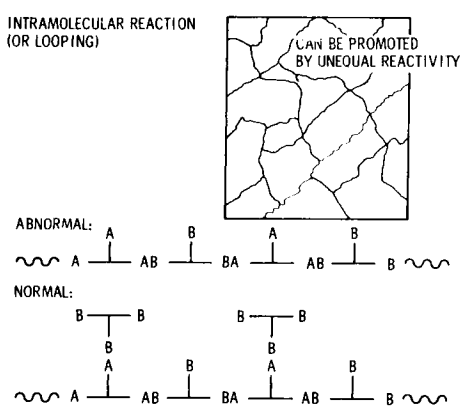

Figure 7.

A POTENTIALLY USEFUL MODEL OF URETHANE SOLID PROPELLANT BINDERS

I. DETERMINE NUMBER OF EFFECTIVE CHAINS, ν_e

II. ACCOUNT FOR SIDE REACTION

Figure 8.

J. Moacanin*

FINITE DEFORMATION THEORY

Propulsion requirements for spacecraft applications on projected missions where solid propellant motors are candidates for use will make severe demands on the state of the art of current technology because of the duration and complexity of anticipated duty cycles. The ability to predict the mechanical behavior of solid propellant grains is predicated on the best understanding of material characterization, grain stress analysis, and proven failure criteria.

Sufficiently accurate experiments in multiaxial (even biaxial) deformation are exceedingly difficult to perform. Therefore, much effort has been expended at JPL to learn to what extent uniaxial experiments can yield the necessary material property parameters. Uniaxial tests are much simpler to carry out, and the results are more accurate.

During last year, a formulation was developed which allows the determination of the isothermal stored energy function for incompressible rubber-like materials from simple uniaxial extension data. The approach was based on the previously postulated separability property for the configurational entropy of an elastomer. Now, these results have been generalized to the non-isothermal case. By postulating entropy separability:

$$S(\lambda_1,\lambda_2,\lambda_3,T) = s(\lambda_1,T) + S(\lambda_2,T) + s(\lambda_3 T) \tag{1}$$

where λ_1, λ_2, and λ_3 are the stretch ratios in the x, y, and z directions, respectively, one derives a thermal-elastic free energy function. For a simple relationship between the stress-temperature coefficient and λ, which was found to hold for natural rubber, the following approximate free energy function is obtained:

$$F = TK \sum_{i=1}^{3} \lambda_i (\ell n \lambda_i - 1) \tag{2}$$

which for isothermal conditions reduces to the Valanis-Landel approximate isothermal stored energy function:

$$F = W(\lambda_1,\lambda_2,\lambda_3) = 2\mu \sum_{i=1}^{3} \lambda_i(\ell n \lambda_i - 1) \tag{3}$$

where μ is the shear modulus.

Using the new formulism along with literature data on natural rubber, it was demonstrated that uniaxial tension-temperature measurements can be used to calculate μ. To unequivocally demonstrate the separability for the non-isothermal case, it is planned to carry out biaxial tension-temperature experiments.

Separate biaxial experiments on non-crosslinked polymers are in progress. These studies will provide information on viscous, i.e., irreversible, processes involved in long-chain deformation, and will be necessary in considerations of time-dependent effects.

*Propulsion Division, Polymer Research Section

SUMMARY OF RESULTS

- THERMAL ELASTIC FREE ENERGY FUNCTION DERIVED
- APPROXIMATE FUNCTION (i.e., FOR $h(\lambda) = k\ln\lambda$) FOR ISOTHERMAL CONDITION REDUCES TO VALANIS-LANDEL APPROXIMATE ISOTHERMAL STORED ENERGY FUNCTION
- NATURAL RUBBER SHEAR MODULUS CALCULATED FROM STRESS-STRAIN AND STRESS-TEMPERATURE COEFFICIENT EXPERIMENTS SHOW GOOD AGREEMENT (3.7 vs 3.9 kg/cm^2); HENCE, CAN CALCULATE ISOTHERMAL FUNCTION FROM EITHER DATA

Figure 5.

BIAXIAL DATA

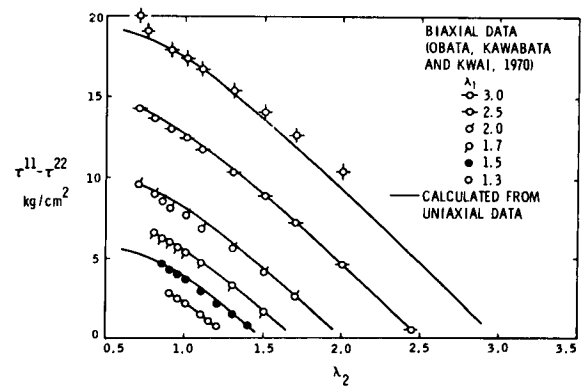

Figure 6.

CONCLUSIONS

- NON-ISOTHERMAL FREE ENERGY FUNCTION CAN BE CALCULATED FROM UNIAXIAL TENSION-TEMPERATURE DATA AS FUNCTION OF STRETCH RATIO
- CONSISTENCY OF APPROACH DEMONSTRATED FOR BIAXIAL ISOTHERMAL EXPERIMENTS
- TO GET PROOF FOR BIAXIAL NON-ISOTHERMAL CONDITIONS NEED BIAXIAL STRESS-TEMPERATURE EXPERIMENTS

Figure 7.

FUTURE WORK

- BIAXIAL EXPERIMENTS UNDER NON-ISOTHERMAL CONDITIONS
- BIAXIAL EXPERIMENTS ON NON-CROSSLINKED POLYMERS

Figure 8.

POWER

R. J. Stirn*

SOLAR CELL RESEARCH

Because solar cell performance at low temperatures and low light intensities, such as first experienced beyond the orbit of Mars, is critically dependent on the cell p/n junction characteristics, an investigation of the junction properties of silicon solar cells has been undertaken. In last year's presentation (JPL Document 701-135), preliminary results of the measured diffusion and recombination current components obtained from dark forward current-voltage curves were given as measured on small area mesas of the cell over a range of temperatures. Also discussed were the ubiquitous current shunts, which were shown to be highly localized.

The effect of current shunting and of the recombination current component on the light current-voltage characteristics was calculated for Jupiter-type conditions and is shown in Fig. 1. It is seen that recombination (increasing I_{02}, the reverse saturation current due to recombination in the space-charge region of the junction) drastically lowers the voltage output of the cell (V_{mp}) without much affecting the current, while shunting (R_{sh}) affects both voltage and current, although not open-circuit voltage (V_{oc}). The effect of R_{sh} on V_{mp} and cell efficiency η is shown in Fig. 2, and that of I_{02} on the same two quantities as well as V_{oc} is shown in Fig. 3. The latter figure also indicates typical experimental values of V_{mp}, V_{oc}, and η as well as the expected improved values if shunting were eliminated, and if I_{02} for an entire 2-x-2-cm cell were equal to that measured over most areas of the cell on etched mesas. In this case (Jupiter environment), the cell efficiency can be increased by 50%.

The variability of I_{02} across the 2 x 2 cm solar cell is consistent with scanning electron microscope pictures which show a variable current collection from the diffused region (Fig. 4) – probably due to precipitates. A surface picture (Fig. 5) shows no external cause to explain the patchy effect.

To determine at what temperatures and voltages either diffusion or recombination current dominates, Figs. 6 and 7 were drawn using measured values. When either one dominates, closed expressions for calculating V_{oc} and V_{mp} exist. However, we see that for V_{mp} most experimental points are in neither area. (The lowest temperature points are limited by shunting.) The experimental V_{oc} points deviate from the predicted curve using I_{01} and the band gap temperature dependence. This is because the I_{02} value is larger when averaged over an entire 2 x 2 cm cell, effectively moving the hatched area to the upper right.

Further work in FY'73 will investigate the I_{02} term using low-energy proton radiation damage. Such work will also allow a determination of solar cell radiation degradation caused the junction alone. Contracts to the University of Pennsylvania and to MIT have been let to aid in the irradiation and in measurements.

A contract to the University of Arizona has been let to investigate the feasibility of replacing the diffused p/n junction in silicon with a field-induced inversion layer p/n junction (Fig. 8). If successful, collection efficiencies should be improved at shorter wavelengths where the light absorption is high.

*Guidance and Control Division, Guidance and Control Systems and Research Section

CALCULATED LIGHT I-V CHARACTERISTICS

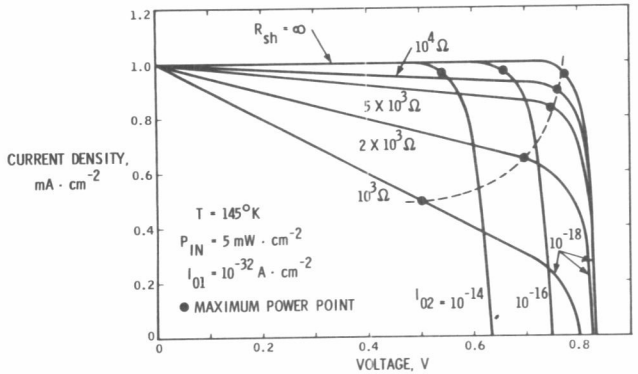

Figure 1.

EFFECT OF SHUNT RESISTANCE

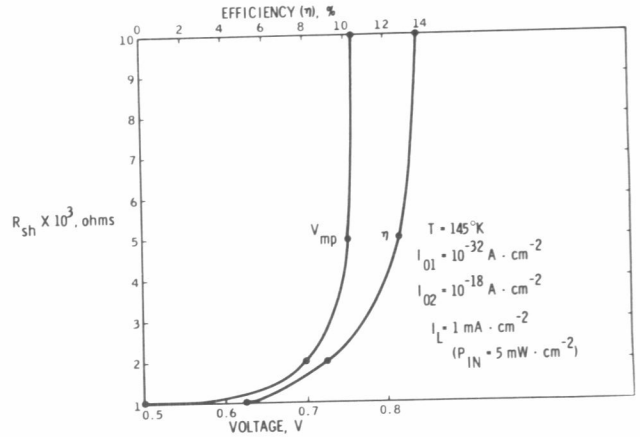

Figure 2.

EFFECT OF RECOMBINATION CURRENT

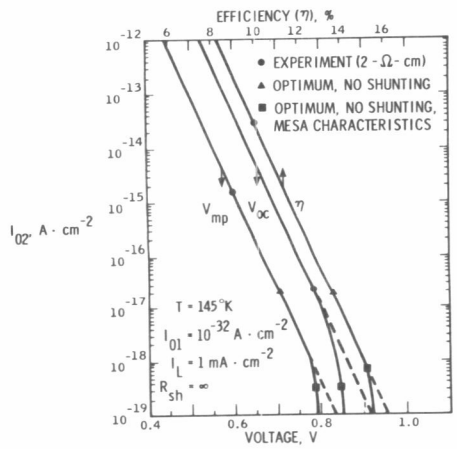

Figure 3.

SEM MONTAGE (SECONDARY ELECTRONS)

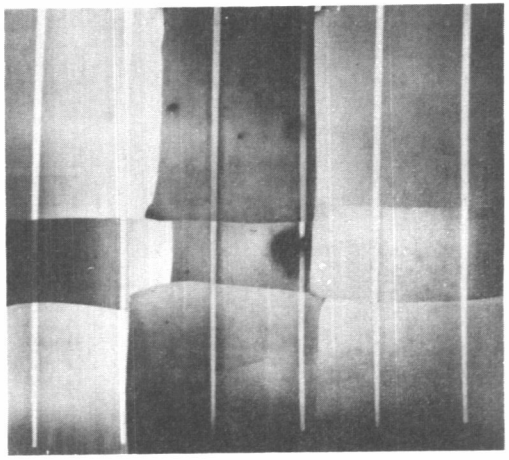

Figure 4.

SEM MONTAGE (INDUCED CONDUCTIVITY)

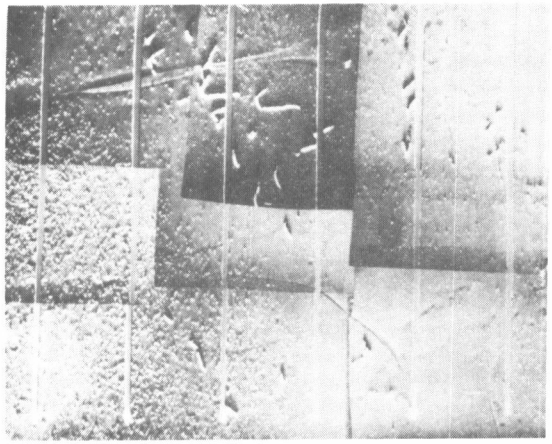

Figure 5.

RATIO OF MEASURED JUNCTION CURRENTS

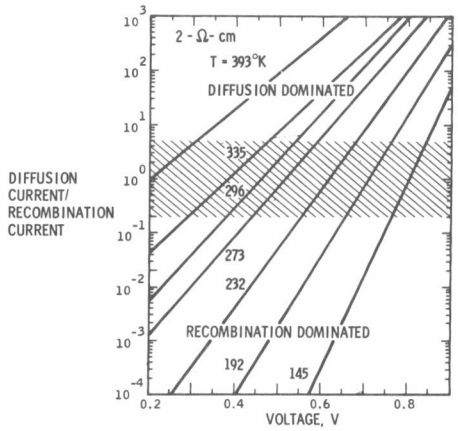

Figure 6.

JUNCTION CURRENT REGIMES

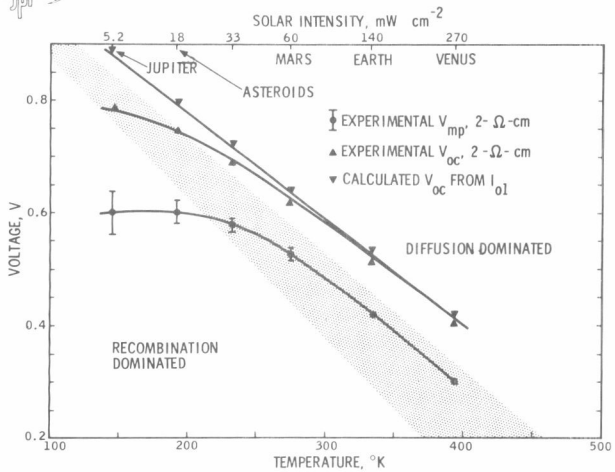

Figure 7.

INVERSION LAYER CELL PROGRAM (U OF ARIZONA)

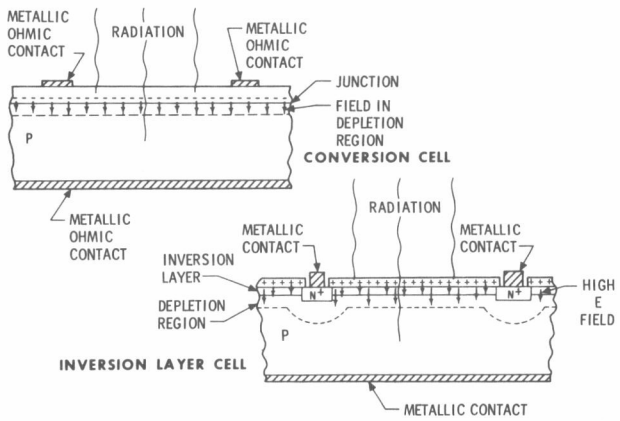

Figure 8.

R. J. Stirn*

LASER BEAM PHOTOVOLTAIC CONVERSION

One of the principal non-military motivations for development of high-energy lasers is the transmission of power through space (Figs. 1 and 2). The most likely candidate for the required energy converter is a photovoltaic device because we have had experience with them as solar cells and as photon detectors and for the reasons listed in Fig. 3. Useful operation can be expected in the wavelength range from a few tenths to one micron with efficiencies from 20 to 40% depending on the laser wavelength and intensity. Some reasons for the expected two-to-four-times improvement in efficiency in silicon solar cells over that obtained in sunlight are listed in Fig. 4.

The first phase of this new task is to determine the expected performance of silicon solar cells over a wide range of intensities and wavelengths and to ascertain how best to optimize the efficiency by changes in the junction depth, base resistivity, grid configuration, and anti-reflection coating. Monochromator measurements are being performed to determine the absolute junction collection efficiency of silicon cells with a range of 0.2-to-2-micron-deep junctions and 0.1-to-90-ohm-cm base resistivities. An example is shown in Fig. 5 for a fixed initial (pre-diffusion) base resistivity of 9.0 ohm-cm. The dependence on junction depth at short wavelengths is obvious. The measurements are to be extended further in the short wavelength region by replacing the tungsten light source with a zenon arc-lamp. It was found that the diffusion length, which is resistivity-dependent, was not the same between cells of the same lot and, in particular, varied greatly between cells having diffusion junction depths even though the initial base resistivity was the same. The latter effect is apparently caused by the different temperature-time schedules of diffusion.

Further photovoltaic measurements will be made with high-intensity laser energy at 488.0, 514.5, and 614.7 nm using ion lasers and between about 520 and 700 nm using a tunable dye laser pumped with the argon ion laser (Fig. 6). These measurements will include the light current-voltage characteristics which will allow a determination of the dependence of the voltage and current on light intensity and of the series resistance.

Improved anti-reflection coatings will be investigated analytically and experimentally. Present coatings are too absorbing in the short wavelength regime. Calculations will be made to predict the equilibrium temperatures expected for various intensity levels, which, with the measured collection efficiencies, junction characteristics, and series resistances, will enable final conversion efficiencies to be computed for varying wavelengths and intensities.

Other semiconductor materials will be investigated later as will be the feasibility of using Schottky barrier solar cells, such as are being developed now at JPL on GaAs. The latter may be especially interesting for application with very-short-wavelength lasers (less than 0.5 micron) where the high absorption of light in semiconductors (Fig. 7) becomes a problem in p/n junction devices.

*Guidance and Control Division, Guidance and Control Systems and Research Section

COLLECTION EFFICIENCY vs JUNCTION DEPTH

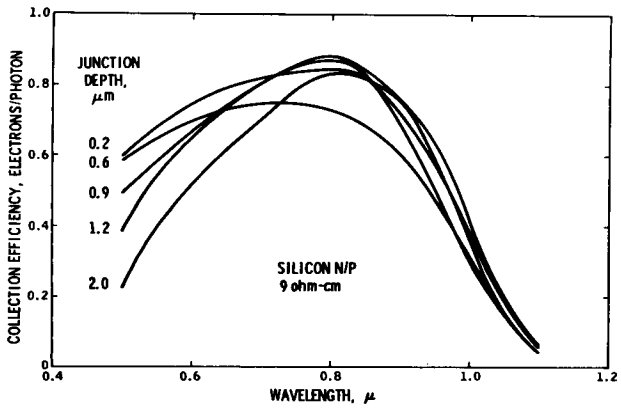

Figure 5.

EXPERIMENTAL SETUP

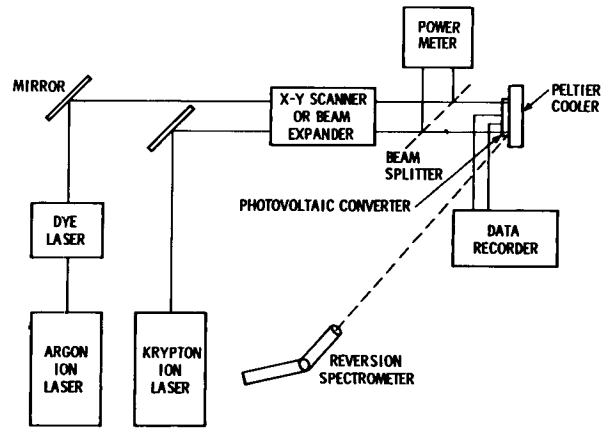

Figure 6.

REPRESENTATIVE ABSORPTION COEFFICIENTS

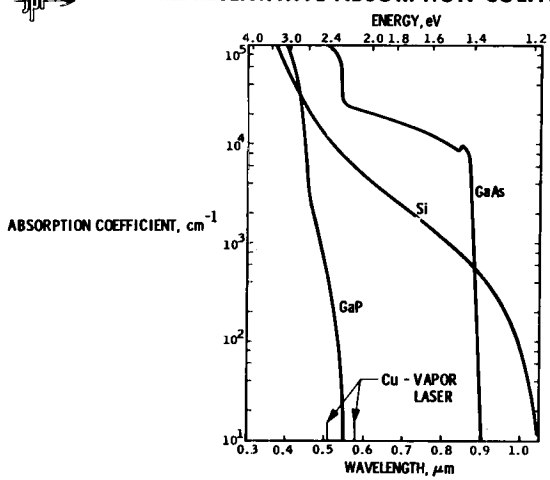

Figure 7.

Werner von Hartmann*

PULSE CHARGING OF BATTERIES

The objective of this work is to improve the performance of spacecraft batteries and their chargers to permit spaceflights of long duration (up to 12 years).

Pulse charging, involving the use of pulsed current rather than direct current for charging, opens new possibilities for the control of battery problems, some of which become significant after extended cycling and some of which are part of new batteries. The ability to produce pulses in various shapes, to introduce negative pulses, to vary frequency and periods of zero current, may well serve to suppress unwanted side reactions in favor of those producing the highest level of charge in the battery.

Missions of extended duration, such as those currently planned, tax present battery technology to its limits. Nickel-cadmium batteries, though known for good cycle life, do nevertheless suffer capacity losses after extended cycling. A reduced charge-discharge efficiency resulting from capacity fading and increased gassing at the nickel electrode are symptomatic for these conditions. In addition, dendrites are known to grow on cadmium electrodes after prolonged cycling thereby endangering battery performance through a short.

On the basis of preliminary results, pulse charging is expected to affect battery performance by reducing capacity fading, controlling gassing during charge, and disrupting dendrite formation and growth. The result of these changes should be higher capacity and longer battery life.

One of the advantages of pulse charging is that it permits high instantaneous charge currents from a low average current source. This feature has considerable merit in view of the fact that certain probes may have limited current capabilities and, that nickel-cadmium batteries suffer under low charge current conditions.

Capacity fading, a symptom seen after repeated cycling, is the result of a gradual agglomeration in the cadmium electrode. This morphological change causes the crystals of cadmium metal to grow at the expense of surface area, and with it, plate capacity. Pulse charging is expected to combat this process through the use of reverse current pulses. These discharge current pulses are thought to release submicroscopic hydrogen bubbles at the electrode surface, scrubbing it and exposing fresh electrochemically active material.

Dendrites, which are known to form whenever strong concentration gradients exist near a partially soluble electrode, grow, penetrating the absorber material and eventually short dissimilar electrodes. The resulting catastrophic failure may be avoided if the concentration gradient is disrupted by reverse migration. Pulse charging has the potential of doing this.

Another reason that pulse charging is thought to be beneficial to battery operation is that it may reduce gassing at the nickel electrode during charge. Oxygen gas is evolved as the result of concentration polarization near the electrode. This polarization which results from hydroxyl ion depletion, can be reduced through the use of pulsed currents. Experiments have shown that concentration polarization can be curtailed under the influence of alternating current.

Preliminary experiments with pulse charging of nickel cadmium cells have shown that the capacity is insensitive to pulse frequency between 15 and 15,000 Hz (Fig. 8) but that the ratio of charge to discharge pulses does influence capacity (Fig. 7). The minimum in capacity near the ratio of 5 indicates the possibility of conflicting mechanisms. Between 1.5 and 5, one mechanism causes the capacity to decline, while at 5 another mechanism gains control, causing the capacity to increase as the current ratio rises. In yet another series of experiments, Mariner 9 spacecraft cells returned slightly more charge after pulse charging than after direct current charging at the same rate (Fig. 10).

Since gassing during charge is not only a parasitic reaction but results in pressure in a sealed cell, present efforts are directed toward assessing the effect of pulse charging on gassing. Equipment is being assembled which will allow cells under charge to be purged with an inert gas. The oxygen swept away in the gas stream will be carried to a detector where the rate and onset of oxygen evolution will be measured as a function of temperature, charge rate, and state of charge. This information should provide the needed data for an understanding of the kinetics of gas evolution at metal-solution interfaces, and also serves as a sensitive and realistic indicator of the effectiveness of pulse charging of batteries.

*Guidance and Control Division, Spacecraft Power Section.

PRESENT STATUS

- EQUIPMENT
- EXPLORATORY MEASUREMENTS

Figure 5.

SQUARE WAVE PULSE CHARGER BLOCK DIAGRAM

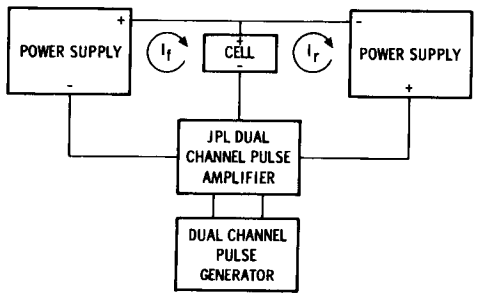

Figure 6.

CAPACITY vs FORWARD-TO-REVERSE CURRENT RATIO

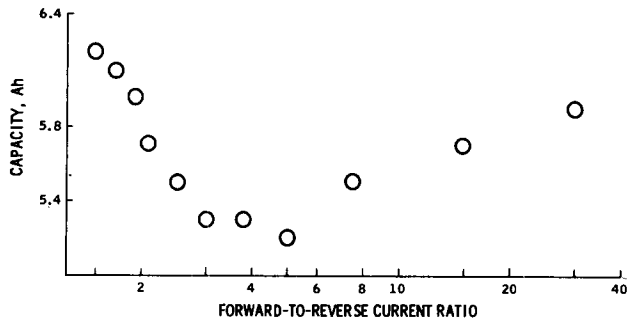

Figure 7.

PRESENT ACTIVITIES

- ESTABLISH EFFECT OF PC ON OXYGEN EVOLUTION
- MEASURE ONSET AND RATE OF OXYGEN EVOLUTION

Figure 11.

OXYGEN MEASUREMENT

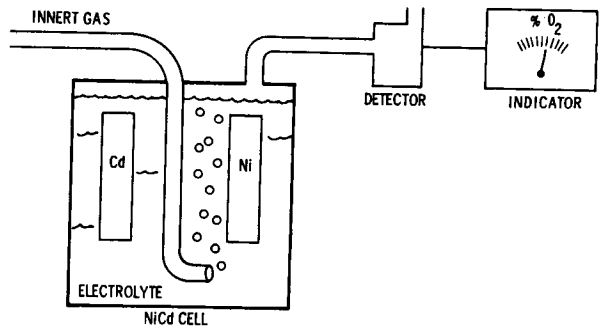

Figure 12.

NEEDED

- FUNDAMENTAL STUDY ON GAS EVOLUTION AT METAL-SOLUTION INTERFACES
- UNIVERSITY CONTRACT?

Figure 13.

D. G. Elliott*

ANALYSIS OF LINEAR INDUCTION MACHINES

The mesh/matrix analysis method for linear induction machines was improved by addition of field shapes from conformal mapping. Inclusion of fringing field permits calculation of the magnetic field and rail current beyond the exit of the iron stators. Calculations for a linear motor show that the field and rail current decay only slowly beyond the exit, causing wasteful ohmic losses. Also, the phase relationship between the field and rail current at both ends is incorrect for thrust production. The mesh/matrix method thus provides the first insight into the reasons for poor performance of linear induction motors.

The overall thrust predicted by the mesh/matrix method agrees within 10% with data from an experimental motor.

A study of accuracy as a function of computation mesh size for a typical linear motor shows that a converged solution requires the full core memory of a UNIVAC 1108 computer and 160 s computing time. A solution requiring half the memory and a third the time, however, gives thrust values only 0.2% different.

The next goal of the work is study of optimum windings for improved efficiency of both transportation linear motors and liquid MHD generators.

*Propulsion Division, Research and Advanced Concepts Section

LINEAR INDUCTION GENERATOR FOR NaK - N_2 CONVERTER

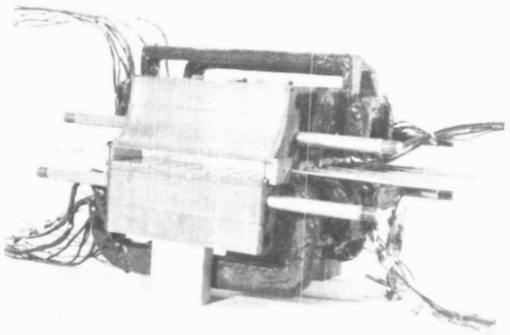

Figure 1.

HIGH-SPEED GROUND TRANSPORTATION WITH LINEAR INDUCTION MOTORS

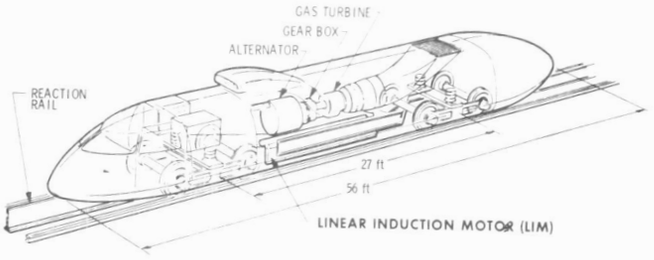

Figure 2.

LINEAR INDUCTION MACHINE

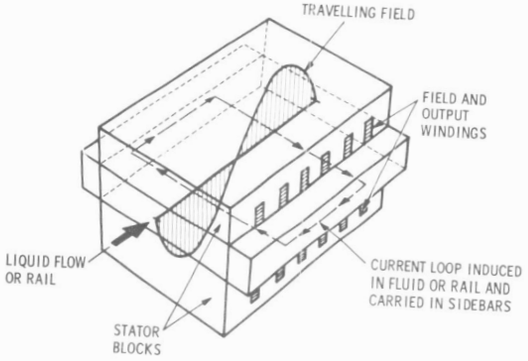

Figure 3.

COMPARISON BETWEEN THEORY AND DATA FOR A LINEAR INDUCTION MOTOR

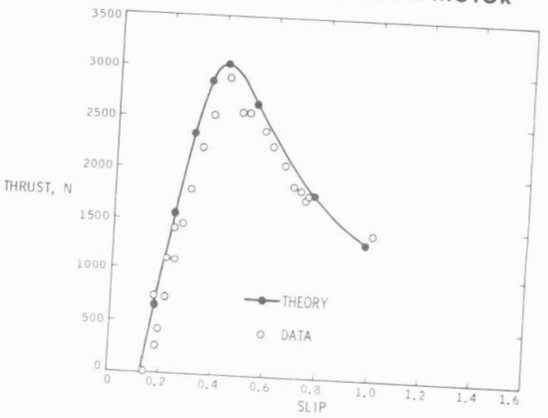

Figure 4.

EFFECT OF MESH SIZE ON ACCURACY AND COMPUTER REQUIREMENTS

NUMBER OF MESHES PER SLOT PITCH	TOTAL NUMBER OF MESHES	MEMORY REQUIREMENT, WORDS	COMPUTING TIME, sec	THRUST, NEWTONS
1	73	28 000	8	1744
2	145	62 000	55	1723
3	217	117 000	160	1720

Figure 5.

LINEAR MOTOR FIELD AND RAIL CURRENT DISTRIBUTIONS

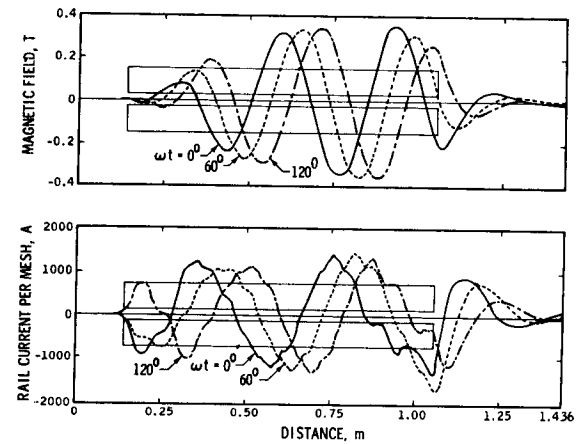

Figure 6.

D.J. Cerini*

NaK-NITROGEN LIQUID METAL MHD CONVERTER

Liquid metal MHD power conversion is one of the more promising methods for generating electric power in space. One type of system employs cesium as the thermodynamic working fluid and lithium as the electrical working fluid in a Rankine cycle operating at 1000°C. This type of system is capable of ac electrical power generation in the multihundred-kilowatt range.

A room-temperature converter has been tested with NaK and nitrogen as the working fluids to demonstrate the feasibility of liquid-metal MHD power generation. The experimental converter consists of the four primary components required in a flight converter: a nozzle, separator, generator, and diffuser. The working fluids are mixed at a pressure of 160 N/cm^2 in the nozzle inlet and flow through the convergent-divergent nozzle to high velocity and low pressure. The flow leaves the nozzle at velocities up to 125 m/s at 5% of the pure liquid density.

The flow impinges along the 70-cm long lower surface of the separator channel which is inclined 18 deg to the flow direction. The centrifugal force causes the liquid to coalesce to a film 15 cm wide by 1 cm high at the separator exit. The flow leaves the separator channel with a tenfold density increase over the nozzle exit conditions. The flow coalescence, resulting in a sevenfold stagnation pressure increase, is achieved at the expense of a 15% velocity loss and a 4% mass loss to the nitrogen exhaust. The wedge-shaped inlet of the generator diverts the bulk of the gas flow and prevents it from entering the generator.

The generator channel is formed by two stator blocks that contain the polyphase linear induction generator windings. The magnetic field, produced by excitation of these windings, interacts with the flow of the liquid metal to reduce the kinetic energy of the liquid stream. The power extracted from the flow is inductively coupled into the stator windings.

The flow leaves the generator channel with sufficient velocity to allow recovery of pressure in the diffuser for return to the nozzle. The diffuser is a divergent duct which typically produces pressure rise of 70% of the isentropic rise for a 50% void-fraction flow.

The experimental NaK-nitrogen converter is approximately 1 m wide by 1.5 m high by 3 m long. It is the approximate size of an 1000°C Cs-Li flight type converter operating at a nozzle inlet pressure of 95 N/cm^2 with a system output of 75 kWe.

To date, the NaK-nitrogen converter has been operated over the range of nozzle pressures of 100 to 160 N/cm^2 and generator excitation levels up to 80% of maximum. The maximum power output obtained was 20 kW at a nozzle inlet pressure of 160 N/cm^2 with 58 kg/s of NaK and 3.2 kg/s of nitrogen flow.

The preliminary results from the experimental program can be summarized as follows:

(1) The converter has good hydraulic and electrical operating characteristics.

(2) No unexpected losses have been found.

(3) Power output is consistent with the Cs-Li cycle analysis.

*Propulsion Division, Research and Advanced Concepts Section

NaK - NITROGEN MHD CONVERTER EXPERIMENT

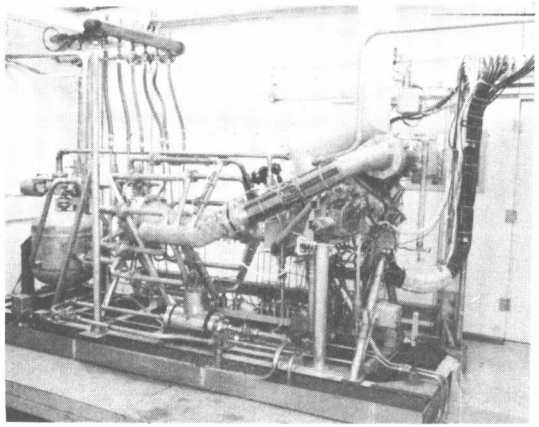

Figure 5.

NaK - NITROGEN MHD CONVERTER NET OUTPUT POWER

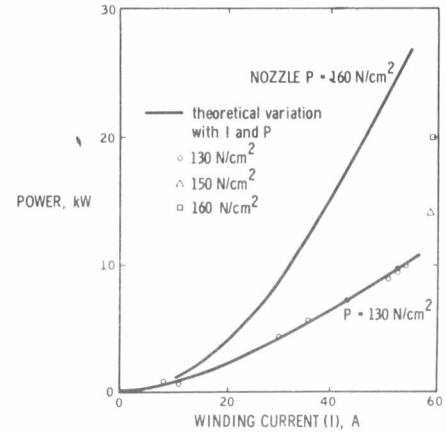

Figure 6.

NaK - NITROGEN MHD CONVERTER

	DESIGN	TEST
NOZZLE INLET PRESSURE	160 N/cm^2	160 N/cm^2
NOZZLE EXIT PRESSURE	18 N/cm^2	19 N/cm^2
NaK FLOW RATE	70 kg/s	67 kg/s
NITROGEN FLOW RATE	3.5 kg/s	3.6 kg/s
GENERATOR INLET VELOCITY	82 m/s	74 m/s
GENERATOR EXIT VELOCITY	65 m/s	61 m/s
GENERATOR PRESSURE	41 N/cm^2	28 N/cm^2
FREQUENCY	350 Hz	350 Hz
VOLTAGE	480 v	400 v
OUTPUT POWER	30 kw	20 kw

Figure 7.

MAIN RESULTS

- GOOD STARTUP AND OPERATING CHARACTERISTICS
- NO UNEXPECTED LOSSES
- POWER OUTPUT CONSISTENT WITH Cs-Li CYCLE ANALYSIS

Figure 8.

COMMUNICATIONS AND INFORMATION SCIENCES

William M. Whitney*

JPL ROBOT RESEARCH PROGRAM

Objectives. The long-range goal of this research is to provide NASA with strength in the advanced computer science disciplines of robotics and artificial intelligence. Such strength will manifest itself in the knowledge and experience of people within NASA who will have contributed to the growth of these fields and who will have developed tools and approaches germane to the needs of future NASA programs and projects. The short-range objective is to design and construct a robot breadboard, operating initially in an indoor laboratory, by January 1975. The breadboard will focus the research activities and demonstrate an ability to integrate sensory and motor functions into a coordinated total system that can perform in a realistic environment.

Justification. For missions not too far from earth, operations with unmanned spacecraft can be carried out by direct control from ground stations, as was done for the Surveyor lunar landers and the Russian Lunakhod rover. When the remote spacecraft or station is far enough from earth that the round-trip communication time is longer than a few minutes, such a control method becomes inefficient and costly, and places severe demands on the communication channel and on the ground-support organizations. For such missions, particularly those for which the spacecraft will be in environments unpredictable in detail in advance, a semiautonomous control mode is needed, one which will permit man to schedule and plan only major tasks and sequences of events, which the remote machines will then execute autonomously. The work being undertaken in this program will provide such an option. At the same time, it will give NASA capability in a rapidly developing branch of computer science that promises numerous applications outside the space program.

Approach. The initial breadboard will be designed to provide selected sensory and motor functions that would be required on a roving vehicle on the surface of Mars. The rover will consist of a vehicle or cart, on which will be mounted a stereo TV sensor, a laser ranging device, a mechanical arm, a small minicomputer for input-output control and multiplexing, and various other sensors to assist locomotion and manipulation. The rover will be complemented by a supervisor consisting of a human operator, display units, and a computing system consisting of a medium-sized local computer for real-time control of the vehicle and a large remote time-shared computer for manipulator and vehicle task planning and for TV and laser data processing. Initially, the rover will be operated indoors and will be tethered for communications and power.

The performance requirements for January 1975 are that the rover should be able, on command, to move to a designated location, to pick up a designated rock, or to deploy selected scientific instrument packages, all autonomously. These tasks present a number of challenging research and system-integration problems that have not been solved for robots operating in natural environments.

Progress and Plans. During the past year, the overall goals of the program and the characteristics of the robot breadboard have been defined, as described above. A detailed program plan is being prepared to forecast probable costs and schedule. Some implementation of the major hardware components has been started, and research is under way to solve the problems associated with vehicle and manipulator control, TV and laser data representation and interpretation, and software system organization. It is expected that, by the end of the present fiscal year, firm approaches will have been adapted in all areas, and the program will have passed from the planning and design phase to full-scale implementation.

*Astrionics Division; Manager, Astrionics Research Section.

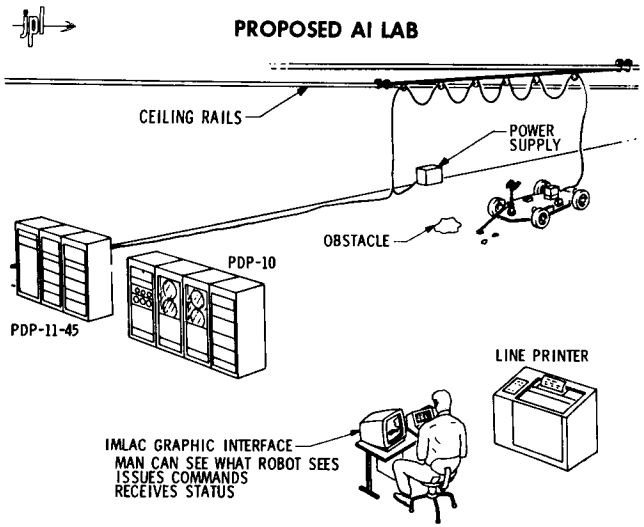

Figure 5.

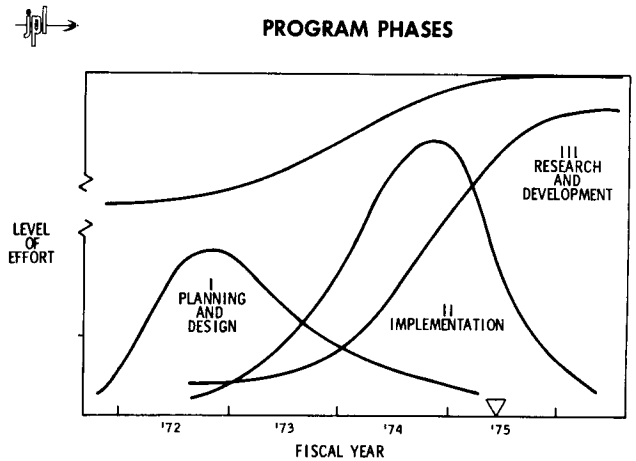

Figure 6.

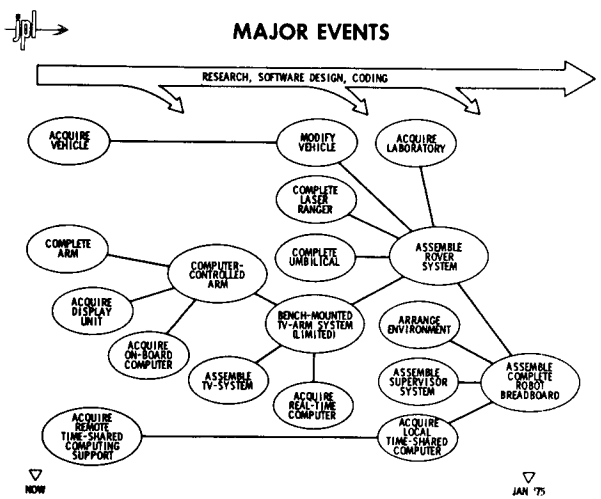

Figure 7.

ROBOT SYSTEM PROBLEMS

(PHASES I, II)

- STRUCTURE OF MODULAR SYSTEM (HARDWARE AND SOFTWARE) THAT CAN ACCOMMODATE CHANGES WITHOUT MAJOR REDESIGN
- INTEGRATION OF HARDWARE AND SOFTWARE ELEMENTS INTO COORDINATED TOTAL SYSTEM
- SUCCESSFUL HANDLING OF DETAILS
  - "LOW LEVEL" vs "HIGH LEVEL" PROBLEMS

Figure 8.

SPEAKERS FROM AI COMMUNITY AT JPL SEMINARS, JUNE 1971 - JUNE 1972

D. LUCKHAM	U.C.L.A. AND STANFORD	16 JUNE 1971
B. RAPHAEL	STANFORD RESEARCH INSTITUTE	24 JUNE 1971
P. HART	STANFORD RESEARCH INSTITUTE	23 AUGUST 1971
D. BOBROW	(FORMERLY) BOLT BERANEK & NEWMAN	22 OCTOBER 1971
A. NEWELL	CARNEGIE-MELLON UNIVERSITY	27 OCTOBER 1971
T. SHERIDAN	M.I.T.	29 OCTOBER 1971
S. AMAREL	RUTGERS UNIVERSITY	23 NOVEMBER 1971
J. McCARTHY	STANFORD UNIVERSITY	10 DECEMBER 1971
A. KLINGER	U.C.L.A.	28 JANUARY 1972
E. FREDKIN	M.I.T.	21 MARCH 1972
A. SAMUEL	STANFORD UNIVERSITY	12 APRIL 1972
J. SKLANSKY	U.C. IRVINE	4 MAY 1972
D. MICHIE	UNIVERSITY OF EDINBURGH	8 MAY 1972
C. ROSEN	STANFORD RESEARCH INSTITUTE	30 JUNE 1972
P. HART	STANFORD RESEARCH INSTITUTE	30 JUNE 1972

Figure 13.

R. J. McEliece*

CODING THEORY AND LINEAR PROGRAMMING

The work described in this presentation deals with the theory of binary error-correcting codes. In particular it describes some recent research (by the author and Drs. Howard Rumsey, Jr., and Lloyd Welch of JPL's Telecommunications Division) which yields estimates of the performance of such codes far superior to any previously known.

When it is necessary to transmit one of several different messages over a telecommunications channel (e.g., S/C experimental outcomes, command or ranging data, etc.) it is frequently also necessary to *encode* the messages into a binary digital format suitable for transmission over the channel. For example in the Mariner photographs of Mars, each "spot" of a photo was encoded into one of 64 possible binary sequences of length 32 before transmission to earth. Similarly command, ranging, and telemetry data from spacecraft which are transferred along NASA ground lines are encoded into 1200 bit blocks prior to transmission.

When the channel being used to transmit these binary encoded messages, *code words* for short, is "noisy" in the sense that what is received is not always exactly the same as what is sent, it is obviously valuable to have the various codewords differ from each other as much as possible, so that even if a message is received in somewhat garbled form it can be correctly interpreted or at least not misinterpreted.

Thus a *binary error correcting code* consists of a set of binary codewords that are different enough from each other to enable the receiver to correctly interpret a somewhat garbled version of one of them. For example, consider the code consisting of the four codewords of length five $\{00000, 00111, 11100, 11011\}$. Let us suppose the second codeword (00111) is transmitted over the channel, and that it is received with an error in the fourth position, i.e., as 00101. The received message differs from the first codeword in two positions, the second in one, the third in three, and the fourth in four positions. Hence, a clever receiver will decide correctly that codeword two was transmitted, in spite of the fact that an error occurred.

Thus we are led to ask the following question: What is the largest number M of binary codewords of length n which can be chosen so that they all differ from each other in at least d positions? We denote this number by M(n,d). For example in the code of the previous paragraph d=3 and so $M(5,3) \geq 4$.

In the past 20 years there has been a very large amount of research done on the problem of calculating (or at least estimating) M(n,d) for various n and d. Last year, we at JPL developed a new technique which is considerably stronger than any of the older methods of dealing with the problem. Following is a brief sketch of the method.

If c and c' denote codewords, define the *distance* between them, d(c,c'), as the number of positions in which they differ. The distance between two codewords is thus a quantitative measure of their mutual distinguishability.

Let C be a code containing M codewords $c_1, c_2, \ldots, c_M$ of length n such that distinct codewords c_i and c_j have $d(c_i, c_j) \geq d$. For each integer $i = 0,1,2, \ldots, n$ define A_i as the number of pairs (c_j, c_k) of codewords from C such that $d(c_j, c_k) = i$, divided by M. Then it is easy to see that $A_0 = 1$, $A_1 = A_2 = \ldots = A_{d-1} = 0$, and $A_0 + A_1 + \ldots A_n = M$.

The important new fact discovered about binary error-correcting codes is that certain linear combinations of the numbers $A_0, A_1, \ldots, A_n$ must be nonnegative. These linear inequalities can then be combined with the simple facts about the A_i given in the previous paragraph via the well-developed theory of *linear programming* to give startling improvements over all other known techniques for estimating M(n,d). Indeed, over 90% of the previously published estimates for M(n,d) can be improved by our technique.

*Telecommunications Division, Communications Systems Research Section

A QUICK LOOK AT THE FAMOUS KNOWN BOUNDS ON M(n, d) - IN ASYMPTOTIC FORM

- THE RATE R OF A CODE IS DEFINED AS

$$R = \frac{1}{n} \log_2 M$$

R TELLS US WHAT FRACTION OF EACH CODEWORD CARRYING INFORMATION; THE REMAINDER COMBATS THE NOISE

EXAMPLE: $R = 6/32$ FOR THE MARINER 1971 BLOCK CODE. ($M = 64$ CODEWORDS OF LENGTH $n = 32$)

- AN IMPORTANT PROBLEM IS THE CALCULATION OF THE LIMIT

$$R(D) = \lim_{n \to \infty} \frac{1}{n} \log_2 M(n, Dn) \quad 0 \le D \le 1$$

Figure 5.

THE KNOWN BOUNDS

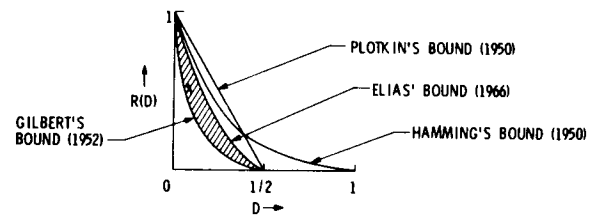

P: $R \le 1-2D$
H: $R \le 1-H(D/2)$
E: $R \le 1-H((1-\sqrt{1-2D})/2)$
G: $R \ge 1-H(D)$

$H(x) = -x \log_2 x - (1-x) \log_2 (1-x)$

- R(D) LIES SOMEWHERE, NOBODY KNOWS WHERE, IN THE SHADED REGION

Figure 6.

THE NEW FACT

$C = \{c_1, c_2, \ldots, c_M\}$ ANY CODE. DEFINE FOR $i = 0, 1, \ldots, n$

$A_i = \frac{1}{M} \times$ THE NUMBER OF PAIRS (c_j, c_k) OF CODEWORDS WITH $d(c_j, c_k) = i$.

- EASILY SEEN THAT $A_0 = 1$, $A_0 + A_1 + \ldots + A_n = M$ AND $A_1 = A_2 = \ldots = A_{d-1} = 0$ (d = MINIMUM DISTANCE OF C).
- DEFINE A POLYNOMIAL B(x)

$$\sum_{j=0}^{n} B_j x^j = \sum_{i=0}^{n} A_i (1-x)^i (1+x)^{n-i}$$

- THEN $B_j \ge 0$ FOR ALL j

Figure 7.

HOW DO WE USE THE NEW FACT?

- EACH B_j CAN BE WRITTEN AS A LINEAR COMBINATION OF THE A_i's

$$B_j = \sum_{i=0}^{n} A_i K_j(i), \text{ WHERE}$$

$$K_j(i) = \sum_{k=0}^{n} (-1)^k \binom{i}{k}\binom{n-i}{j-k}$$

- HENCE AFTER A LITTLE MANIPULATION THE PROBLEM OF ESTIMATING M(n, d) CAN BE STATED AS A LINEAR PROGRAMMING PROBLEM:

MAXIMIZE $A_0 + A_1 + \ldots + A_n$ ($= M =$ # CODEWORDS)

SUBJECT TO: $A_0 = 1$, $A_1 = A_2 = \ldots = A_{d-1} = 0$ $\left(\text{MIN. DISTANCE} \ge d\right)$

$A_i \ge 0$ FOR ALL i

$\sum_{i=0}^{n} A_i K_j(i) \ge 0$ ($B_j \ge 0$ TRANSLATED)

Figure 8.

PHYSICS AND CHEMISTRY

Gary Russell*

LASER KINETICS

Because laser power propagation in space requires lasers with high efficiencies operating at a small wavelength to minimize laser beam divergence, a theoretical study has been initiated to systematically search for lasants with these properties. CW lasers currently operating in the visible and ultraviolet are inefficient because their lasants are generally ionized gases with inherently low quantum efficiencies. Therefore, this study has been focused on the search for metallic vapor lasants which have potentially high efficiencies when used in a multiple pulsed mode of operation.

These lasants are characterized by upper lasing levels a few ev above the ground state and metastable lower lasing levels, making the attainment of population inversion by electron collisions an inherently transient process. The energy level diagrams of several promising metallic vapors - bismuth, germanium, and copper are shown in Figs. 1-3.

The existence of the two laser transitions in copper, λ = 5782 and 5106 Å, has already been experimentally verified. Bismuth has two possibilities, one in the near infrared at 9152 Å and one in the visible at 4724 Å. Germanium, in addition to two transitions in the visible, has two possible transitions in the ultraviolet. The lasant physical characteristics are shown in Figs. 4 and 5. Note that bismuth looks very attractive as a lasant for a multiple pulsed flowing laser because of its high vapor pressure at low temperatures and low heats of fission and sublimation.

Currently a theory is being formulated which describes the pulsed laser-discharge characteristics of metallic vapor - buffer gas mixtures. The theory deals with the determination of the electron temperature and density simultaneously with the populations of the metallic vapor excited states for a given temporal distribution of current. Ionization rates and elastic and inelastic electron energy losses due to the buffer gas are included in the analysis. The theory has been completed for copper and has been able to accurately predict the lasing wavelengths, laser pulse delay times, and pulse widths for the JPL supersonic copper vapor laser. Some representative results obtained for copper using helium as the buffer gas are shown in Figs. 6-8 where the buffer gas pressure is varied. The effect of increasing the buffer gas pressure is to raise the laser peak power per pulse, shorten the delay time after initiation of the current pulse, and decrease the pulse width. However, as shown in Fig. 7, the energy density per pulse has a maximum where the laser efficiency has not yet dropped appreciably, indicating that the best performance for a copper vapor laser is achieved with a helium-copper number density ratio between ten and one hundred.

*Propulsion Division, Research and Advanced Concepts Section

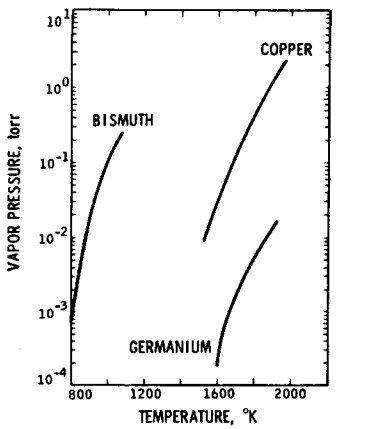

Figure 5.

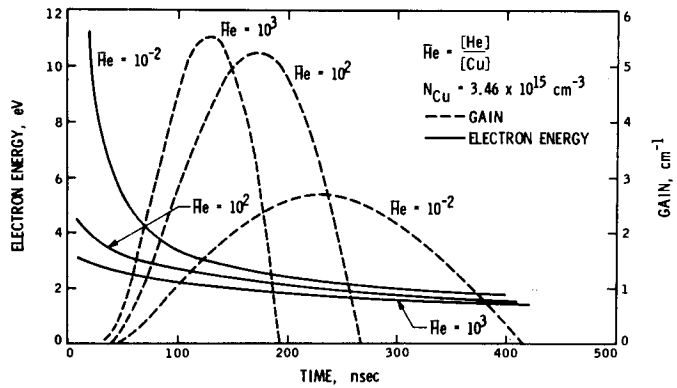

Figure 6.

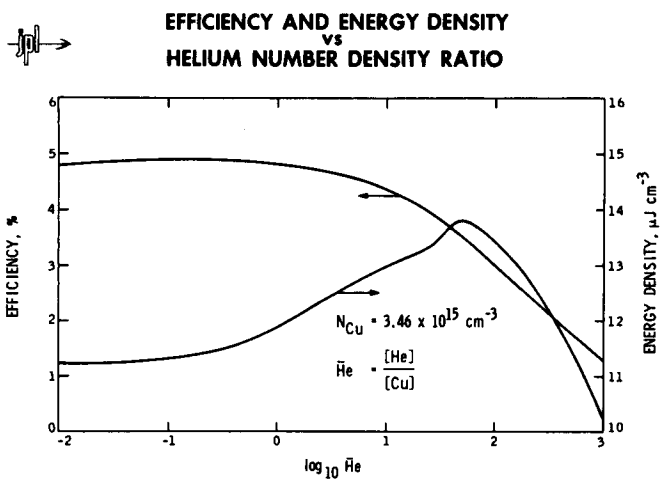

Figure 7.

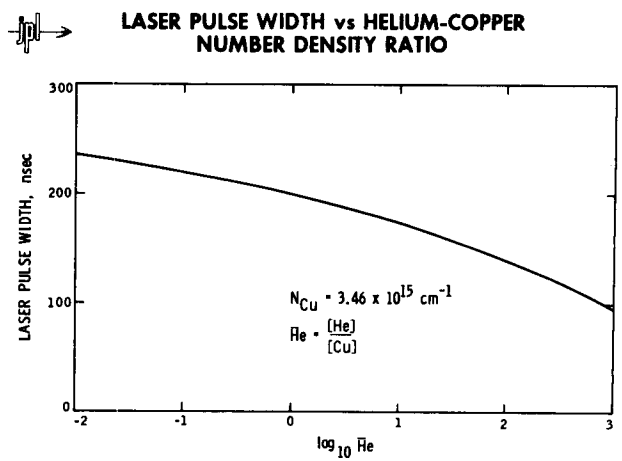

Figure 8.

RTOP 503-10-01
Quantum Electronics
Che Jen Chen*

METALLIC VAPOR DISCHARGE TUBE EXPERIMENT

This experiment is designed to study the lasing characteristics of some metallic vapors which, because of their energy level structures, may lase in the short wavelength visible and ultraviolet regions. The optical efficiency is in general very high. Such metals, if found, can be used as lasants for high-power laser space applications.

A radiation furnace with tantalum as a heating element is used to heat the alumina laser discharge tube. The metals to be studied are held in a boron nitride bucket hanging in the center of the discharge tube. The bucket can also be heated electrically by a tungsten winding embedded in the wall of the bucket to supply more energy for heat of vaporization of the metal. A conventional optical cavity is arranged along the length of the discharge tube. The schematic diagram of the experimental setup is shown in Fig. 1. The spectral line shape of the metal vapors without an optical cavity under different excitation schemes is first studied by using a high resolving power spectrometer (both grating and interference types) to detect the existence of the inverted levels. The narrowing of the line width due to the induced emission indicates the levels responsible for the emission are inverted. An example of a copper inverted level is shown in Fig. 2. An optical cavity for the particular wave length is then designed to study the characteristics of the laser. Laser gain, power, pulse width, relaxation (or recovery) time of the lasant, and the effect of buffer gases are measured.

Currently, copper vapor is being investigated. The pulse width of the copper laser varies with the pressure of the buffer gas for a fixed temperature of the discharge tube. There is an optimum pressure as shown in Figs. 3 and 4. The energy of each copper laser pulse also varies with the buffer gas pressure as shown in Fig. 5. The optimum condition is also revealed in this measurement. The effect of discharge current repetition rate on the copper laser performance is shown in Fig. 6. The pulse width, energy, and power of the laser pulse are decreased by increasing the repetition rate. The recovery (or relaxation) time for copper lasant is about 1 s. Under these specific conditions the long recovery time indicates the necessity of utilizing a high-speed flowing system to obtain higher repetition rates.

In future work, measurements will be carried out for some other metals, which appear to be promising as a lasant in the short wave length region, such as germanium, bismuth, thallium, etc.

*Propulsion Division, Research and Advanced Concepts Section

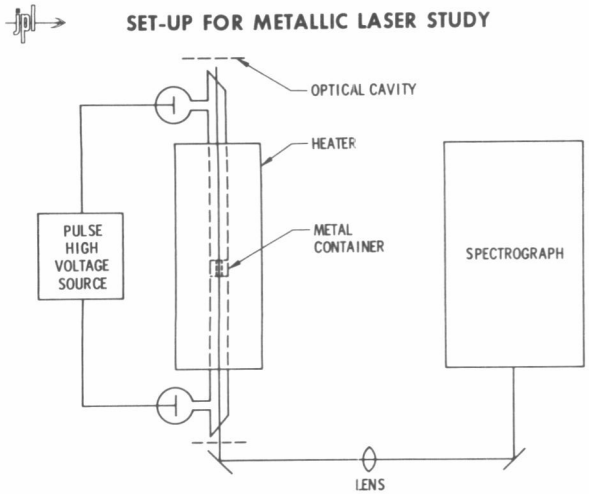

Figure 1.

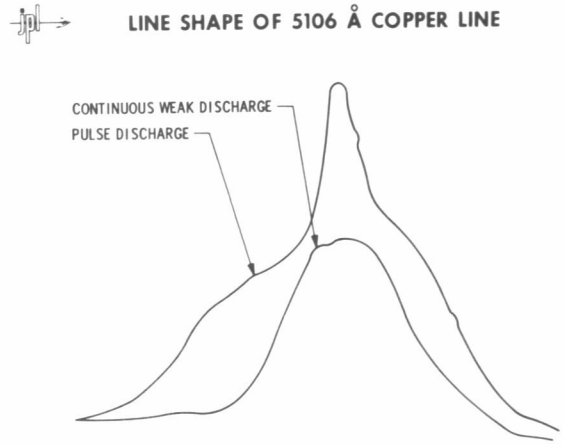

Figure 2.

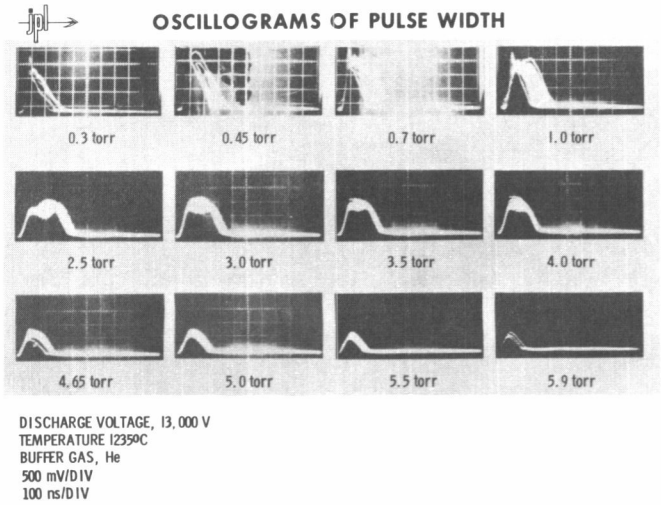

Figure 3.

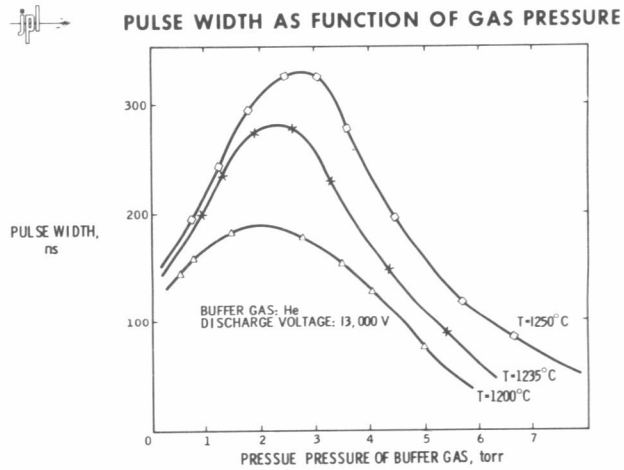

Figure 4.

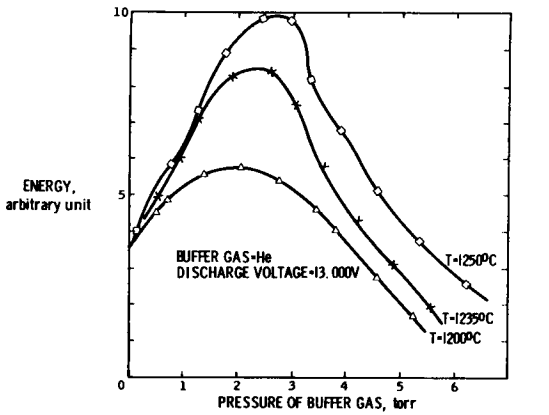

Figure 5.

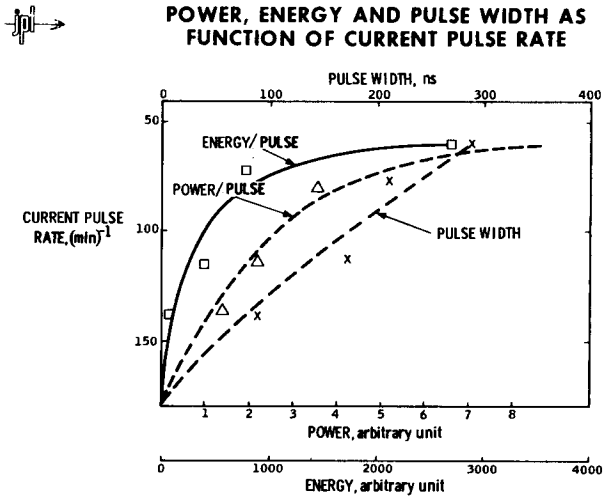

Figure 6.

RTOP 503-10-01
Quantum Electronics
Noble Nerheim*

SUPERSONIC ELECTRIC DISCHARGE COPPER VAPOR LASER

The objective of this work is to investigate the properties of a high-power copper-vapor laser. This laser, which oscillates at 5106 and 5782 Å, is operated by passing a high current pulse through copper vapor. The laser kinetics precludes CW operation; therefore, high average power can be attained only by rapid pulsing. Because of the slow relaxation of the copper plasma, it is necessary to rapidly replenish the copper lasant, utilizing a high-velocity flow, to make a high repetition rate effective.

In this work, a high-velocity flow was obtained by expanding a heated mixture of copper vapor, argon, and helium through a supersonic nozzle. A schematic of the experiment is shown in Fig. 1. The arc heater supplies energy to a helium-argon mixture which then vaporizes the copper and provides the high temperature supersonic flow of the gas-vapor mixture. Figure 2 is a photograph of the insulated plenum chamber, the two-dimensional nozzle, and the electrode assembly. Figure 3 shows the device mounted in the vacuum chamber.

Figure 4 shows a typical discharge current trace and the power output at 5106 Å. These experimental results are compared with the predictions of a theoretical model of the copper vapor laser kinetics, developed at JPL, in Fig. 5. This illustration shows that both the laser pulse width and the delay time are in good agreement with the prediction.

Appropriate mirror coatings were used to vary the laser cavity transmittance from 3.8% to 48% for both individual and simultaneous oscillation at 5106 and 5782 Å. The results obtained from these experiments are shown in Fig. 6. The illustration indicates that the power at 5106 Å is much larger than at 5782 Å and, further, that the sum of the power of the two lines is about equal to the power obtained when both lines oscillated simultaneously. It was found that the power increased almost linearly with the amount of copper injected over the range investigated. Increasing the cavity pressure from 2 to 8 torr increased the peak power of the 5106 Å line, but the pulse width decreased so that the total energy remained almost constant. The 5782-Å oscillation was nearly extinguished at 8 torr. The maximum energy density measured to date was 2.5 $\mu J/cm^3$.

Future plans include optimizing the average power per unit volume by determining the maximum pulse repetition rate and investigating conditions for maximum power per pulse. In addition, some effort will be devoted to determining scaling parameters and quality of the output beam.

*Propulsion Division, Research and Advanced Concepts Section

SUPERSONIC COPPER VAPOR LASER FACILITY

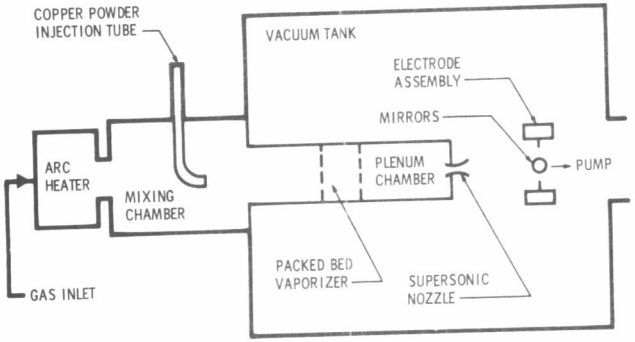

Figure 1.

VIEW OF INSULATED PLENUM CHAMBER, NOZZLE FACE, AND ELECTRODE ASSEMBLY

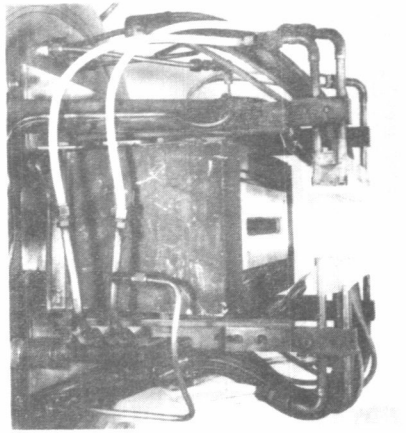

Figure 2.

PHOTOGRAPH OF ASSEMBLED EXPERIMENT

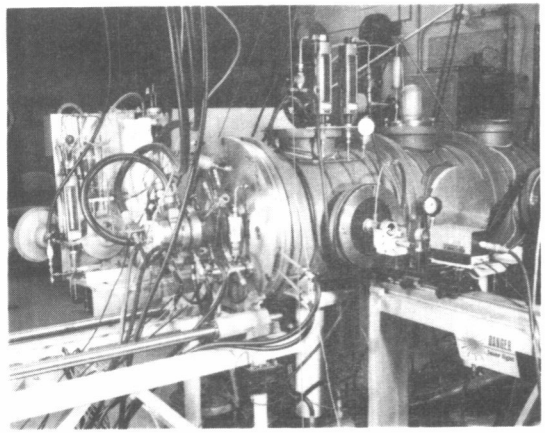

Figure 3.

CURRENT AND LASER POWER AS A FUNCTION OF TIME

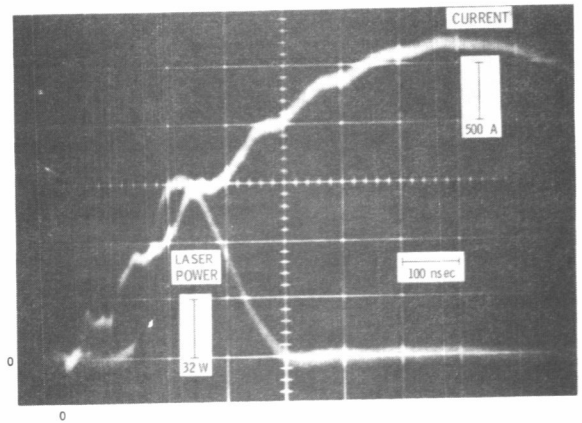

Figure 4.

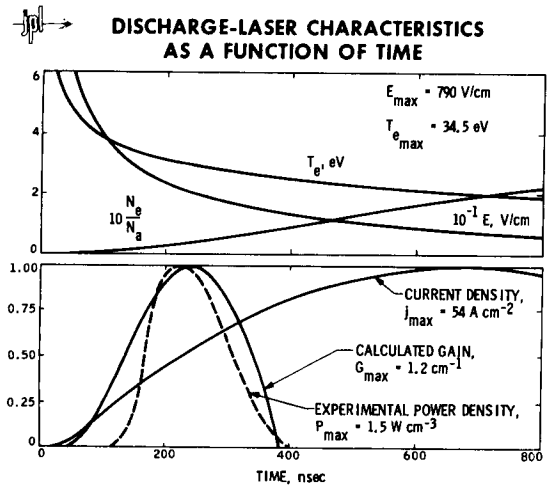

Figure 5.

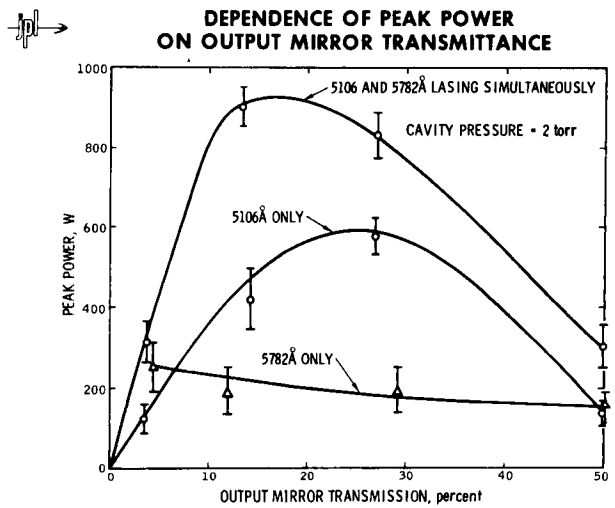

Figure 6.

RTOP 503-10-01
Quantum Electronics
D. D. Elleman*

NUCLEAR ZEEMAN MASER

The principal emphasis of this task is to investigate experimental and theoretical techniques for producing population inversion in nuclear Zeeman levels and to study the feasibility of using this phenomenon for producing stimulated emission in the radio frequency region of the electromagnetic spectrum.

The experimental work conducted in the previous year was devoted to investigation of various methods of producing population inversion in the nuclear levels. This work has been completed and two techniques have proven successful. However, successful population inversion in itself is not a sufficient condition to guarantee laser action. If the upper Zeeman levels are depopulated by processes other than stimulated emission, such as spontaneous emission or spin lattice relaxation, then laser action may not be possible.

It can be shown that spontaneous emission plays only a very minor role at the frequencies at which we are looking in the nuclear Zeeman maser. However, spin lattice relaxation processes can play a very dominate role in the depopulation of the upper levels; for this reason, a rather extensive program of measurement of relaxation processes has been conducted this past year.

Very pure single crystals of ZnF_2 have been used to measure the spin lattice relaxation time of the ^{19}F nuclei. The original results from these experiments showed a relatively large scatter in the experimental points. Relaxation times varied from approximately 145 to 182 ms. This variation was several orders of magnitude larger than was anticipated with the available equipment. A more careful analysis of the data showed that the relaxation time was dependent on the crystal orientation in the magnetic field. This result was quite unexpected and had never been reported by previous workers in the field. Figure 1 shows a plot of the spin lattice relaxation time versus crystal orientation. Figure 2 is a polar plot of the same data.

Similar relaxation time measurements have been conducted on Ca F_2 single crystals which have a simpler crystal structure. The results of these experiments are shown in Fig. 3. These results indicate that this phenomenon is probably universal and not a characteristic of just the Zn F_2 structure. In addition, measurement of the spin-spin relaxation time T_2 have been made on the Ca F_2 crystal. (These results are shown in Fig. 4.) As can be seen, there is a close correlation between T_2 and T_1 relaxation times. The T_2 relaxation time is related to the resonance line width. Recent work at JPL and Caltech has shown that there are techniques available to narrow the line width in these solids; that is, we can greatly increase the T_2 relaxation time in the crystal.

Future experiments, as well as theoretical work, will be conducted to see if this type of increase in T_2 will carry over as an increase in the spin lattice relaxation time. If indeed this is possible, it would lead to a significant improvement in the feasibility of using the Zeeman levels as a master source.

*Space Sciences Division, Physics Section

RTOP 503-10-03
Plasma Dynamics
Wesley Huntress*

PHYSICS OF MOLECULAR INTERACTIONS

In order to design efficient magnetohydrodynamic (MHD) generators, and nuclear and magnetogasdynamic dynamic lasers, a great deal of information is needed on the nonequilibrium properties of their working fluid. Thus, data are needed on the excitation and deactivation of ions and molecules, recombination and ionization rate processes and their associated nonequilibrium radiative losses. In this task we are particularly interested in the behavior of weakly ionized plasmas and we are currently using ion cyclotron resonance techniques to measure such processes as collisions between ions and their parent molecules, collisions frequencies, reaction rates and charge transfer rates versus ion temperature.

There is a variety of these processes which can place an ion in an excited state from which it can then subsequently radiate and, if certain conditions are satisfied, a laser could be constructed using such a mechanism. Figure 2 shows some of these possible mechanisms. The processes that we have been investigating with ion cyclotron resonance (ICR) techniques during the past year are the charge transfer reactions between rare gas ions (X^+) and various small molecules M as shown in Fig. 3. As indicated in the slide, after reaction, the molecular ion $(M^+)^*$ can be left in an excited state from which it can then subsequently radiate. In order to have sufficient ions in an excited state, the charge transfer rate has to be relatively large. Figure 4 summarizes the measurement of the reaction rates for this type of charge transfer reaction and as can be noted, many of these reactions have relatively large rate constants. There are other types of processes that can deactivate an excited state ion such as $(N_2^+)^*$ as shown in the slide. If the decomposition of $(N_2^+)^*$ into N^+ and N is fast, this would have a deleterious effect for the application of the $(N_2^+)^*$ as a laser medium. Recent modification to the ICR spectrometer will allow measurement of the relative rates for the production of $(N_2^+)^*$ and N^+ and N. This work should be completed within the next 6 months.

The flowing afterglow ion laser is currently being constructed and Fig. 6 shows a schematic diagram of the system as it is now planned. The results of the ICR measurement have been used in the design of the flowing afterglow system and these measurements. Figure 7 summarizes some of the more pertinent advantages of the chemical ion laser.

*Space Sciences Division, Physics Section

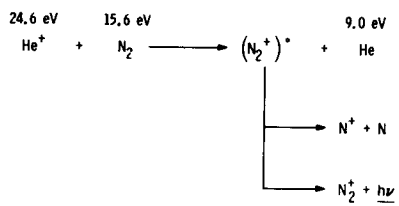

Figure 5.

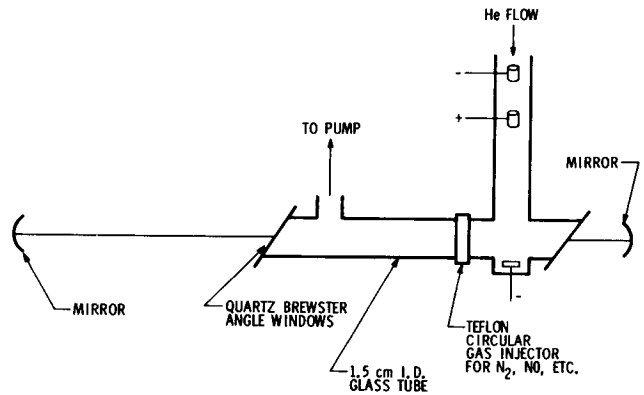

Figure 6.

ADVANTAGES OF CHARGE TRANSFER CHEMICAL ION LASERS

- SELECTIVE EXCITATION PROCESS
- INITIALLY NO MOLECULAR IONS
- LARGE RATE CONSTANTS FOR IONS
- WAVELENGTHS FROM I.R. TO U.V.
- FAST DEPOPULATION OF LOWER LEVEL

Figure 7.

S. Trajmar*

ELECTRON IMPACT SPECTROSCOPY

This program is concerned with the physics of electron-molecule (atom) collisions. The many processes that can occur in such collisions are studied and cross sections for them are determined. Electron impact excitation can also be exploited from the point of view of spectroscopy, and many excitations that cannot be studied by the methods of optical spectroscopy, are conveniently studied by the methods of electron impact spectroscopy. Especially important is spin-exchange scattering which leads to the production of metastable species.

We have extensively utilized the methods of electron impact spectroscopy and carried out pioneering work in this field. Our capabilities are the result of the construction of unique, special-purpose electron impact spectrometers.

The major efforts of the past year are summarized as follows:

Measurements with Apparatus A have been continuing on Xe, N_2, CO, O_2 and H_2O. For Xe, differential and integral cross sections have been determined for elastic scattering and for the lowest lying electronic states at 20 and 40 eV impact energies. These electron impact excitation processes constitute the pumping mechanism in Xe lasers, and the measurements have been carried out specifically to supply cross sections for laser model calculations. The program also turned out to be scientifically rewarding. The measured angular distributions supply information for intermediate angular momentum, coupling a rarely studied case occurring in the heavier rare gases, as well as in Ge, Sn, Br, etc. Publications covering the other molecules are listed.

A new high-resolution molecular-beam/electron-beam apparatus (B) capable of ion, electron and photon coincidence measurements has been put into operation and performed as designed. It is presently being utilized to complete measurements that could not be done on Instrument A. Its performance in energy resolution and angular coverage is shown in Figs. 1 and 2.

An instrument (C) for measuring cross sections for electron-metallic vapor collision processes has been constructed. The electron-scattering part has been checked out on N_2, and a Cu atomic beam furnace is being installed. Electron impact excitation cross sections for Cu will be determined. These cross sections are needed for predicting and understanding the high-power Cu-laser system. No such measurements exist at the present time.

A new program has been initiated to extend our measurements to the very low impact energy region (below 1 eV), to the study of metastable species and free radicals, and to superelastic collisions. These processes are the most important ones occurring in plasmas, but it is rather difficult to study them. An instrument (E) is being constructed to carry out these studies in cooperation with Dr. R. Hall, RRA, University of Paris. The construction is financed by a JPL Director's Fund grant.

Theoretical calculations to supplement and to help in integrating the experimental measurements are being carried out by Dr. N. Winter (RRA) in cooperation with Professor A. Goddard (Caltech) and are financed by a Caltech President's Fund grant. Similar active cooperations are carried out with Professors A. Kupperman (Caltech), G. A. Segal (USC), H. S. Taylor (USC), D. G. Truhlar (University of Minnesota), and with Drs. D. C. Cartwright (Aerospace), W. J. Hunt (University of California, Berkeley), and J. K. Rice (Sandia).

*Space Sciences Division, Physics Section

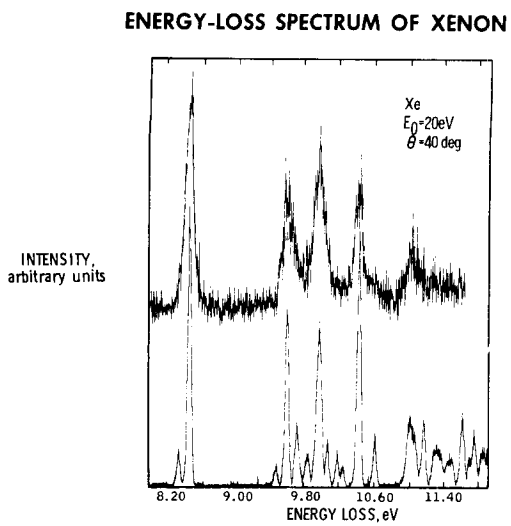

Figure 1.

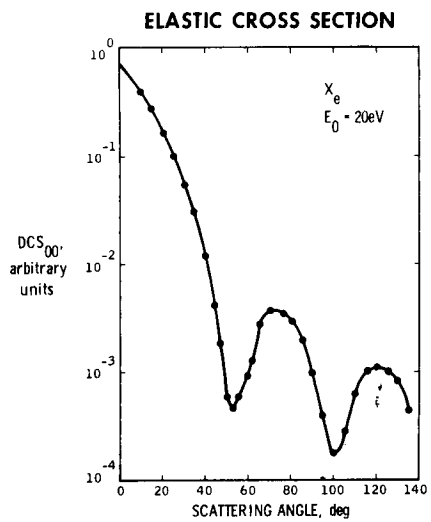

Figure 2.

RTOP 503-10-03
Plasma Dynamics
K. Shimada*

THERMIONICS RESEARCH

The objectives of thermionics research are to investigate: (1) physical parameters of cesium plasma and (2) electron and ion emission/collection properties of electrodes in contact with cesium vapor. Specific objectives are to apply results of these investigations to improve performance of thermionic converters at lower-than-conventional operating temperatures at which the life of converters is greatly increased.

The plasma parameters were measured from volt-ampere characteristics of a Langmuir probe immersed in a cesium plasma which was formed in a simulated thermionic converter as was reported last year. The results this year were obtained with a smaller interelectrode gap (2 mm) and at higher cesium temperatures (up to 533K). It was verified that the potential profiles in the gap closely resemble those computed in small-gap thermionic converters. However, it was also found that the density of ions generated in unignited modes, including the anode glow mode, were not large enough to efficiently neutralize the electron space charge.

Electron emission properties of tantalum electrodes having a controlled amount of oxygen and the electron collection properties of Ta_2O_5-coated electrodes were determined in a metal-ceramic Marchuck tube (Fig. 1) in which cesium discharge was formed. Electron emission or collection did not vary markedly for an oxygen content varying between 0.1 and 0.3 atomic percent, but the electron emission was almost an order of magnitude larger than that from a non-oxygenated electrode under cesiated conditions. Electron collection properties of the Ta_2O_5-coated electrode, indicated by the work function ϕ of that electrode, were excellent as ϕ was approximately 1.4 eV which is nearly 0.3 eV lower than a planar tantalum electrode at collector temperatures (Fig. 2). The effect of oxygen on other physical parameters is shown in Fig. 3.

Lastly an experimental device (Fig. 4) for investigation of the effect of argon on cesium discharge has been procured and operated. The device is unique in that it allows introduction of argon gas into the device without losing cesium. Cesium breakdown phenomena will be critically examined as controlled amounts of argon are introduced to explore the possibility of using similar devices for current choppers in power conditioners.

*Guidance and Control Division, Guidance and Control Systems of Research Section

SAMPLE PROBE

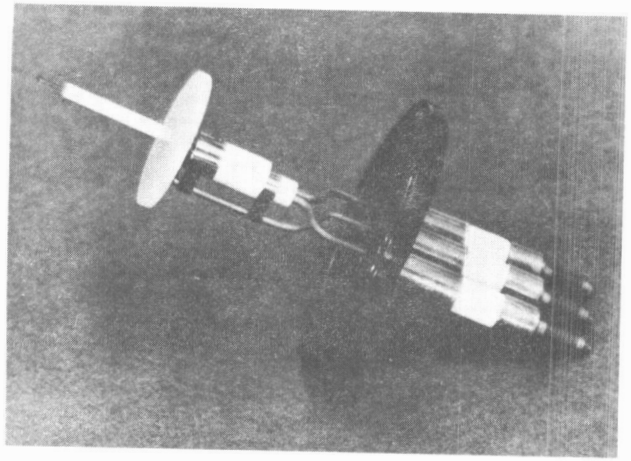

Figure 5.

ARGON-CESIUM DIODE

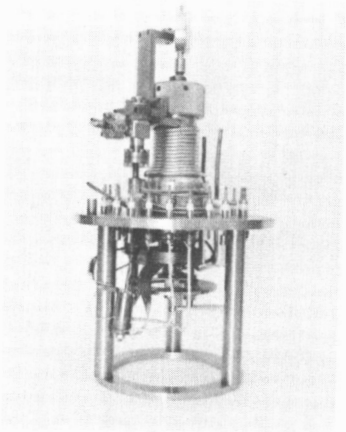

Figure 6.

ARGON INJECTION SYSTEM

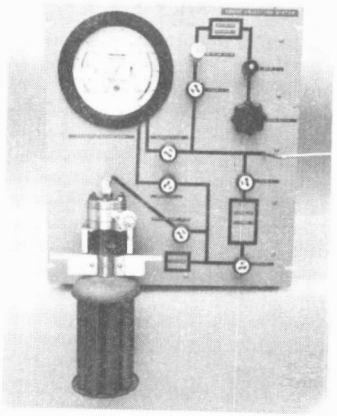

Figure 7.

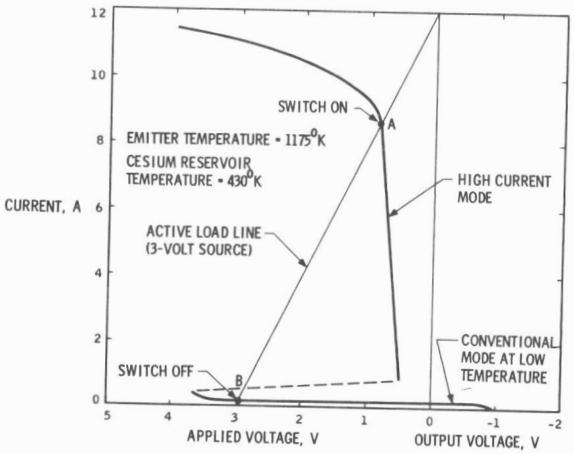

Figure 8.

RTOP 503-10-03
Plasma Dynamics
K. Shimada*

LASER PLASMADYNAMIC CONVERTER

The objective of the task is to investigate means for efficiently converting laser energy into electrical energy for application to laser power transmission. The specific method under investigation utilizes cesium metal as a source of cesium ions which are to be generated by the laser radiation.

As shown in Fig. 1, an experimental laser plasmadynamic (LPD) converter has a hemispherical ion collector electrode and a cesium pool in contact with another electrode. The laser light is introduced through an optical window into the cesium chamber and onto the surface of cesium. Cesium vapor with extremely high density will be formed when the high-intensity laser beam strikes the surface of the cesium. The cesium gas will interact strongly with the laser beam in the same manner as blow-off materials of solid surfaces. The interaction results in cesium ionization. The collection of ions and electrons to produce electric power will be achieved by driving those charged particles along the electric field which exists in the gap between two electrodes having different work functions (Fig. 2).

Calculations show that an electric current of 16 A/cm^2 at 1V can be obtained at a conversion efficiency of 22% (Fig.3). Since this efficiency depends strongly on the efficiency of ionization, the interaction between the laser and the cesium liquid will be investigated first. For this purpose another device, shown in Fig. 4, is being fabricated. Spatial and energy distributions of cesium ions and neutrals will be determined in this device.

The first irradiation experiment is being planned with a TEA CO_2 laser mainly because of the magnitude of its power (40 W average, 2 MW peak/pulse). Higher efficiencies would be obtainable with lasers with shorter wavelengths where resonant excitation and ionization of cesium are more likely to occur.

*Guidance and Control Division, Guidance and Control Systems and Research Section

LPD CONVERTER

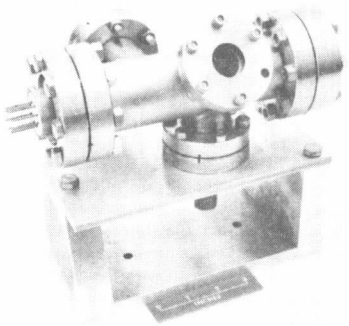

Figure 5.

LASER IRRADIATION SETUP

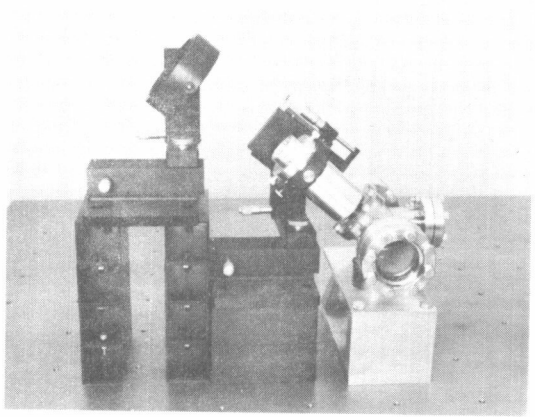

Figure 6.

LASER PLASMA ANALYZER

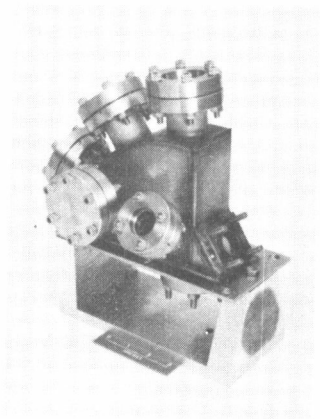

Figure 7.

IDEAL CONVERTER EFFICIENCY

SAMPLE CALCULATION

OUTPUT POWER DENSITY (P_{OUT}) FOR J = 16 A/cm^2 AT 1 V = 16 W/cm^2

ION FLUX DENSITY NEEDED TO GENERATE 16 A/cm^2 = $2.2 \times 10^{-2} \frac{gm}{sec\text{-}cm^2}$

POWER DENSITY NEEDED FOR EVAPORATION (P_V) = 11.0 W/cm^2

POWER DENSITY NEEDED FOR IONIZATION (P_I) = 62.2 W/cm^2

TOTAL INPUT POWER DENSITY $P_{IN} = P_V + P_I$ = 73.2 W/cm^2

CONVERTER EFFICIENCY $\eta = \frac{P_{OUT}}{P_{IN}}$ = 22%

Figure 8.

Melvin M. Saffren*

SUPERFLUID HELIUM ORBITAL EXPERIMENTS

The objective of this task is to devise concepts for superfluid helium experiments to be carried out in weightlessness in the Physics and Chemistry Laboratory in Space, and to determine the feasibility of these concepts by means of earth-based experiments.

The experiments are meant to help understand, by means of studying the breakdown of superfluidity in freely suspended HeII drops, the nature of superfluidity itself. In addition, these drops can be used as models for other superfluid "drops" such as atomic nucleii and neutron stars. The experiments also allow study of novel phenomena in HeII and novel measurement of HeII properties. Finally, these experiments together with others being planned in another task will provide data for the efficient design of weightless HeII cooling systems for spacecraft instruments and devices.

In the last ten months, nearly a dozen more experiment concepts have been added to the original dozen. Most noteworthy of the new concepts are experiments that involve non-simply connected rotating HeII drops of toroidal shape, and those that involve highly electrically charged spherical drops. The toroidal drops can be used to study the decay into vortices of "persistent" non-simply connected superfluid flows of high circulation in the absence of constraining walls. The absence of walls in this and the other experiment distinguishes them from those which heretofore have been carried out on HeII. In fact, two theories of vortex formation in HeII that have been published in the last year indicate that it is the microscopic rigid imperfections in container walls that are responsible for vortex formation in earth-based experiments. The experiments on highly charged drops can be used, according to our calculations, to verify the recently published suggestion that electrons or alpha-particles will form a two-dimensional lattice on the surface of HeII for sufficiently high values of the charge density.

To establish the basic feasibility of most of the nearly two dozen planned experiments, the following must be demonstrated: methods for forming, positioning, rotating, oscillating, fissioning, observing flows, and generating vortices (other than by means of rotation) in freely suspended HeII drops. It must also be demonstrated that the lifetime of such drops will be sufficiently long for meaningful measurements to be carried out.

The primary method for forming, positioning, oscillating, and fissioning the drops utilizes acoustic pressure – the dynamic pressure of sound waves. We have already demonstrated in the laboratory that an acoustic standing wave excited in a spherical resonator in normal gravity can be used to collect and levitate styrofoam bits at the center of the resonator. A soap bubble, meant to represent a drop, has also been levitated to help demonstrate the absence of any instability tending to disrupt a drop. To simulate drop formation in weightlessness, tests are now being planned which will utilize the neutral buoyancy of water drops in chloroform-hexane solutions. Drop tower tests of the resonator will be carried out in another task as will the tests for the acoustic excitation of freely suspended fluid drops. However, laboratory demonstration of a backup method for forming a drop by means of drop accretion will be carried out under the present task. Drop accretion, in which pairs of oppositely directly smaller droplets are repeatedly fired at an accreting drop, also provides a backup method for drop oscillation and rotation, and not just drop formation.

Drop lifetime for a 1-cm HeII drop at 1.8° K has been calculated, indicating that the drop radius would decrease 10^{-6} cm in an hour – hardly observable. Preliminary laboratory tests on pendant HeII drops indicate the persistence of drops even of 1 mm and 2 mm radius for more than 30 minutes. Any HeII loss in the drops could be accounted for by small heat leak along the surface substrate from which the drops were suspended. However, a less equivocal test is planned in which a 1-cm superconducting sphere freely levitated by a magnetic field is coated with HeII simulating a free HeII drop; the rate of rise of the sphere measures the loss of HeII.

A levitated HeII-coated superconducting sphere is, in fact, currently being used in tests now in progress to test the feasibility of rotating a free drop by rotating the vapor surrounding it. In the tests, the coupling of the liquid to the vapor is measured by the rate at which such a sphere, once made to spin, loses its angular velocity. The results of these tests are of some interest in themselves, indicating that the accommodation coefficient of gaseous helium atoms to an HeII surface – measuring the "sticking" of a free atom to the surface – is very much lower than has been heretofore assumed. However, even this low coupling allows a 1-cm drop to be spun up to an angular velocity of 1 rps in 40 s by rotating the vapor 1 rps faster than the instantaneous angular velocity of the drop. Nonetheless, backup methods for drop rotation are still being considered.

It is planned to generate vortices in the drop by rotating small superconducting spheres suspended in the drop, the spheres being made to rotate by imposition of a strong magnesic field, an effect quite akin to the Einstein-de Haas effect manifested by magnetic materials subjected to an imposed magnetic field. The method will be tested in the laboratory by levitating tiny superconducting spheres in HeII using a non-uniform field and causing them to rotate by imposition of a strong uniform field.

*Space Sciences Division

FORMATION

- ACOUSTIC PRESSURE

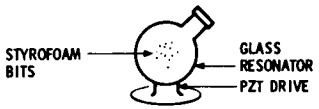

- ACCOMPLISHED
  - LEVITATION
  - BUBBLE
- PLANNED
  - NEUTRAL BUOYANCY
  - DROP TOWER (MS/MS)
    - ACTUAL FORMATION
    - OVERDRIVE ABSENT

Figure 5.

FORMATION (contd)

- ACCRETION

- ACCOMPLISHED
  - WATER DROP COALESCENCE
- PLANNED
  - "STACK" SIMULATION
  - DROP TOWER
    - He II
    - DAMP OSCILLATIONS

Figure 6.

LIFETIME

- ACCOMPLISHED
  - CALCULATION
  - PENDANT DROP

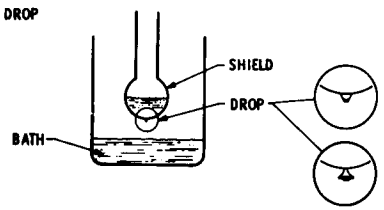

- PLANNED
  - COATED SPHERE

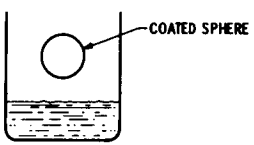

Figure 7.

ROTATION

- VAPOR-LIQUID COUPLING
  - COATED SPHERE SPINDOWN
    - CALIBRATION
    - TEST
    - NEW RESULTS
- PLANNED
  - ACCRETION
- BACKUP
  - DIELECTROPHORESIS
  - ACOUSTIC ROTATION

Figure 8.

SUPERCONDUCTING DEWAR

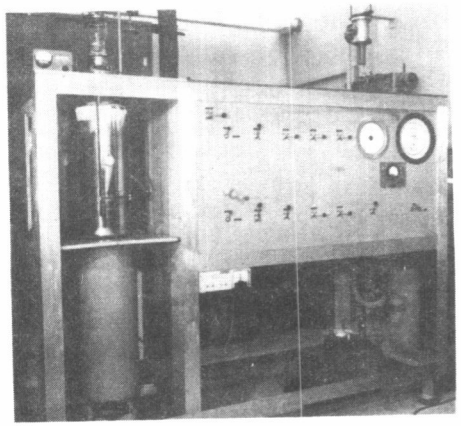

Figure 9.

SPHERE LEVITATION

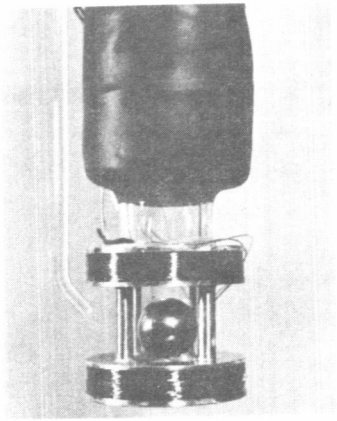

Figure 10.

VORTEX GENERATION

- PLANNED
- GYROMAGNETIC EFFECT

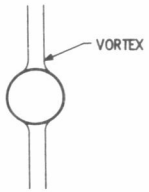

- SUPERCONDUCTING POWDERS

Figure 11.

Melvin M. Saffren*

STUDY FOR A PHYSICS AND CHEMISTRY LABORATORY IN SPACE

The objective of this task, contracted to us by LaRC, is twofold: first, define classes of physics and chemistry experiments which could justifiably be carried out on the Physics and Chemistry Laboratory in Space proposed for the Space Shuttle, and, second, exemplify each class by experiment concepts which appear to merit a detailed study of their feasibility.

In pursuing this objective, possible experiments are judged according to three criteria: scientific worth, richness of potential applications, and the impossibility or impracticality of their being performed on earth. The first two criteria serve to eliminate experiments which were mere curiosities, or which provoke a "so-what" response. The third criterion eliminated, among others, gravity wave detection experiments.

The approach to the task consisted of the formation of a JPL working group in which experiments proposed by each member would be intensely scrutinized by the rest of the group. Some of the proposed experiments were originated by the proposer, others were stimulated by experiments in the literature which appeared to be seriously marred by their having to be performed on earth. Still others arose during discussion, and some had been proposed before in other studies. From time to time, members of the group or the entire group, met with scientists from local universities to discuss or solicit experiment concepts. The reaction of university scientists to the possibility of performing experiments on the Space Shuttle was extremely interesting. If they were merely informed of the unique environment of Shuttle and asked to suggest experiments, their reaction was quite negative. If instead, they were approached with particular experiments in their specialty that the working group had come up with – though no one in the group was an expert in that specialty – the reaction was positive, even when the experiments suggested by the group were rejected. We feel there is an important lesson here for those who would solicit Shuttle experiments from university and other outside scientists.

Consideration of experiment classes by the working group has already led to the suggestion of two facilities for the Physics and Chemistry Laboratory – a drop dynamics and zero-g positioning facility, and a wall-less chemistry facility. Furthermore, six experiment concepts have so far been proposed for study of their feasibility, and three of these have university scientists as co-proposers. The six experiments and two facility proposals have been submitted to Langley Research Center (LaRC) for consideration, along with proposals from other centers, by an *ad hoc* committee of NSF convened by LaRC for further evaluation.

*Space Sciences Division

DROP DYNAMICS AND ZERO-G POSITIONING

- He II DROP
- APPLICATIONS
  - METEOROLOGY
    - ADIABATIC CONDENSATION
    - COALESCENCE
    - DROPLET GROWTH
    - SNOWFLAKES
    - SEEDING
  - COSMOLOGY
    - PULSARS
    - GRAVITATIONAL SYSTEMS
      - GALAXIES
      - DUST CLOUDS

Figure 5.

DROP DYNAMICS AND ZERO-G POSITIONING (contd)

- APPLICATIONS
  - NUCLEAR PHYSICS
  - LIQUIDS AND GASES -- ZERO-G
    - FUELS
    - CRYOGENS
    - LIFE SUPPORT
  - GEOPHYSICS
    - DYNAMO
    - FLUID CORE DAMPING
  - CONTAMINATION -- ZERO-G
  - SPACE MANUFACTURING
    - CONVECTION -- ZERO-G
      - SURFACE TENSION
      - THERMAL EXPANSION
    - DROP DYNAMICS
    - ACOUSTIC CONTROL AND DISPERSION

Figure 6.

WALL-LESS CHEMISTRY

- NO WALL DEEXCITATION
- LONG PATH LENGTH - LOW PRESSURE
- LOW BACKGROUND
- SOLAR EXCITATION SOURCE

Figure 7.

APPLICATIONS

- REACTIONS LONG-LIVED METASTABLES
- NEW SYNTHESES AND MANUFACTURE
- PLANETARY ATMOSPHERES
  - SOLAR FLUX
  - METASTABLES
- REACTIONS ON SNOWS DUSTS
- COMET CHEMISTRY
- CONTAMINATION AND OUTGASSING
- FLAME CHEMISTRY - MIXED FLAMES
- BEAM EXPERIMENTS

Figure 8.

Melvin M. Saffren*

INFRARED ACTIVE JOSEPHSON JUNCTIONS

The objective of this task is to study, theoretically and experimentally, the effect of infrared radiation on Josephson junctions containing substances in the junction barrier with levels that can be excited by the radiation. It is hoped that such junctions will allow more sensitive detection of infrared radiation than is now possible with conventional Josephson weak-line detectors, and that these junctions will also extend the range of detection to wavelengths perhaps as low as 1_{μ}. Furthermore, these novel infrared active junctions may allow the remote detection of a specific molecular species to which the detector is tuned.

Until early this year, the work on active junctions had been solely theoretical. At that time, work began to study active junctions experimentally as well. This portion of the work is being carried out in conjunction with another task in which similar junctions are used to study tunneling spectroscopy.

Theory. The response of an active junction to infrared radiation has now been calculated using our modified transfer-Hamiltonian model of the junction. The effect of the radiation on the tunneling electrons is taken into account using the Tien-Gordon approximation, and the effect of radiation on the infrared active barrier site is taken into account by assuming a non-zero probability of occupation of its excited levels. Even this crude model of an irradiated infrared active junction requires the rather sophisticated method of temperature-dependent Green's functions for its solution. The resulting expression of the junction in terms of its current-voltage characteristic is complicated and awaits numerical evaluation which we plan to carry out in the next few months. Nevertheless, some interesting qualitative features of the response are already evident. First of all, if the radiation amplitude is made to vanish, the twice-differentiated characteristic does display the spectrum of the active site – the well known "Lambe - Jaklevic" peaks – and this serves as a check on the calculation. For non-zero values of the radiation amplitude, the calculation indicates that a Lambe - Jaklevic peak will decrease in amplitude for radiation having photon energy greater than the peak. Furthermore, if the radiation is capable of exciting a particular Lambe - Jaklevic peak, that peak will appear again at a lower voltage. The amplitude of this displaced peak depends, however, on the magnitude of the coupling of the tunneling electrons to the active site. When the coupling is appreciable, the appearance of the additional peak constitutes a new method of detecting radiation. Evaluation of typical couplings is planned.

These effects on the characteristic have been described as perturbations by the radiation on the unperturbed characteristic determined by the site. Conversely, the characteristic of the irradiated active junction can be analyzed in terms of the effect of an active site on the pure radiation characteristic. As is well known, this radiation characteristic manifests so-called "voltage steps." At voltages below the voltage corresponding to the superconducting energy gap of the electrodes, these steps are the Josephson steps, and above the voltage, the steps are the photon-assisted tunneling or single-particle steps. The present calculation shows that the effect of an active site on the characteristic is the addition of new Josephson and single particle steps displaced from the original steps. Again the amplitude of these new features depends on the coupling of the tunneling electrons to the active sites. When the level spacing of a site is resonant with the incident radiation, the additional steps fall on top of the original ones, and the amplitude of the steps does appear to be enhanced. However, the actual enhancement depends not only on the strength of the electron-site coupling but also on the strength of the coupling of the radiation to the site. More careful calculation of the enhancement will have to treat interference effects between the direct photon excitation of the tunneling electrons and their indirect excitation by a photon-excited level of a site. Conceivably, these effects could lead not to enhancement but diminution of the steps. We hope to calculate these effects in the coming year. These same considerations apply to another portion of the characteristic; namely, the critical value of the zero-voltage current (supercurrent). While the present calculation indicates that an active site resonant with the radiation lowers the value of the critical current, interference can modify this conclusion.

The present calculation also neglects another potentially important effect – modification of the effective barrier height by a site when it is excited by the

*Space Sciences Division

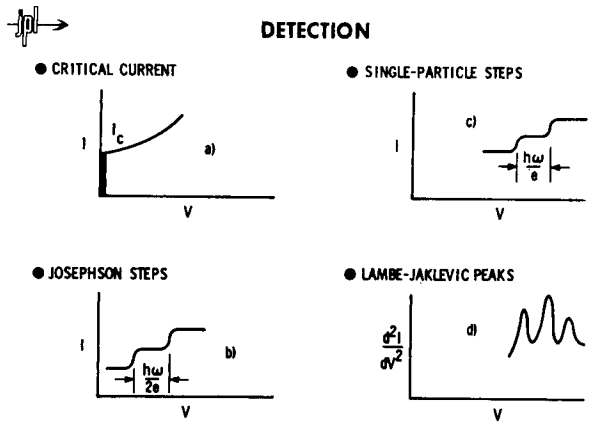

Figure 3.

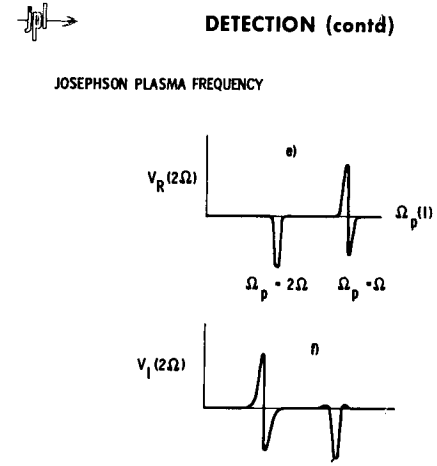

Figure 4.

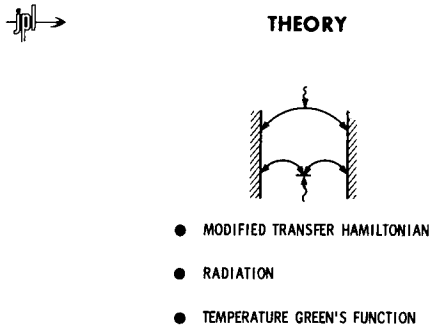

Figure 5.

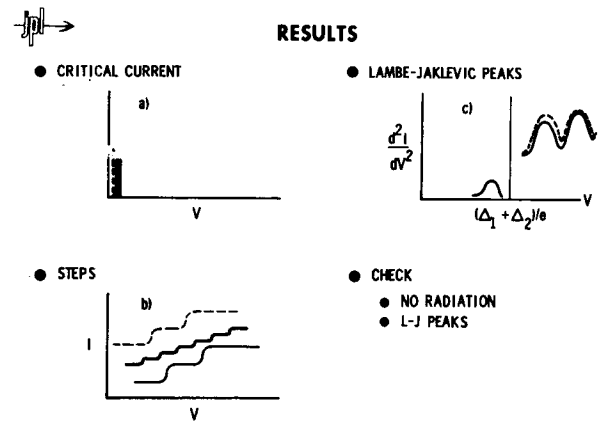

Figure 6.

PLANNED

- COMPUTE COUPLINGS
- COMPUTE CHARACTERISTICS
- INCLUDE INTERFERENCE
  - PHOTON → ELECTRON
  - PHOTON → ACTIVE SITE → ELECTRON
- EFFECT OF RADIATION ON COUPLING
  - BARRIER HEIGHT
  - PLASMA FREQUENCY
- SEMICONDUCTOR JUNCTIONS

Figure 7.

EXPERIMENT

- JUNCTIONS FABRICATED
- APPARATUS CONSTRUCTED
- IR INTO DEWAR
- OH BENDING

Figure 8.

ALUMINUM JUNCTION

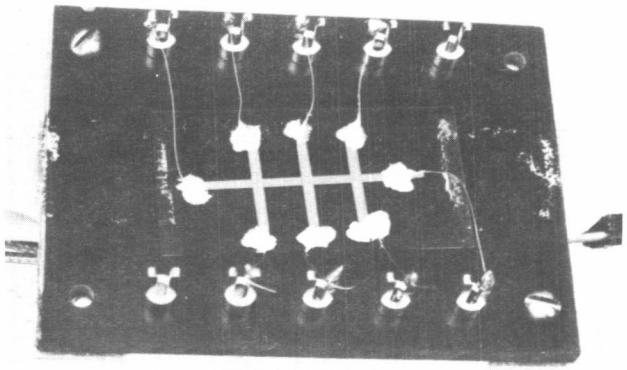

Figure 9.

APPARATUS TO MEASURE CHARACTERISTIC

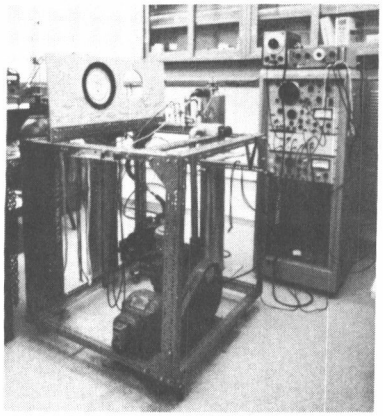

Figure 10.

LAMBE-JAKLEVIC EFFECT

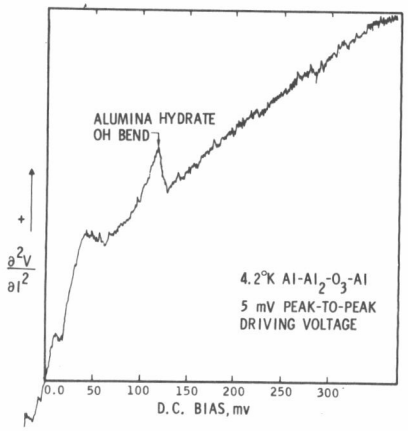

Figure 11.

PLANNED

- SPUTTERING APPARATUS
- JUNCTIONS
  - ELECTRODES
  - ACTIVE MATERIAL
- IR INTO JUNCTION
- RADIATION EXPERIMENTS
  - FREQUENCY
  - INTENSITY
  - TEMPERATURE

Figure 12.

Randall K. Kirschman*

SUPERCONDUCTIVITY RESEARCH

We have been fabricating and studying superconducting structures of the type developed by Harris A. Notarys and James E. Mercereau, who are presently at Caltech, and with whom we are cooperating. There are several reasons for studying this particular structure. It is a metallic, thin-film structure and superior to other types of superconducting structures in regard to the practical aspects of long life, stability, ruggedness, and reproducibility. The primary application we have in mind for this structure is that of a detector for astronomical observations in the infrared region of 0.1 to 3 mm. The detector will have high sensitivity, fast response, and the ability to operate in a narrow-band, tunable mode. Such a detector is actively being sought by astronomers, since it would make the hitherto neglected 0.1 - 3 mm region more accessible. Various theoretical studies have indicated that detectors using superconducting structures would have sensitivities and response times that are orders of magnitude better than presently obtainable. In addition, superconducting detectors based on the Notarys-Mercereau structure could be operated as tunable narrow-band detectors as well as broad-band detectors. Such detectors could find use in spacecraft instruments such as the infrared astronomy satellite as well as in ground-based observatories.

Other applications for this structure include sensitive measurement of magnetic properties, voltage, and current.

During the past year, several important developments have resulted from the cooperative effort between the Cryogenics Laboratory at JPL and the Low Temperature Physics Laboratory at Caltech. First, sensitivity measurements made at low frequencies (10 MHz to 0.5 GHz) gave results that confirmed the applicability of the theory developed at Caltech for this type of superconducting structure. Second, observations of frequency response have been extended to 240 GHz (approximately 1.3 mm). Measurements of frequency response are presently limited by technical difficulties, and a higher value is expected. Third, fabrication techniques for structures using refractory superconductors (such as niobium and tantalum) have progressed to the point where operating structures can be produced reliably and controllably. These are more durable and stable than earlier structures that used tin, lead, or indium; they are also expected to have a higher frequency response. The emphasis has been on developing fabrication methods employing photolithographic and chemical techniques that lend themselves to automated fabrication.

Future work includes extending measurements of sensitivity to microwave frequencies, extending measurements of frequency response, and developing methods to improve coupling of infrared radiation to the structures. Close cooperation will be maintained with the Low Temperature Physics Laboratory at Caltech in this research.

The results of parts of this work were presented at the Applied Superconductivity Conference in Annapolis, Maryland (May 1-3, 1972), and will appear in an IEEE journal. A more extensive report has been submitted to the Journal of Low Temperature Physics.

*Engineering Mechanics Division, Structures, Dynamics, and Materials Section.

NOTARYS-MERCEREAU SUPERCONDUCTING STRUCTURE

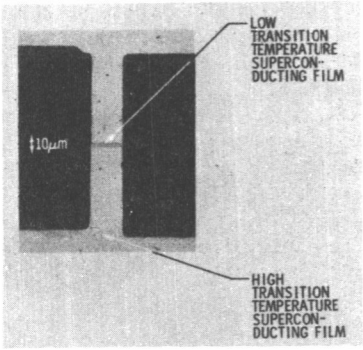

PRACTICAL ADVANTAGES

- A THIN-FILM STRUCTURE
- RUGGED, STABLE
- LONG USEFUL LIFE
- SIMPLE, CONTROLLABLE FABRICATION

Figure 1.

RELEVANCE

- PRIMARY APPLICATION
  - DETECTOR FOR INFRARED ASTRONOMY (0.1 - 3 mm)
  - FEATURES
    - SENSITIVE
    - FAST
    - NARROW-BAND MODE POSSIBLE
    - TUNABLE
  - USES
    - SATELLITE DETECTOR
    - MOLECULAR IDENTIFICATION
    - SPECTRAL SCANNING
    - IR IMAGING ARRAYS

Figure 2.

RELEVANCE (contd)

- OTHER APPLICATIONS
  - MEASUREMENT
    - MAGNETIC FIELDS
    - MAGNETIC PROPERTIES
    - VOLTAGE
    - CURRENT
  - COMMUNICATION
    - MICROWAVE (MILLIMETER) REGION
- AN INTERESTING, UNIQUE STRUCTURE
  - NOT WELL UNDERSTOOD
  - NOT A JOSEPHSON JUNCTION

Figure 3.

FABRICATION

- RECENT WORK
  - CAN NOW MAKE STRUCTURES USING "HARD" SUPERCONDUCTORS RELIABLY AND REPRODUCIBLY
  - HAVE ABANDONED EARLIER TYPE USING "SOFT" SUPERCONDUCTORS
- IMPORTANCE
  - GREATER RELIABILITY AND STABILITY
  - USEFUL TEMPERATURE RANGE DOUBLED
  - TECHNIQUES ARE ADAPTABLE TO AUTOMATED FABRICATION
- FUTURE WORK
  - DEVELOP FABRICATION TECHNIQUES FOR MORE COMPLEX STRUCTURES AND ARRAYS

Figure 4.

FREQUENCY RESPONSE

- RECENT WORK
  - HAVE EXTENDED OBSERVATIONS TO 240 GHz (1.3 mm) FROM 90 GHz (3 mm) LAST YEAR
- IMPORTANCE
  - STRUCTURE IS NOW KNOWN TO WORK WITHIN REGION OF INTEREST (0.1 - 3 mm)
- FUTURE WORK
  - WILL TRY TO PUSH RESPONSE TO COVER ENTIRE REGION OF INTEREST

Figure 5.

SENSITIVITY TO ELECTROMAGNETIC RADIATION

- RECENT WORK
  - MEASUREMENT OF SENSITIVITY AT LOW FREQUENCY (10 MHz - 0.5 GHz)
- IMPORTANCE
  - HELPS TO DEVELOP A PRACTICAL UNDERSTANDING OF STRUCTURE
- FUTURE WORK
  - EXTEND MEASUREMENTS TO HIGHER FREQUENCY (>0.5 GHz)
  - DEVELOP METHODS OF EFFICIENTLY COUPLING IR RADIATION TO STRUCTURE

Figure 6.

Alan Rembaum*

SUPERCONDUCTIVITY AT HIGH TEMPERATURE

The possibility of synthesizing a system according to the excitonic model of superconductivity proposed by Ginzburg was explored using a layered structure. Single crystals of MoS_2 (hexagonal and rhombohedral polymorphs) grown by the chemical transport technique as well as natural molybdenite were intercalated with the complete series of alkali metals. Stochiometries and X-ray data of all intercalates were determined by chemical and X-ray analysis, and a complete indexing of X-ray patterns of $K_{0.4}MoS_2$ and $Rb_{0.3}MoS_2$ was achieved. The results of chemical analysis of samples in which 100% intercalation occurred confirmed that the alkali intercalates are characterized by definite stochiometries. The X-ray results showed insignificant changes in the a_o axis and considerable expansion of Co axis (ΔCo; 6.745, 2.704, 4.286, 4.899 and 7.312 Å for $Li_{0.4}MoS_2$, $Na_{0.3}MoS_2$, $K_{0.4}MoS_2$, $Rb_{0.3}MoS_2$ and $Cs_{0.3}MoS_2$, respectively). All intercalated crystals were superconducting (T_{onset}; 3.7, 4.1, 6.1, 6.25 and 6.30K for $Li_{0.4}MoS_2$, $Na_{0.3}MoS_2$, $K_{0.4}MoS_2$, $Rb_{0.3}MoS_2$ and $Cs_{0.3}MoS_2$ respectively). The onset of superconductivity was the same for both the perpendicular and parallel orientation. The determination of superconducting transition temperature was followed by critical magnetic field and resistivity measurements as a function of temperature and orientation. Potassium intercalated MoS_2 has been found to be characterized by a critical magnetic field of 40 kgauss at 5.25°K. The slope of the critical field versus critical temperature (42 kG/K) is only a factor of 3.5 smaller than the highest slope yet found.

The study of the resistivity of a single crystal of MoS_2 before and after intercalation as a function of temperature revealed that MoS_2 behaves like a typical semiconductor, the resistivity decreasing with increase of temperature, while $K_{0.4}MoS_2$ exhibited characteristics of a metal, the resistivity decreasing with decrease of temperature. The superconductivity of intercalated MoS_2 is believed to be caused by an electron transfer from the alkali metal to an empty band of MoS_2, resulting in an increase in electron density as well as in the density of states at the Fermi Surface.

*Propulsion Division, Polymer Research Section

HEXAGONAL AND RHOMBOHEDRAL MoS_2

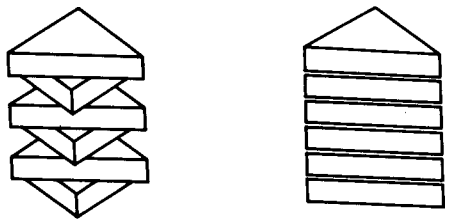

DISTANCE BETWEEN LAYERS
6.147 Å (2H)
6.122 Å (3R)

HEXAGONAL MoS_2; ADJACENT LAYERS IN ANTIPARALLEL ORIENTATION

RHOMBOHEDRAL MoS_2; ALL LAYERS IN PARALLEL ORIENTATION

Figure 5.

RESULTS

- CHANGES OF LATTICE CONSTANTS ON INTERCALATION BUT NO CHANGE IN CRYSTAL STRUCTURE
- DETERMINATION OF STOICHIOMETRY
- COMPLETE INDEXING OF X-RAY DIFFRACTION PATTERNS OF MoS_2 $K_{0.4}MoS_2$ AND $Rb_{0.3}MoS_2$
- DETERMINATION OF SUPERCONDUCTING TRANSITION TEMPERATURE OF ALL ALKALI METAL INTERCALATES
- DETERMINATION OF RESISTIVITY AS A FUNCTION OF ORIENTATION AND TEMPERATURE OF MoS_2 AND $K_{0.4}MoS_2$
- DETERMINATION OF CRITICAL MAGNETIC FIELD AS A FUNCTION OF TEMPERATURE

Figure 6.

CHEMICAL AND X-RAY DATA FOR INTERCALATED MoS_2

COMPOUND	C_0(Å)	a_0(Å)	ΔC_0(Å)	Δd_0(Å)*
MoS_2 (2H)**	12.2943	3.1603		
Li_xMoS_2 ($0.4 \le x \le 1.0$)	19.039	(-)†	6.745	3.372
Na_xMoS_2 ($0.3 \le x \le 0.6$)	14.998	(-)†	2.704	1.352
$K_{0.4}MoS_2$ (2H)	16.5804	3.2036	4.286	2.143
$K_{0.4}MoS_2$ (3R)††	24.7915	3.2072	6.422	2.141
$Rb_{0.3}MoS_2$ (2H)	17.1937	3.2039	4.899	2.450
$Cs_{0.3}MoS_2$	19.606	(-)†	7.312	3.656

* CHANGE IN INTERPLANAR SPACING, d_0

**2H REPRESENTS THE HEXAGONAL POLYMORPH

† DATA IS NOT REFINED

†† 3R REPRESENTS THE RHOMBOHEDRAL POLYMORPH

Figure 7.

EXPANSION OF Co AXIS AS A FUNCTION OF ATOMIC SIZE

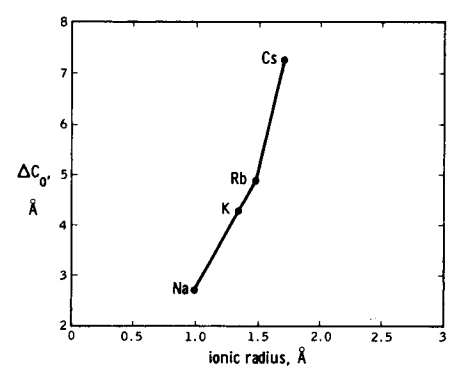

Figure 8.

BAND STRUCTURE

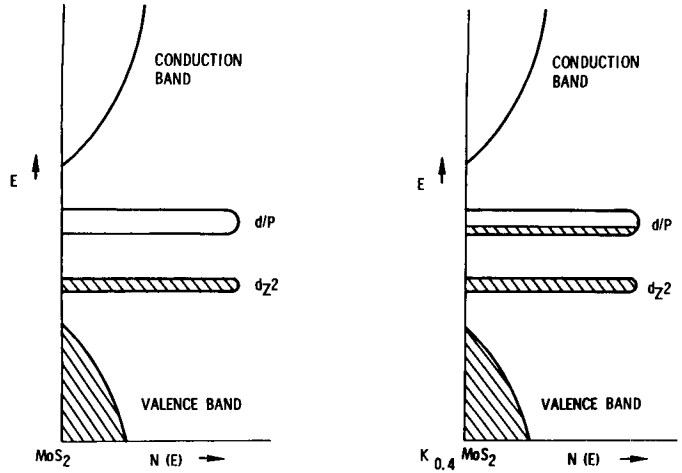

Figure 12.

CONCLUSIONS

- THE A_xMoS_2 STRUCTURES HAVE A HIGHER SUPERCONDUCTING TRANSITION TEMPERATURE THAN ANY OTHER LAYERED INTERCALATES KNOWN
- THE HIGH CRITICAL MAGNETIC FIELD MAY HAVE PRACTICAL APPLICATIONS
- INTERCALATED MoS_2 IS A METAL
- THE SUPERCONDUCTIVITY MECHANISM IS NOT EXCITONIC

Figure 13.

FUTURE WORK

- INTERCALATION OF METALS WITH HIGH IONIZATION POTENTIALS
- INTERCALATION OF POLARIZABLE ORGANIC COMPOUNDS INTO METALLIC LAYERED STRUCTURES
  - DYES AND RELATED STRUCTURES
  - INTERLAYER SYNTHESIS
- DETERMINATION OF TRANSPORT PROPERTIES AND SUPERCONDUCTIVITY
- DETERMINATION OF CRITICAL MAGNETIC FIELDS

Figure 14.

Christer Svensson*

ELECTRONIC PROPERTIES OF THIN INSULATING FILMS

Insulating films are of great importance in microelectronics of today. In metal oxide semiconductor (MOS) circuits the properties of the insulating film used will probably give the ultimate limitation of performance and life of the circuits. Of particular interest are dielectric breakdown and charge instabilities. Neither the dielectric breakdown phenomenon nor some charge instabilities are understood, and one objective of this program is to gain a better understanding of these phenomena.

Since silicon dioxide is the most widely used insulator in MOS circuits, we have initiated an investigation of these films and have found time-dependent breakdown mechanisms (probably defect-related). This means that an MOS circuit which has passed all tests still may fail due to breakdown after a long time of operation. The phenomenon will be further investigated.

In a new class of electronic devices – charge-storage-memory devices – the properties of the insulating films will be of even greater importance. In a charge storage device one of the insulating films is used both for injecting charge at very high fields (writing mode) and for insulating these charges from the environment at low fields (storage mode). The insulator must therefore be able to withstand very high fields without destruction or degradation and to be a very good insulator at low fields. In some charge-storage devices the insulator is also used for the charge storage itself using charge trapping (in the MNOS device).

We have started to investigate a charge-storage device of the metal-insulator-metal-oxide-silicon (MIMOS) type. We are particularly interested in memories with a writing speed of about 1 μs and with storage times ranging from a week to several years.

Last year Dr. Joseph Maserjian reported on the progress of using thin silicon dioxide as the oxide in the MIMOS device. For the storage electrode and outer insulator, aluminum and aluminum nitride were investigated. However, this combination in the MIMOS structure exhibited instabilities due to unstable properties of the aluminum layer. Another approach is to replace the Al-AlN combination with molybdenum-silicon nitride. With this new combination we have been able to make simple MIMOS structures.

The performance of these devices is under investigation, but we have found that they can be used with 1 μs writing speed and about one week of storage time. However, there are still some problems to be solved. We have observed that the thin oxide is destroyed after many writing cycles (on the order of 1000 cycles). This is believed to be caused by charge-trapping in the oxide. We are also working with high voltages – about 30 volts. These voltages must be reduced to get a practical memory device, and this will be done by reducing the insulator thicknesses. We need also to demonstrate the possibility of putting MIMOS devices together in large memory arrays. This work is in progress under a different task.

*Astrionics Division, Astrionics Research Section. Dr. Svensson is an exchange scientist from Chalmers University of Technology, Sweden, replacing Dr. Joseph Maserjian (who is presently at Chalmers University replacing Dr. Svensson) for six months.

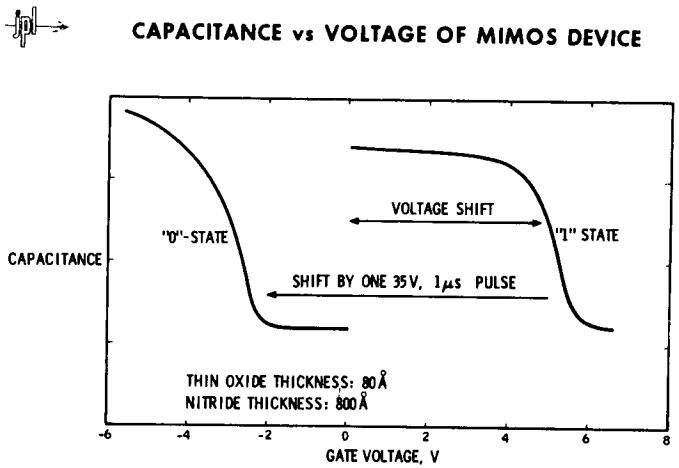

Figure 4.

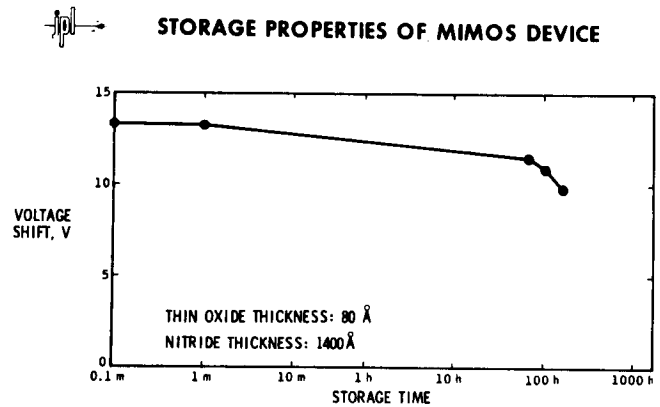

Figure 5.

George Lewicki*

MAGNETO-OPTIC INFORMATION STORAGE ON MnBi FILMS

The objective of this work is to study materials and phenomena useful for optical storage. In such storage, an optical beam both stores and retrieves information from the storage medium. Storage of holograms gives rise to the possibility of a 10^{12}-bit random-access memory with no moving parts. Such an approach is being considered in industry. Here we are thinking in terms of a task more directly related to JPL's needs – namely, frame-by-frame storage of television pictures. This technique, if shown feasible, could lead to storage of a thousand TV frames with power, weight, and volume characteristics, each down at least a factor of ten over those of tape recorders presently used for this task.

Currently we are studying the preparation of ferromagnetic MnBi films and the use of optical storage techniques on them. Information is stored as the value of magnetization in localized areas of the film. This magnetization is controlled by the joint action of a magnetic field and localized heating from a focused laser beam; it is read out by the same beam used for writing, because of the magneto-optic effect coupling optical properties of magnetization.

Films are prepared by sequentially evaporating layers of bismuth and manganese on a substrate, and heating the composite structure to allow reaction of the elements to form MnBi. At this time last year, uncontrolled oxygen contamination of the Mn layer was identified as the main problem in the preparation of films. We did not have the freedom of alleviating this problem by more rapid evaporation of the Mn, inasmuch as the rate of evaporation was found to be one of the variables controlling the kinetics of the reaction. Since that time we have assembled and put into operation a vacuum system achieving sufficiently low pressures to prevent oxygen contamination. This vacuum system uses bake-out, cryogenic pumping, and titanium gettering. Blank-off pressures are in the low 10^{-9} torr range and those during evaporations in the low 10^{-8} range. The system has allowed reproducible preparation of films.

A systematic study of the growth of one kind of MnBi film has just been completed. Measurements of the Faraday rotation and the Kerr rotation from the front and back surfaces of films with various thicknesses and composition were used to deduce the fact that a film is made up of four layers. Details of the measurements and the arguments used to arrive at this conclusion have been submitted for publication (Ref. 1). There is an MnBi layer sandwiched in between two compounds of manganese and bismuth of unknown composition. On top of the sandwich is a layer of excess manganese. The sandwiching layers are sufficiently optically attenuating to cause an appreciable reduction (at least by a factor of 2) of the magneto-optic effect necessary for the technical application of MnBi films. We have a work order with Caltech for backscattering measurements aimed at determining the composition of the sandwiching layers (this is funded by a JPL Director's Discretionary Fund Task).

Future work will be in the general direction delineated as follows. We have found a second way of obtaining MnBi films from superimposed films of the constituents. The ways in which films of the constituents are evaporated are different; consequently, the kinetics of the reaction are different. We intend to carry out Faraday measurements and Kerr measurements from front and back surfaces to determine whether these films are also layered. On completion of this work, we will carry out laser-recording experiments on both types of films to determine the limitations of this storage technique as far as MnBi films are concerned.

REFERENCE

1. Lewicki, G., and Guisinger, J. E., "Whither Goest the MnBi?" submitted for publication in J. Appl. Phys.

*Astrionics Division, Astrionics Research Section.

FUTURE WORK

- ANALYSIS OF SECOND TYPE OF MnBi FILM BY KERR AND FARADAY MEASUREMENTS
- COMPARISON OF THE TWO TYPES OF FILMS IN TERMS OF DISCRETE BIT SWITCHING AND ANALOGUE RECORDING

Figure 5.

LASER RECORDING

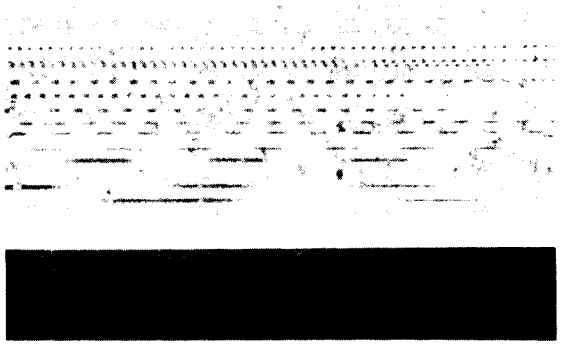

Figure 6.

Alex Shumka*

SPACE-CHARGE-LIMITED CURRENTS (SCLC) IN SOLIDS

The overall objective is to investigate space-charge-limited currents (SCLC) in semiconductors and insulators and particularly in those solids (such as silicon) that are of practical importance. Results of such an effort will not only contribute toward a better understanding of space-charge mechanisms in practical solid-state devices but will also pave the way toward realizing a new class of devices based on these phenomena, of which the solid-state triode is one example. These new devices, because of their known and expected electrical properties – such as a high frequency response, a low sensitivity to temperature changes, a high radiation resistance, and a high temperature operation, will be particularly useful for practical application. The specific objectives are to investigate the fluctuation phenomenon (noise) in SCLC and the effect of radiation damage on SCLC.

Noise in SCLC has been subjected to a considerable amount of theoretical analyses without any reliable experimental data to substantiate these theories. Previous experimental attempts have been plagued not only by excessive 1/f noise, which we have found to be largely dependent on the fabrication techniques, but also by effects due to ionized impurities, traps, field-dependent mobility and carrier heating (Ref. 1). Last year we reported on silicon structures exhibiting ideal solid-state-diode characteristics in which the intrinsic properties of SCLC, such as noise, can be investigated. These silicon solid-state diodes have provided a unique opportunity to measure the intrinsic thermal noise properties – that is, for the case in which the carriers are in thermal equilibrium with the lattice.

According to theory (Ref. 2), a Nyquist relation exists for SCLC noise – that is, $S_V = 4kT\ (2r)$ where S_V is the spectral density of the voltage noise, k the Boltzman constant, T the lattice temperature, and 2r the equivalent noise resistance in which r is the ac impedance. Our experimental results (Ref. 3) show that the noise spectra of the diode at room temperature ($T = 300^{o}K$) for various biasing currents exhibit low 1/f components and have a flat band at higher frequencies as expected. The important result is that we have been able to show that the noise equivalent resistance is $(2 \pm 7\%)r$. At present this work is extended to noise measurements at various temperatures to establish the proportionality of T and to higher frequencies where r is frequency-dependent due to transit-time effects. The completion of this task is expected to give a complete experimental verification of the theory. All the noise measurements are made in collaboration with Prof. M-A. Nicolet and Dr. J. Golder of Caltech.

A high resistance to radiation damage has been attributed to SCLC in solids and has added greatly to their importance for practical application. However, there is a lack of experimental results to substantiate these claims. To obtain quantitative data on the effect of radiation damage on SCLC we have irradiated several silicon solid-state diodes with neutrons (>3 MeV) and with protons (140 MeV). Preliminary measurements on proton-irradiated samples show that fluences of $9 \times 10^{12}\ cm^{-2}$ can have a significant effect on SCLC. A measure of radiation resistance is expected from further experimental work. These results will then be used for comparison with other similarly irradiated devices to determine the relative differences in radiation tolerances. A determination of the types and amount of displacement damage produced by the energetic protons in SCLC is also under investigation. We have already succeeded in detecting the presence of at least three different energy levels associated with the displacement damage. Similar measurements will be made on samples irradiated with energetic neutrons.

REFERENCES

1. Nicolet, M-A., Bilger, H. R., and Shumka, A., Solid-State Electron *14,* 667 (1971).

2. Shumka, A., Solid-State Electron *13,* 145 (1970).

3. Shumka, A., Golder, J., Nicolet, M-A., JPL Quarterly Technical Review, Vol. 2, No. 2, 72 (1972).

*Astrionics Division, Astrionics Research Section.

RADIATION DAMAGE INVESTIGATION

- WHY
  - HIGH TOLERANCE TO RADIATION DAMAGE IMPORTANT FOR PRACTICAL APPLICATION
  - NO EXPERIMENTAL DATA TO SUBSTANTIATE THE CLAIM OF A HIGH RADIATION RESISTANCE FOR SCLC
- HOW
  - SILICON STRUCTURES IRRADIATED WITH ENERGETIC NEUTRONS AND PROTONS TO MEASURE THE EFFECT OF RADIATION DAMAGE ON SCLC

Figure 5.

SCLC IN PROTON IRRADIATED SILICON

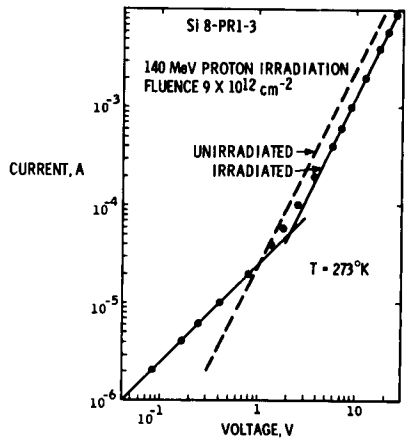

Figure 6.

SUMMARY

- NOISE
  - MEASURED COMPLETE NOISE SPECTRA FOR ONE TEMPERATURE
  - FOUND AGREEMENT BETWEEN EXPERIMENT AND THEORY
  - MEASUREMENTS AT VARIOUS TEMPERATURES AND AT HIGHER FREQUENCIES IN PROGRESS
- RADIATION TOLERANCE
  - OBSERVED SIGNIFICANT EFFECT OF RADIATION DAMAGE ON SCLC
  - DETECTED SEVERAL DEFECT LEVELS DUE TO PROTON DAMAGE
  - DETERMINATION OF RADIATION TOLERANCE AND IDENTIFICATION OF DEFECTS IN PROGRESS

Figure 7.